The Astronomical Journal, 123:1111–1148, 2002 March

THE OBSERVED OFFSET DISTRIBUTION OF GAMMA-RAY BURSTS FROM THEIR HOST GALAXIES: A ROBUST CLUE TO THE NATURE OF THE PROGENITORS[1,2]

J. S. Bloom, S. R. Kulkarni, and S. G. Djorgovski
Palomar Observatory, 105-24, California Institute of Technology, Pasadena, CA 91125
Received 2000 October 10; accepted 2001 November 27

ABSTRACT

We present a comprehensive study to measure the locations of gamma-ray bursts (GRBs) relative to their host galaxies. In total, we find the offsets of 20 long-duration GRBs from their apparent host galaxy centers by utilizing ground-based images from Palomar and Keck and space-based images from the *Hubble Space Telescope* (*HST*). We discuss in detail how a host galaxy is assigned to an individual GRB and the robustness of the assignment process. The median projected angular (physical) offset is $0\farcs17$ (1.3 kpc). The median offset normalized by the individual host half-light radii is 0.98, suggesting a strong connection of GRB locations with the UV light of their hosts. This provides strong observational evidence for the connection of GRBs to star formation. We further compare the observed offset distribution with the predicted burst locations of leading stellar-mass progenitor models. In particular, we compare the observed offset distribution with an exponential disk, a model for the location of collapsars and promptly bursting binaries (e.g., helium star–black hole binaries). The statistical comparison shows good agreement, given the simplicity of the model, with the Kolmogorov-Smirnov probability that the observed offsets derive from the model distribution of $P_{\rm KS} = 0.45$. We also compare the observed GRB offsets with the expected offset distribution of delayed merging remnant progenitors (black hole–neutron star and neutron star–neutron star binaries). We find that delayed merging remnant progenitors, insofar as the predicted offset distributions from population synthesis studies are representative, can be ruled out at the 2×10^{-3} level. This is arguably the strongest observational constraint yet against delayed merging remnants as the progenitors of long-duration GRBs. In the course of this study, we have also discovered the putative host galaxies of GRB 990510 and GRB 990308 in archival *HST* data.

Key words: astrometry — cosmology: miscellaneous — cosmology: observations — gamma rays — methods: statistical

On-line material: color figures

1. INTRODUCTION

For some 30 years since the discovery of gamma-ray bursts (GRBs; Klebesadel, Strong, & Olson 1973), a basic understanding of the nature of the brief intense flashes of gamma-rays remained elusive. Throughout much of the 1970s and 1980s the prevailing view was that GRBs arise from the surface of neutron stars in and around our Galaxy (see Lamb 1995 for a review), though by the mid-1990s the isotropic distribution of GRBs on the sky (see Fishman & Meegan 1995) served as the cornerstone of mounting evidence suggesting an extragalactic origin (see Paczyński 1995 for a review). The main impedance to progress was the difficulty of localizing bursts to an accuracy high enough to unequivocally associate an individual GRB with some other astrophysical entity. In large measure the localization problem was due to both the transient nature of the phenomena and the fact that the incident direction of gamma-rays is difficult to pinpoint with a single detector; for example, the typical 1 σ uncertainty in the location of a GRB using the Burst and Transient Source Experiment was 4°–8° in radius (Briggs et al. 1999). The Interplanetary Network (IPN; see Cline et al. 1999) localized GRBs by using burst arrival times at several spacecraft throughout the solar system and provided accurate localizations (3 σ localizations of about a few to hundreds times square arcminutes) to ground-based observers; however, the localizations were reported with long time delays (days to months after the GRB).

The crucial breakthrough came in early 1997, shortly following the launch of the *BeppoSAX* satellite (Boella et al. 1997). On-board instruments (Frontera et al. 1997; Jager et al. 1997) were used to rapidly localize the prompt and long-lived hard X-ray emission of the GRB of 1997 February 28 (GRB 970228) to a 3 σ accuracy of $3'$ (radius) and relay the location to ground-based observers in a matter of hours. Fading X-ray (Costa et al. 1997) and optical (van Paradijs et al. 1997) emission, the so-called afterglow, associated with GRB 970228 were discovered. Ground-based observers noted (Metzger et al. 1997b; van Paradijs et al. 1997) a faint nebulosity in the vicinity of the optical transient (OT) afterglow. Subsequent *Hubble Space Telescope* (*HST*) imaging resolved the nebulosity (Sahu et al. 1997) and showed that the morphology was indicative of a distant galaxy (Sahu et al. 1997). Three years later, we now know the redshift of this faint blue galaxy is $z = 0.695$ (Bloom, Djorgovski, & Kulkarni 2001).

[1] Partially based on observations with the NASA/ERA *Hubble Space Telescope*, obtained at the Space Telescope Science Institute, which is operated by the Association of Universities for Research in Astronomy, Inc., under NASA contract NAS 5-26555.

[2] In addition, some of the data presented herein were obtained at the W. M. Keck Observatory, which is operated as a scientific partnership among the California Institute of Technology, the University of California, and the National Aeronautics and Space Administration, and was made possible by the generous financial support of the W. M. Keck Foundation.

The next prompt localization of a GRB yielded the first confirmed distance to the GRB through optical absorption spectroscopy: GRB 970508 occurred from a redshift $z \geq 0.835$ (Metzger et al. 1997a). The first radio afterglow was detected from GRB 970508, which, through observations of scintillation, led to the robust inference of superluminal motion of the GRB ejecta (Frail et al. 1997). These measurements (along with the dozen other redshifts now associated with individual GRBs) have effectively ended the distance scale debate and solidified GRBs as one of the most energetic phenomena known (see Kulkarni et al. 2000; Frail et al. 2001).

The cosmological nature of GRBs now frames our basic understanding of the physics of GRB phenomena.[3] The general energetics are well constrained: given the observed fluences and redshifts, approximately 10^{51}–10^{53} ergs in gamma-ray radiation is released in a matter of a few seconds in every GRB. The GRB variability timescale suggests that this energy is quickly deposited by a "central engine" in a small volume of space (radius of $\sim$300 km) and is essentially optically thick to gamma-ray radiation at early times. This opaque fireball of energy then expands adiabatically and relativistically until the gamma-ray radiation can escape; the emitting surface of the GRB is likely to be 10^{15}–10^{17} cm from the explosion site and probably arises from the interaction of internal shocks initiated by the central engine (e.g., Fenimore, Ramirez-Ruiz, & Wu 1999). Only a small amount of baryonic matter ($\sim 10^{-5}\ M_{\odot}$) can be entrained with the fireball since too much baryonic matter, a condition referred to as the "baryonic loading" problem, would essentially stall the relativistic expansion of the fireball. The transient afterglow phenomenon is thought to be due to synchrotron radiation arising from the interaction of the relativistic ejecta and the ambient medium surrounding the burst site (see van Paradijs, Kouveliotou, & Wijers 2000; Kulkarni et al. 2000; Djorgovski et al. 2002b for reviews). The relativistic nature of the expanding shock (which also gives rise to the GRB) is required to avoid the so-called compactness problem (see Piran 1999) and, as mentioned above, was observationally confirmed with radio scintillation measurements of the afterglow of GRB 970508 (Frail et al. 1997).

While the GRB emission and the afterglow phenomenon are now reasonably well understood, one large outstanding question remains: What makes a gamma-ray burst? Specifically what are the astrophysical objects, the "progenitors," that produce gamma-ray bursts? To date several theoretical considerations appear to implicate the progenitors as stellar-mass systems involving a compact source, probably a black hole (BH). First, the implied (isotropic) energy release in gamma-rays is typically 10^{-3}–10^{-1} times the rest-mass energy of the Sun. The estimated efficiency of conversion of the initial input energy (either Poynting flux or baryonic matter) to gamma-rays ranges from $\sim$1% (e.g., Kumar 1999) to as much as $\sim$60% (e.g., Kobayashi & Sari 2001); therefore, the best-guess estimate of the total energy release is roughly comparable to the rest-mass energy of 1 $M_{\odot}$. Second, the variability timescale (a few milliseconds) observed implies that the energy deposition takes place in a small region of space (radius of $c \times 1$ ms $\approx$ 300 km). Third, the inferred rate of GRB occurrence, about four per day in the universe above current detection thresholds, and the lack of burst repetition (e.g., Hakkila et al. 1998) suggest that GRB events are rare ($\sim 10^{-7}$ yr^{-1} Galaxy^{-1}; Fenimore, Epstein, & Ho 1993; Wijers et al. 1998) and catastrophically destroy the individual progenitors.

The progenitor models that most naturally explain these observables in the GRB phenomena fall in to two broad classes—the coalescence of binary compact stellar remnants and the explosion of a massive star ("collapsar"). An active galactic nucleus (AGN) origin is another possibility; however, the variability timescale still requires the energy source to be a stellar-mass object (Carter 1992; Cheng & Wang 1999). We briefly summarize the popular progenitor models and refer the reader to Fryer, Woosley, & Hartmann (1999) for a more in-depth review. In both the collapsar and the merging remnant class of progenitors a spinning BH is formed. The debris, either from the stellar core of the collapsar or a tidally disrupted neutron star, forms a temporary accretion disk (or "torus"), which then falls into the BH, releasing a fraction of the gravitational potential energy of the matter. In this general picture (see Rees 1999 for a review), the lifetime of the accretion disk accounts for the duration of the GRB, and the light-crossing time of the BH accounts for the variability timescale. The GRB is powered by the energy extracted either from the spin energy of the hole or the from the gravitational energy of the infalling matter.

The coalescing compact binary class (Paczyński 1986; Goodman 1986; Eichler et al. 1989) was favored before the first redshift determination because the existence of coalescence events of double neutron star binaries (NS-NS) was assured; at least a few NS-NS systems in our Galaxy (e.g., PSR 1913+16 and PSR 1534+12) will merge in a Hubble time thanks to the gravitational radiation of the binary orbital angular momentum (see Taylor 1994). Further, the best estimate of the rate of NS-NS coalescence in the universe (e.g., Phinney 1991; Narayan, Paczyński, & Piran 1992) was comparable to an estimate of the GRB rate (Fenimore et al. 1993; Wijers et al. 1998). Recently, stellar evolution models have suggested that black hole–neutron star binaries (BH-NS) may be formed at rates comparable to or even higher than NS-NS binaries (e.g., Bethe & Brown 1998), though no such systems have been observed to date. There are other merging remnant binaries that may form GRBs, notably merging black hole–white dwarf (BH-WD) binaries (Fryer & Woosley 1998) and black hole–helium star (BH-He) binaries (see Fryer et al. 1999).

The collapsar class is composed of rotating massive stars, either isolated or in a binary system, whose iron core subsequently collapses directly to form a black hole (Woosley 1993). To avoid baryon loading the progenitor star should have lost most, if not all, of its extended gas envelope of hydrogen by the time of collapse. The progenitors of collapsars—likely Wolf-Rayet stars—are then closely related to the progenitors of hydrogen-deficient supernova, namely, type Ib/Ic supernovae (see MacFadyen & Woosley 1999). Perhaps one distinguishing difference is that high angular momentum is necessary in collapsars. High angular momentum centrifugally supports a transient torus around the BH, creating a natural timescale for mass-energy injection. The efficiency of energy conversion is also helped around a spinning BH. Further, angular momentum creates

[3] The emergent picture described herein is reserved to the so-called long duration GRBs, those lasting for a duration $\gtrsim$2 s, since no short-duration bursts have yet been well localized on rapid timescales ($\lesssim$few days).

a natural rotation axis along which large density gradients allow for the expanding blast wave to reach relativistic speeds.

How can this large variety of viable GRB progenitors be distinguished? Direct associations with other known astrophysical entities is possible. For massive stars, the energy release from the collapse of the core of the star, just as in supernovae, is sufficient to explode the star itself. This may result in a supernova-like explosion at essentially the same time as a GRB. The first apparent evidence of such a supernova associated with a cosmological GRB came with the discovery of a delayed bright red bump in the afterglow light curve of GRB 980326 (Bloom et al. 1999b). The authors interpreted the phenomena as due to the light-curve peak of a supernova at redshift $z \sim 1$. Later, Reichart (1999) and Galama et al. (2000) found similar red bumps in the afterglow of GRB 970228. Merging remnant progenitor models (e.g., BH-NS and NS-NS systems) have difficulty producing these features in a light curve on such long timescales, and so the supernova interpretation, if true, would be one of the strongest direct clues that GRBs come from massive-star explosions. However, the supernova story is by no means complete. For instance, in only one other GRB (000911) has marginal ($\sim 2\ \sigma$) evidence of a supernova (SN) signature been found (Lazzati et al. 2001); further, many GRBs do not appear to show any evidence of SNe signatures (e.g., Hjorth et al. 2000). Even the "supernova" observations themselves find plausible alternative explanations (such as dust echoes) that do not strictly require a massive-star explosion (Esin & Blandford 2000; Reichart 2001; Waxman & Draine 2000). We note, however, that all other plausible explanations of the observed late-time bumps require high-density environments found most readily in star-forming regions.

Chevalier & Li (2000) emphasize that if a GRB comes from a massive star, then the explosion does not take place in a constant-density medium but in a medium enriched by constant mass loss from the stellar winds. One would expect to see signatures of this wind-stratified medium in the afterglow (e.g., bright sub-millimeter emission at early times, increasing "cooling frequency" with time; see Panaitescu & Kumar 2000; Kulkarni et al. 2000). However, afterglow observations have been inconclusive (Kulkarni et al. 2000), with no unambiguous inference of GRBs in such a medium.

Recent work has begun to focus on the immediate environments of GRBs as a means toward divining the nature of the progenitors. This has come primarily from detections of line features now in five GRB afterglows (e.g., GRB 970508 and GRB 970828; Piro et al. 1999; Yoshida et al. 1999). The most recent and convincing detection so far comes from observations of the afterglow of GRB 991216 (Piro et al. 2000). Individually, the observational significance of the line detections are marginal, but on the whole there appears to be a good case for line-emission features in the afterglow of some GRBs. If so, the inescapable conclusion is that there must exist dense matter in the vicinity of the explosion (e.g., Weth et al. 2000; Vietri et al. 1999; Lazzati, Campana, & Ghisellini 1999), a seeming discordance with the expectations of NS-NS merger models.

We emphasize that even the connection of GRBs to stellar-mass progenitors has yet to be established. The most compelling arguments we have outlined (e.g., temporal variability) rely on theoretical interpretations of the GRB phenomena. Further, direct observational results (SN signatures and transient Fe line emission) are not yet conclusive.

In this paper we examine the observed locations of GRBs with respect to galaxies. We find an unambiguous correlation of GRB locations with the UV light of their hosts, providing strong indirect evidence for the connection of GRBs to stellar-mass progenitors. Beyond this finding, we aim to use the location of GRBs to distinguish between stellar-mass progenitor models. In § 2 we review the expectations of GRB locations from each progenitor model. Then in §§ 3 and 4 we discuss the instruments, techniques, and expected uncertainties involved in constructing a sample of GRB locations about their host galaxies. In § 5 we comment on the data reductions specific to each GRB in our sample. The observed distribution is shown and discussed in § 6 and then statistically compared with the expected offset distribution of leading progenitor models (§ 7). Last, in § 8 we summarize and discuss our findings.

2. LOCATION OF GRBs AS A CLUE TO THEIR ORIGIN

Before the detailed modeling of light curves was used to constrain the nature of supernovae progenitors, the location of supernovae in and around galaxies provided important clues to the nature of the progenitors (e.g., Reaves 1953; Johnson & MacLeod 1963). For instance, only Type Ia supernovae have been found in elliptical galaxies, naturally leading to the idea that the progenitor population can be quite old, whereas the progenitors of Type II and Type Ibc are likely to be closely related to recent star formation (see van Dyk 1992 for review). Further, in late-type galaxies, Type Ibc and Type II supernovae appear to be systematically closer to H II star-forming regions than Type Ia supernovae (e.g., Bartunov, Tsvetkov, & Filimova 1994). This is taken as strong evidence that the progenitors of Type Ibc and Type II SNe are massive stars (see Filippenko 1997).

Since the most massive stars explode soon ($\lesssim 10^7$ yr) after zero-age main sequence (ZAMS), we expect GRBs from collapsars to be observed in galaxies undergoing vigorous star formation (i.e., late-type, irregular, and starburst galaxies). Merging neutron stars on the other hand require a median time to merge of $\sim(2\text{–}10) \times 10^8$ yr since ZAMS (e.g., Phinney 1991; Narayan et al. 1992; Portegies Zwart & Spreeuw 1996; Bloom, Sigurdsson, & Pols 1999d). The instantaneous rate of GRBs from binary mergers, then, is more a function of the integrated (as opposed to instantaneous) star formation rate in its parent galaxy. So if GRBs arise from the death of massive stars we do not expect early-type (i.e., elliptical and S0) host galaxies, whereas GRBs from merging remnants could occur in such galaxies. In principle, because of the significant time from ZAMS to the mergers of NS-NS and BH-NS binaries, such merging remnants should produce GRBs at preferentially *lower* redshift than collapsars and promptly bursting binaries (BH-He). In practice, though, distinguishing the GRB(z) rate from the SFR(z) rate is extremely difficult without tens if not hundreds more GRB redshift measurements (e.g., Bloom et al. 1999d).

More importantly, independent of galaxy type, the locations of GRBs within (or outside) galaxies provide a powerful clue toward distinguishing the progenitor scenarios. Massive stellar explosions occur very near their birth site, likely in active H II star-forming regions, because the time

since ZAMS is so small. BH-He binaries will merge quickly and so are also expected to be located near star-forming regions (Fryer et al. 1999). In stark contrast, NS-NS and NS-BH binaries merge far from their birth site. These stellar remnant progenitors will merge after at least one of the binary members has undergone a supernova. Each supernova is thought to impart a substantial "kick" to the resulting neutron star (see Hansen & Phinney 1997); for those binary systems that survive both supernovae explosions the center of mass of the remnant binary itself will receive a velocity boost on the order of a few hundred kilometers per second (e.g., Brandt & Podsiadlowski 1995). That is, NS-NS or NS-BH binaries will be ejected from their birth site. The gradual angular momentum loss in the binary due to gravitational radiation causes the binary to coalesce (or "merge"), which then leads to a GRB. The exact time until merger ($\sim 10^6$–10^9 yr) depends on the masses of the remnants and binary orbit parameters. Population synthesis models have all shown that roughly one-third to one-half of NS-NS and BH-NS binary mergers will occur beyond 10 kpc in projection from the centers of their hosts (Bloom et al. 1999d; Fryer et al. 1999). The exact distribution of merger sites depends sensitively on the gravitational potential of the host and the (radial) distribution of massive-star birth sites.

How have locations of GRBs within (or outside) galaxies impacted our understanding of the progenitors of GRBs thus far? As mentioned above, the first accurate localization (van Paradijs et al. 1997) of a GRB by way of an optical transient afterglow revealed GRB 970228 to be spatially coincident with a faint galaxy (Sahu et al. 1997; Fruchter et al. 1999c, Fruchter, Thorsett, & Pian 1999b; Bloom et al. 2001). Though the nearby galaxy was faint, van Paradijs et al. (1997) estimated the a posteriori probability of a random location on the sky falling so close to a galaxy by chance to be low. As such, the galaxy was identified as the host of GRB 970228. Sahu et al. (1997) further noted that the OT appeared offset from the center of the galaxy, thereby calling into question an AGN origin. Soon thereafter Bloom et al. (1998a) found, and then Fruchter & Pian (1998) confirmed, that GRB 970508 was localized very near the center of a dwarf galaxy. Given that underluminous dwarf galaxies have a weaker gravitational potential with which to bind merging remnant binaries, both Paczyński (1998) and Bloom et al. (1998a) noted that the excellent spatial coincidence of the GRB with its putative host found an easier explanation with a massive-star progenitor rather than NS-NS binaries.

Once the afterglow fades, one could study in detail its environment (analogous to low-redshift supernovae). Unfortunately, however, the current instrumentation available for GRB observations cannot pinpoint or resolve individual GRB environments on the scale of tens of parsecs unless the GRB occurs at a low redshift ($z \lesssim 0.2$) and the transient afterglow is well localized. At higher redshifts (as for all GRBs localized to date), only the very largest scales of galactic structure can be resolved (e.g., spiral arms), even by *HST*. Therefore, the locations of most individual GRBs do not yield much insight into the nature of the progenitors. Instead, the observed *distribution* of GRBs in and around galaxies must be studied as a whole and then compared with the expectations of the various progenitor models. This is the aim of the present study. As we will demonstrate, while not all GRBs are well localized, the overall distribution of GRB offsets proves to be a robust clue to the nature of the progenitors.

In this paper we present a sample of GRB offset measurements that represents the most comprehensive and uniform set compiled to date. Every GRB location and host galaxy image has been reanalyzed using the most uniform data available. The compilation is complete with well-studied GRBs until 2000 May. Throughout this paper we assume a flat Λ cosmology (e.g., de Bernardis et al. 2000) with $H_0 = 65\ \mathrm{km\ s^{-1}\ Mpc^{-1}}$, $\Omega_M = 0.3$, and $\Lambda_0 = 0.7$.

3. DATA: SELECTION AND REDUCTION

The primary goal of this paper is to measure the offsets of GRBs from their hosts when the necessary data are available. Ideally this could be accomplished using a data set of early-time afterglow and late-time host imaging observed using the same instrument under similar observing conditions. The natural instrument of choice is *HST*, given its exquisite angular resolution and astrometric stability. While most hosts have been observed with *HST* at late times, there are only a handful of early-time *HST* detections of GRB afterglows. On the other hand, early ground-based images of GRB afterglows are copious but late-time seeing-limited images of the hosts give an incomplete view of the host as compared with an *HST* image of the same field. Moreover, ground-based imaging is inherently heterogeneous, taken with different instruments, at different signal-to-noise levels, and through a variety of observing conditions; this generally leads to poorer astrometric accuracy. Bearing these imperfections in mind we have compiled a data set of images that we believe are best suited to find offsets of GRBs from their hosts.

A listing of the data set compilation is given in Table 2. We include every GRB (up to and including GRB 000418) with an accurate radio or optical location and a deep late-time optical image. There is a hierarchy of preference of imaging conditions and instruments that yield the most accurate offsets; we describe the specifics and expected accuracies of the astrometric technique in § 4.

3.1. *Data Set Selection Based on Expected Astrometric Accuracy*

We group the data sets into five different levels ordered by decreasing astrometric accuracy. Levels 1–4 each utilize differential astrometry and level 5 utilizes absolute astrometry relative to the International Coordinate Reference System (ICRS). Specifics of the individual offset measurements are given in § 4. The ideal data set for offset determination is a single *HST* image in which both the transient and the host are well localized (hereafter self-*HST*); so far, only GRB 970228, 990123, and possibly 991216 fall in this category. The next most accurate offset is obtained when both the early- and late-time images are from *HST* and taken at comparable depth with the same filter (hereafter *HST*→*HST*). In addition to the centering errors of the OT and host, such a set inherits the uncertainty in registering the two epochs (e.g., GRB 970508). Next, an early deep image from ground-based (GB) Keck, Palomar 200 inch (P200), or the Very Large Telescope (VLT) in which the OT dominates is paired with a late-time image from *HST* (e.g., GRB 971214, GRB 980703, 991216, and 000418; hereafter GB→*HST*).

Though in the majority of these cases most of the objects detected in the *HST* image are also detected in the Keck image (affording great redundancy in the astrometric mapping solution), object centering of ground-based data is hampered by atmospheric seeing. The next most accurate localizations use ground-based to ground-based imaging to compute offsets (GB→GB). Last, radio localizations compared with optical imaging (RADIO→OPT) provide the least accurate offset determinations. This is due primarily to the current difficulty of mapping an optical image onto an absolute coordinate system (see § 4.5).

3.2. *Imaging Reductions*

3.2.1. *Reductions of HST Imaging*

Most of the *HST* images of GRB afterglows and hosts were acquired using the *Space Telescope Imaging Spectrograph* (STIS; Kimble et al. 1998). STIS imaging undersamples the angular diffraction limit of the telescope, and therefore individual *HST* images essentially do not contain the full possible astrometric information. To produce a final image that is closer to the diffraction limit, interpixel dithering between multiple exposures is often employed. The image reconstruction technique, which also facilitates removal of cosmic rays and corrects for the known optical field distortion, is called "drizzling" and is described in detail in Fruchter & Hook (1997). We use this technique, as implemented using the IRAF[4] package DITHER and DITHERII, to produce our final *HST* images.

We retrieved and reduced every public STIS data set of GRB imaging from the *HST* archive[5] and processed the so-called "on-the-fly calibration" images to produce a final drizzled image. These images are reduced through the standard *HST* pipeline for bias subtraction, flat-fielding, and illumination corrections by using the best calibration data available at the time of archive retrieval. The archive name of the last image and the start time of each *HST* epoch are listed in columns (2) and (3) of Table 1, respectively.

Some *HST* GRB imaging has been taken using the STIS/Longpass filter (F28x50LP) which, based on its effective red wavelength (central wavelength $\lambda_c \approx 7100$ Å), would make for a good comparison with ground-based *R*-band imaging. However, the Longpass filter truncates the full STIS field of view to about 40% and therefore systematically contains fewer objects to tie astrometrically to ground-based images. Therefore, all the *HST* imaging reported herein was taken in (unfiltered) STIS Clear (CCD50) mode. Unlike the Longpass filter, the spectral response of the Clear mode is rather broad (2000–10000 Å). We use the known optical distortion coefficients appropriate to the wavelength of peak sensitivity $\lambda \approx 5850$ Å of this observing mode to produce final images that are essentially linear in angular displacement versus instrumental pixel location.

The original plate scale of most STIS imaging is $0\farcs05077 \pm 0.00007$ pixel^{-1} (Malumuth & Bowers 1997), though there is a possibility that thermal expansion of the instrument could change this scale by a small amount (see Appendix A). The pixel scale of all our final reduced *HST* images is half the original scale, i.e., $0\farcs02539$ pixel^{-1}.

3.2.2. *Reductions of Ground-based Imaging*

Ground-based images are all reduced using the standard practices for bias subtraction, flat-fielding, and, in the case of *I*-band imaging, fringe correction. In constructing a final image we compute the instrumental shift of dithered exposures relative to a fiducial exposure and co-add the exposures after applying the appropriate shift to align each image. All images are visually inspected for cosmic-ray contamination of the transient, host, or astrometric tie stars. Pixels contaminated by cosmic rays are masked and not used in the production of the final image.

4. ASTROMETRIC REDUCTIONS AND ISSUES RELATED TO DATA SET LEVELS

Here we provide a description of the astrometric reduction techniques for both our ground-based and the *HST* images, and issues related to the five levels of astrometry summarized in § 3.1. A discussion of the imaging reductions and astrometry for the individual cases is given in § 5.

4.1. *Level 1: Self-HST* (*Differential*)

An ideal image is one in which the optical transient and the host galaxy are visible in the same imaging epoch with *HST*. This typically implies that the host galaxy is large enough in extent to be well resolved despite the brilliance of the nearby OT. Of course, a later image of the host is always helpful to confirm that the putative afterglow point source does indeed fade. In this case (as with GRB 970228 and GRB 990123) the accuracy of offset determination is limited mostly by the centroiding errors of the host "center" and optical afterglow. Uncertainties in the optical distortion corrections and the resulting plate scale are typically sub-milliarcsecond in size (see Appendix A).

In principle we expect centering techniques to result in centroiding errors (σ_c) on a point source with a signal-to-noise ratio, SN, of $\sigma_c \approx \phi/\mathrm{SN}$ (see Stone 1989), where ϕ is the instrumental FWHM seeing of the final image. Since ϕ is typically $\sim$75 milliarcsecond (mas) we expect approximately milliarcsecond offset accuracies with self-*HST* images.

4.2. *Level 2: HST→HST* (*Differential*)

Here, two separate *HST* epochs are used for the offset determination. The first epoch is taken when the afterglow dominates the light, and the second, when the host dominates. In addition to the centroiding errors, the astrometric accuracy of this level is limited by uncertainty in the registration between the two images.

In general when two images are involved (here and all subsequent levels), we register the two images such that an instrumental position in one image is mapped to the instrumental (or absolute position) in the other image. The registration process is as follows. We determine the noise characteristics of both the initial and final images empirically, using an iterative sigma-clipping algorithm. This noise, along with the gain and effective read noise of the CCD, are used as input to the IRAF CENTER algorithm. In addition we measure the radial profile of several apparent

[4] IRAF is distributed by the National Optical Astronomy Observatories, which are operated by the Association of Universities for Research in Astronomy, Inc., under cooperative agreement with the National Science Foundation.

[5] See http://archive.stsci.edu.

TABLE 1

GRB Host and Astrometry Observing Log

Name (1)	Telescope Instrument Filter (2)	Date (3)	α (J2000.0) (4)	δ (J2000.0) (5)	Exp. (6)	Δt (7)	Level (8)	Refs. (9)
GRB 970228	*HST* STIS O49001040	1997 Sep 4.75	05 01 46.7	+11 46 54	4600	189	Self-*HST*	1, 2
GRB 970508	*HST* STIS O41C01DIM	1997 Jun 2.64	06 53 49.5	+79 16 20	5000	25	*HST*→*HST*	3, 4
	HST STIS O4XB01I9Q	1997 Aug 6.01	...	...	11568	89	...	5
GRB 970828	Keck LRIS *R* band	1998 Jul 19.4	18 08 34.2	+59 18 52	600	325	RADIO→OPT	6, 7
GRB 971214	Keck LRIS *I* band	1997 Dec 16.52	11 56 26.0	+65 12 00	1080	1.5	GB→*HST*	8
	HST STIS O4T301040	1998 Apr 13.27	...	...	11862	119	...	9
GRB 980326	Keck LRIS *R* band	1998 Mar 28.25	08 36 34.3	−18 51 24	240	1.4	GB→GB	10, 11
	Keck LRIS *R* band	1998 Dec 18.50	...	...	2400	267	...	11
	HST STIS O59251ZWQ	2000 Dec 31.80	...	...	7080	1010	...	12
GRB 980329	Keck NIRC *K* band	1998 Apr 2.31	07 02 38.0	+38 50 44	2520	4.15	GB→GB	13, a
	Keck ESI *R* band	2001 Jan 1.41	...	...	6600	1009	...	a
	HST STIS O65K22YXQ	2000 Aug 27.03	...	...	8012	884	...	14
SN 1998bw (GRB 980425?)...	NTT EMMI *I* band	1998 May 4.41	19 35 03.3	−52 50 45	120	8.5	GB→*HST*	15
	HST STIS O65K30B1Q	2000 Jun 11.98	...	...	1185	778	...	16
GRB 980519	P200 COSMIC *R* band	1998 May 20.48	23 22 21.5	+77 15 43	480	1.0	GB→GB→*HST*	17, 18
	Keck LRIS *R* band	1998 Aug 24.50	...	...	2100	97	...	19
	HST STIS O65K41IEQ	2000 Jun 7.24	...	...	8924	750	...	20
GRB 980613	Keck LRIS *R* band	1998 Jun 16.29	10 17 57.6	+71 27 26	600	3.1	GB→GB→*HST*	21, a
	Keck LRIS *R* band	1998 Nov 29.62	...	...	900	169	...	a
	HST STIS O65K51ZZQ	2000 Aug 20.31	...	...	5851	799	...	22
GRB 980703	Keck LRIS *R* band	1998 Jul 6.61	23 59 06.7	+ 08 35 07	600	3.4	GB→*HST*	23
	HST STIS O65K61XTQ	2000 Jun 18.81	...	...	5118	717	...	24
GRB 981226	Keck LRIS *R* band	1999 Jun 21.57	23 29 37.2	−23 55 54	3360	177	RADIO→OPT(GB)→*HST*	25
	HST STIS O65K71AXQ	2000 Jul 3.56	...	...	8265	555	...	26
GRB 990123	*HST* STIS O59601060	1999 Feb 9.12	15 25 30.3	+ 44 45 59	7200	16.7	Self-*HST*	27

TABLE 1—*Continued*

Name (1)	Telescope Instrument Filter (2)	Date (3)	α (J2000.0) (4)	δ (J2000.0) (5)	Exp. (6)	Δt (7)	Level (8)	Refs. (9)
GRB 990308	Keck LRIS *R* band	1999 Jun 19.26	12 23 11.4	+06 44 05	1000	103	GB→GB→*HST*	28
	HST STIS O65K91E6Q	2000 Jun 19.67	...	...	7782	470	...	29
GRB 990506	Keck LRIS *R* band	1999 Jun 11.25	11 54 50.1	−26 40 35	1560	36	RADIO→OPT(GB)→*HST*	30
	HST STIS O65KA1UYQ	2000 Jun 24.55	...	...	7856	415	...	31
GRB 990510	*HST* STIS O59273LCQ	1999 Jun 17.95	13 38 07.7	−80 29 49	7440	39	*HST*→*HST*	32, 33
	HST STIS O59276C7Q	2000 Apr 29.45	...	...	5840	355	...	34
GRB 990705	NTT SOFI *H* band	1999 Jul 5.90	05 09 54.5	−72 07 53	1200	0.23	GB→GB→*HST*	35
	VLT FORS1 *V* band	1999 Jul 10.40	...	...	1800	4.7	...	35
	HST STIS O65KB1G2Q	2000 Jul 26.06	...	...	8792	386	...	36
GRB 990712	*HST* STIS O59262VEQ	1999 Aug 29.50	22 31 53.1	−73 24 28	8160	48	*HST*→*HST*	37, 38
	HST STIS O59274BNQ	2000 Apr 24.21	...	...	3720	287	...	39
GRB 991208	Keck NIRSPEC *K* band	1999 Dec 16.68	16 33 53.5	+46 27 21	1560	8.5	GB→GB→*HST*	40, 41
	Keck ESI *R* band	2000 Apr 4.54	...	...	1260	118	...	a
	HST STIS O59266ODQ	2000 Aug 3.58	...	...	5120	239	...	42
GRB 991216	Keck ESI *R* band	1999 Dec 29.41	05 09 31.2	+11 17 07	600	13	GB→GB→*HST*	43, a
	Keck ESI *R* band	2000 Apr 4.23	...	...	2600	110	...	a
	HST STIS O59272GIQ	2000 Apr 17.71	...	...	9440	123	...	44
GRB 000301C	*HST* STIS O59277P9Q	2000 Mar 6.22	16 20 18.6	+29 26 36	1440	4.8	*HST*→*HST*	45, 46
	HST STIS O59265XYQ	2001 Feb 25.86	...	...	7361	361	...	47
GRB 000418	Keck ESI *R* band	2000 Apr 28.41	12 25 19.3	+20 06 11	300	10	GB→*HST*	48, 49
	HST STIS O59264Y6Q	2000 Jun 4.23	...	...	2500	47	...	50

NOTE.—Col. (2): Telescopes: (*HST*) *Hubble Space Telescope*; (Keck) W. M. Keck 10 m Telescope II, Mauna Kea, Hawaii; (P200) Hale 200 inch telescope at Palomar Observatory, Palomar Mountain, California; (NTT) European Space Agency 3.5 m New Technology Telescope, Chile; (VLT) Very Large Telescope UT-1 ("Antu"); instruments: STIS (Kimble et al. 1998), ESI (Epps & Miller 1998), LRIS (Oke et al. 1995), COSMIC (Kells et al. 1998), NIRSPEC (McLean et al. 1998), SOFI (Finger et al. 1998), FORS1 (Nicklas et al. 1997); filters: all ground-based observations are listed in standard bandpass filters, while the *HST* STIS images (used for astrometry) are all in Clear mode. The last data set of the *HST* visit is listed. Col. (3): Observation dates in Universal Time, corresponding to the start of the last observation in the data set. Col. (4–5): Position (right ascension is in hours, minutes, seconds, and declination is in degrees, arcminutes, and arcseconds) of the GRB. Col. (6): Total exposure time in seconds. Col. (7): Time in days since the trigger time of the GRB. Col. (8): The comment denotes the astrometric level as in § 4. Col. (9): Reference to the first presentation of the given data set. If two references appear on a given line then the first is a reference to the position of the GRB.

REFERENCES.—(a) This paper; (1) van Paradijs et al. 1997; (2) Fruchter et al. 1999c; (3) Frail et al. 1997; (4) Pian et al. 1998; (5) Fruchter & Pian 1998; (6) Groot et al. 1998a; (7) Djorgovski et al. 2001; (8) Kulkarni et al. 1998a; (9) Odewahn et al. 1998; (10) Groot et al. 1998b; (11) Bloom et al. 1999b; (12) Fruchter et al. 2001b; (13) Larkin et al. 1998; (14) Holland 2000b; (15) Galama et al. 1998; (16) Holland et al. 2000c; (17) Jaunsen et al. 1998; (18) Bloom et al. 1998a; (19) Bloom et al. 1998d; (20) Holland et al. 2000b; (21) Hjorth et al. 1998; (22) Holland 2000e; (23) Bloom et al. 1998a; (24) Bloom & Kulkarni 2000b; (25) Frail et al. 1999; (26) Holland et al. 2000d; (27) Bloom et al. 1999c; (28) Schaefer et al. 1999; (29) Holland 2000a; (30) Taylor et al. 2000; (31) Hjorth 2000; (32) Vreeswijk et al. 1999; (33) Fruchter et al. 1999a; (34) Bloom 2000; (35) Masetti et al. 2000; (36) Holland et al. 2000a; (37) Sahu et al. 2000; (38) Fruchter et al. 2000b; (39) Fruchter et al. 2000d; (40) Frail 1999; (41) Bloom et al. 1999a; (42) Fruchter et al. 2000e; (43) Uglesich et al. 1999; (44) Vreeswijk et al. 2000; (45) Fynbo 2000a; (46) Fruchter et al. 2000c; (47) Fruchter & Vreeswijk 2001a; (48) Mirabal, Halpern, & Wagner 2000; (49) Bloom et al. 2000a; (50) Metzger et al. 2000.

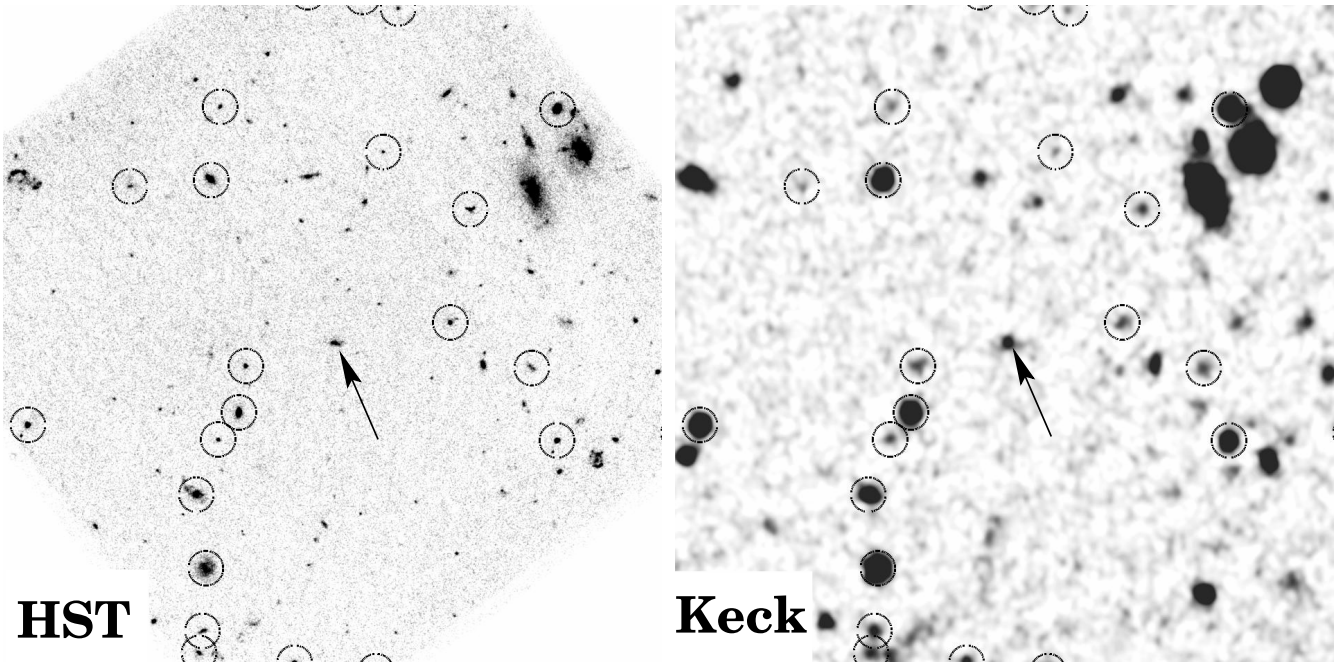

FIG. 1.—Example Keck *R*-band and *HST* STIS Clear images of the field of GRB 981226. Twenty of the 25 astrometric tie objects are circled in both images. As with other Keck images used for astrometry in the present study, most of the faint objects detected in the *HST* images are also detected (albeit with poorer resolution). The optical transient in the Keck image and the host galaxy in the *HST* image are in the center. The field is approximately $50'' \times 50''$, with north up and east to the left.

compact sources in the image and use the derived seeing FWHM (ϕ) as further input to the optimal filtering algorithm technique for centering[6] (OFILTER). For faint stars we use the more stable GAUSSIAN algorithm. Both techniques assume a Gaussian form of the point-spread function which, while not strictly matched to the outer wings of the Keck or *HST* point-spread function (PSF), appears to reasonably approximate the PSF out to the FWHM of the images.

When computing the differential astrometric mappings between two images (such as *HST* and Keck or Keck and the USNO-A2.0 catalog) we use a list of objects common to both epochs, called "tie objects," and compute the astrometric mapping by using the routine IRAF GEOMAP. The polynomial order of the differential fitting we use depends on the number of tie objects. A minimum of three tie objects is required to find the relative rotation, shift, and scale of two images, which leaves only one degree of freedom. The situation is never this bad: in fact, when comparing *HST* images and an earlier *HST* image (or deep Keck image) we typically find 20–30 reasonable tie objects, and therefore we can solve for higher order distortion terms. Figure 1 shows an example Keck and *HST* field of GRB 981226 and the tie objects we use for the mapping. We always reject tie objects that deviate by more than 3 σ from the initial mapping. A full third-order two-dimensional polynomial with cross terms requires 18 parameters, which leaves, typically, $N \approx 30$ degrees of freedom. Assuming such a mapping adequately characterizes the relative distortion, it is reasonable to expect that mapping errors will have an rms error $\sigma \approx 30^{-1/2}\phi/\langle \mathrm{SN} \rangle$, where $\langle \mathrm{SN} \rangle$ is the average signal-to-noise ratio of the tie objects. For example, in drizzled *HST* images $\phi \approx 75$ mas and $\langle \mathrm{SN} \rangle \approx 20$ so that we can expect differential mapping uncertainties at the 1 mas level for *HST*→*HST* mapping. Cross-correlation techniques, such as IRAF CROSSDRIZZLE, can in principle result in even better mapping uncertainties, but, in light of recent work by Anderson & King (1999), we are not confident that the *HST* CCD distortions can be reliably removed at the sub-milliarcsecond level.

4.3. *Level 3: GB→HST (Differential)*

This level of astrometry accounts for the majority of our data set. In addition to inheriting the uncertainties of centroiding errors and astrometric mapping errors described above, we must also consider the effects of differential chromatic refraction (DCR) and optical image distortion in ground-based images. In Appendix A we demonstrate that these effects should not dominate the offset uncertainties. Following the argument above (§ 4.2) the astrometric mapping uncertainties scale linearly with the seeing of ground-based images, which is typically a factor of 10–20 larger than the effective seeing of the *HST* images.

An independent test of the accuracy of the transference of differential astrometry from ground-based images to space-based imaging is illustrated by GRB 990123. In Bloom et al. (1999c) we registered a Palomar 60 inch (P60) image to a Keck image and thence to an *HST* image. The overall statistical uncertainty introduced by this process (see Appendix B for a derivation) is $\sigma_r = 107$ mas (note that in the original paper we mistakenly overstated this error as 180 mas uncertainty). The position we inferred was 90 mas from a bright point source in the *HST* image. This source was later seen to fade in subsequent *HST* imaging, and so our identification of the source as the afterglow from P60→Keck→*HST* astrometry was vindicated. Since the P60→Keck differential mapping accounted for approximately half the error (due to

[6] See L. Davis, http://iraf.noao.edu/iraf/ftp/iraf/docs/apspec.ps.Z.

optical field distortion and unfavorable seeing in P60), we consider ~100 mas uncertainty in Keck→*HST* mapping a reasonable upper limit to the expected uncertainty from other cases. In practice, we achieved rms accuracies of 40–70 mas (see Table 2).

4.4. *Level 4: GB→GB (Differential)*

This level contains the same error contributions as in GB→*HST* level, but in general the uncertainties are larger since the centroiding uncertainties are large in both epochs. The offsets are computed in terms of pixels in late-time image. Just as with the previous levels with *HST*, we assume an average plate scale to convert the offset to units of arcseconds. For the Low Resolution Imaging Spectrometer (LRIS; Oke et al. 1995) and Echellete Spectrograph Imager (Epps & Miller 1998) imaging we assume a plate scale of $0\farcs212$ pixel^{-1} and $0\farcs153$ pixel^{-1}, respectively. We have found that these plate scales are stable over time to better than a few percent; consequently, the errors introduced by any deviations from these assumed plate scales are negligible.

4.5. *Level 5: RADIO→OPT (Absolute)*

Unfortunately, the accuracy of absolute offset determination is (currently) hampered by systematic errors in astrometrically mapping deep optical–infrared imaging to the ICRS. Only bright stars ($V \lesssim 9$ mag) have absolute localizations measured on the milliarcsecond level, thanks to astrometric satellite missions such as *Hipparcos*. The density of *Hipparcos* stars is a few per square degree, so the probability of having at least two such stars on a typical CCD frame is low. Instead, optical astrometric mapping to the ICRS currently utilizes ICRS positions of stars from the USNO-A2.0 Catalog, determined from scanned photographic plates (Monet 1998). Even if all statistical errors of positions are suppressed, an astrometric plate solution can do no better than inherit a systematic 1 σ uncertainty of 250 mas in the absolute position of any object on the sky ($\sigma_\alpha = 0\farcs18$ and $\sigma_\delta = 0\farcs17$; Deutsch 1999). By contrast, very long baseline array (VLBA) positions of GRB radio afterglow have achieved sub-milliarcsecond absolute positional uncertainties relative to the ICRS (Taylor et al. 1999). So, until optical systematic errors are beaten down and/or sensitivities at radio wavelengths are greatly improved (so as to directly detect the host galaxy at radio wavelengths), the absolute offset astrometry can achieve 1 σ accuracies no better than ~300 mas (≈2.5 kpc at $z = 1$). In fact, one GRB host (GRB 980703) has been detected at radio wavelengths (Berger, Kulkarni, & Frail 2001), with the subsequent offset measurement accuracy improving by a factor of ~3 over the optical measurement determined herein (§ 5.10).

There are three GRBs in our sample for which absolute astrometry (level 5) is employed. In computing the location of the optical transient relative to the ICRS we typically use 20–40 USNO A2.0 astrometric tie stars in common with Keck or Palomar images. We then use IRAF CCMAP to compute the mapping of instrumental position (x, y) to the world coordinate system (α, δ).

5. INDIVIDUAL OFFSETS AND HOSTS

Below we highlight the specific reductions for each offset, the results of which are summarized in Table 2. In total there are 21 bursts until 2000 May that have been reliably localized at the arcsecond level and one burst with an uncertain association with the nearby SN 1998bw (GRB 980425). In our analysis we do not include GRB 000210 (Stornelli et al. 2000) because of lack of late-time imaging data. Thereby, the present study includes 20 "cosmological" GRBs plus the nearby SN 1998bw/GRB 980425. Offset measurements should be possible for the recent bursts GRB 000630 (Hurley 2000), 000911 (Hurley et al. 2000a), 000926 (Hurley et al. 2000b) and 010222 (Piro 2001).

To look for the hosts, we generally image each GRB field roughly a few months to a year after the burst with Keck. Typically these observations reach a limiting magnitude of $R \approx 24$–26 mag, depending on the specifics of the observing conditions. If an object is detected within ~1″ from the afterglow position and has a brightness significantly above the extrapolated afterglow flux at the time of observation, this source is deemed the host (most GRB hosts are readily identified in such imaging). If no object is detected, we endeavor to obtain significantly deeper images of the field. Typically these faint host searches require 1–3 hr of Keck (or VLT) imaging to reach limiting magnitudes at the $R \approx 27$ mag level. If no object is detected at the location of the afterglow, *HST* imaging is required and the host search is extended to limiting magnitudes of $R \approx 28$–29 mag. Only three hosts in our sample (GRB 990510, 000301C, and 980326) were first found using *HST* after an exhaustive search from the ground.

Note that the assignment of a certain observed galaxy as the host of a GRB is, to some extent, a subjective process. We address the question of whether our assignments are "correct" in § 6.1, where we demonstrate on statistical grounds that at most only a few assignments in the sample of 20 could be spurious. In § 6.1 we also discuss how absorption and emission redshifts help strengthen the physical connection of GRBs to their assigned hosts.

Irrespective of whether individual assignments of hosts are correct, we uniformly assign the nearest (in angular distance) detected galaxy as the host. In practice this means that the nearest object (i.e., galaxy) brighter than $R \simeq 25$–26 mag detected in Keck imaging is assigned as the host. In almost all cases, there is a detected galaxy within ~1″ of the transient position. For the few cases in which there is no object within ~1″, deeper *HST* imaging *always* reveals a faint galaxy within ~1″. In most cases, the estimated probability that we have assigned the "wrong" host is small (see § 6.1). After assigning the host, the center of the host is then determined, except in a few cases, as the centroid near the brightest component of the host system. In a few cases in which there is evidence for significant low surface brightness emission (e.g., GRB 980519) or the host center is ambiguous we assign the approximate geometric center as the host center.

A summary of our offset results is presented in Table 2. Since all our final images of the host galaxies are rotated to the cardinal orientation before starting the astrometric mapping process, these uncertainties are also directly proportional to the uncertainties in α and δ. It is important to note, however, that the projected radial offset is a positive-definite number and the probability distribution is not Gaussian. Thereby, the associated error (σ_r) in offset measurements does not necessarily yield a 68% confidence region for the offset (see Appendix B) but is, clearly, indicative of the precision of the offset measurement.

TABLE 2

MEASURED ANGULAR OFFSETS AND PHYSICAL PROJECTIONS

Name (1)	X_0 East (arcsec) (2)	Y_0 North (arcsec) (3)	R_0 (arcsec) (4)	R_0/σ_{R_0} (5)	z (6)	D_θ (kpc arcsec^{-1}) (7)	X_0 (proj) (kpc) (8)	Y_0 (proj) (kpc) (9)	R_0 (proj) (kpc) (10)
GRB 970228	-0.033 ± 0.034	-0.424 ± 0.034	0.426 ± 0.034	12.59	0.695	7.673	-0.251 ± 0.259	-3.256 ± 0.259	3.266 ± 0.259
GRB 970508	0.011 ± 0.011	0.001 ± 0.012	0.011 ± 0.011	1.003	0.835	8.201	0.090 ± 0.090	0.008 ± 0.098	0.091 ± 0.090
GRB 970828	0.440 ± 0.516	0.177 ± 0.447	0.474 ± 0.507	0.936	0.958	8.534	3.755 ± 4.403	1.510 ± 3.815	4.047 ± 4.326
GRB 971214	0.120 ± 0.070	-0.070 ± 0.070	0.139 ± 0.070	1.985	3.418	7.952	0.954 ± 0.557	-0.557 ± 0.557	1.105 ± 0.557
GRB 980326	0.125 ± 0.068	-0.037 ± 0.062	0.130 ± 0.068	1.930	$\sim$1	...	...	...	...
GRB 980329	-0.037 ± 0.049	-0.003 ± 0.061	0.037 ± 0.049	0.756	$\lesssim$3.5	...	...	...	...
GRB 980425	-10.55 ± 0.052	-6.798 ± 0.052	12.55 ± 0.052	241.4	0.008	0.186	-1.964 ± 0.010	-1.265 ± 0.010	2.337 ± 0.010
GRB 980519	-0.050 ± 0.130	1.100 ± 0.100	1.101 ± 0.100	11.00	...	...	...	...	...
GRB 980613	0.039 ± 0.052	0.080 ± 0.080	0.089 ± 0.076	1.174	1.096	8.796	0.344 ± 0.454	0.703 ± 0.707	0.782 ± 0.666
GRB 980703[a]	-0.054 ± 0.055	0.098 ± 0.065	0.112 ± 0.063	1.788	0.966	8.553	-0.460 ± 0.469	0.842 ± 0.555	0.959 ± 0.536
GRB 981226	0.616 ± 0.361	0.426 ± 0.246	0.749 ± 0.328	2.282	...	...	...	...	...
GRB 990123	-0.192 ± 0.003	-0.641 ± 0.003	0.669 ± 0.003	223.0	1.600	9.124	-1.752 ± 0.027	-5.849 ± 0.027	6.105 ± 0.027
GRB 990308	-0.328 ± 0.357	-0.989 ± 0.357	1.042 ± 0.357	2.919	...	...	...	...	...
GRB 990506	-0.246 ± 0.432	0.166 ± 0.513	0.297 ± 0.459	0.647	1.310	9.030	-2.221 ± 3.901	1.499 ± 4.632	2.680 ± 4.144
GRB 990510	-0.064 ± 0.009	0.015 ± 0.012	0.066 ± 0.009	7.160	1.619	9.124	-0.584 ± 0.082	0.137 ± 0.109	0.600 ± 0.084
GRB 990705	-0.865 ± 0.046	0.109 ± 0.049	0.872 ± 0.046	18.86	0.840	8.217	-7.109 ± 0.380	0.896 ± 0.399	7.165 ± 0.380
GRB 990712	-0.035 ± 0.080	0.035 ± 0.080	0.049 ± 0.080	0.619	0.434	6.072	-0.213 ± 0.486	0.213 ± 0.486	0.301 ± 0.486
GRB 991208	0.071 ± 0.102	0.183 ± 0.096	0.196 ± 0.097	2.016	0.706	7.720	0.548 ± 0.789	1.410 ± 0.744	1.513 ± 0.750
GRB 991216	0.211 ± 0.029	0.290 ± 0.034	0.359 ± 0.032	11.08	1.020	8.664	1.828 ± 0.251	2.513 ± 0.295	3.107 ± 0.280
GRB 000301C...	-0.025 ± 0.014	-0.065 ± 0.005	0.069 ± 0.007	9.821	2.030	9.000	-0.222 ± 0.130	-0.581 ± 0.046	0.622 ± 0.063
GRB 000418	-0.019 ± 0.066	0.012 ± 0.058	0.023 ± 0.064	0.358	1.118	8.829	-0.170 ± 0.584	0.109 ± 0.514	0.202 ± 0.564

NOTE.—The observed offsets (X_0, Y_0) and associated Gaussian uncertainties include all statistical errors from the astrometric mapping and OT + host centroid measurements. The observed offset, $R_0 = (X^2_0 + Y^2_0)^{1/2}$, and σ_{R_0} (constructed analogously to eq. [B4]) are given in col. [4]. Note that $R_0 - \sigma_{R_0} \leq R \leq R_0 + \sigma_{R_0}$ is not necessarily the 68% percent confidence region of the true offset since the probability distribution is not Gaussian (see eq. [B3]). The term R_0/σ_{R_0} in col. [5] indicates how well the offset from the host center is determined. In general, we consider the GRB to be significantly displaced from the host center if $R_0/\sigma_{R_0} \gtrsim 5$. In col. [6], z is the measured redshift of the host galaxy and/or aborption redshift of the GRB complied from the literature (see Kulkarni et al. 2000). In col. [7], D_θ is the conversion of angular displacement in arcseconds to projected physical distance.

[a] Using radio detections of the host and afterglow, Berger et al. 2001 find a more accurate offset of $X_0 = -0.032 \pm 0.015$ and $Y_0 = 0.025 \pm 0.015$ ($R_0 = 0.040 \pm 0.015$), consistent with our optical results; see § 5.10.

TABLE 3
HOST DETECTION PROBABILITIES AND HOST NORMALIZED OFFSETS

Name (1)	$R_{c,\mathrm{host}}$ (mag) (2)	A_{R_c} (mag) (3)	P_{ch} (4)	R_{half} (obs) (arcsec) (5)	R_{half} (calc) (arcsec) (6)	r_e (kpc) (7)	r_0 (8)
GRB 970228	24.60 ± 0.20	0.630	0.00935	0.345 ± 0.030	0.316 ± 0.095	1.6	1.233 ± 0.146
GRB 970508	24.99 ± 0.17	0.130	0.00090	0.089 ± 0.026	0.300 ± 0.090	0.4	0.124 ± 0.129
GRB 970828	25.10 ± 0.30	0.100	0.07037		0.296 ± 0.089	1.5	1.603 ± 1.780
GRB 971214	25.65 ± 0.30	0.040	0.01119	0.226 ± 0.031	0.273 ± 0.082	1.1	0.615 ± 0.321
GRB 980326	28.70 ± 0.30	0.210	0.01878	0.043 ± 0.028	0.116 ± 0.035	0.2	3.023 ± 2.532
GRB 980329	27.80 ± 0.30	0.190	0.05493	0.245 ± 0.033	0.168 ± 0.050	1.3	0.152 ± 0.202
GRB 980425	14.11 ± 0.05	0.170	0.00988	18.700 ± 0.025	...	2.1	0.671 ± 0.003
GRB 980519	25.50 ± 0.30	0.690	0.05213	0.434 ± 0.041	0.279 ± 0.084	2.2	2.540 ± 0.332
GRB 980613	23.58 ± 0.10	0.230	0.00189	0.227 ± 0.031	0.352 ± 0.106	1.2	0.392 ± 0.338
GRB 980703	22.30 ± 0.08	0.150	0.00045	0.169 ± 0.026	0.392 ± 0.117	0.9	0.663 ± 0.385
GRB 981226	24.30 ± 0.01	0.060	0.01766	0.336 ± 0.030	0.327 ± 0.098	1.7	2.227 ± 0.996
GRB 990123	23.90 ± 0.10	0.040	0.01418	0.400 ± 0.028	0.341 ± 0.102	2.2	1.673 ± 0.117
GRB 990308	28.00 ± 0.50	0.070	0.31659	0.213 ± 0.028	0.156 ± 0.047	1.1	4.887 ± 1.776
GRB 990506	24.80 ± 0.30	0.180	0.04365	0.090 ± 0.027	0.308 ± 0.092	0.5	3.297 ± 5.196
GRB 990510	27.10 ± 0.30	0.530	0.01218	0.167 ± 0.041	0.205 ± 0.061	0.9	0.393 ± 0.111
GRB 990705	22.00 ± 0.10	0.334[a]	0.01460	1.151 ± 0.030	0.400 ± 0.120	5.7	0.758 ± 0.045
GRB 990712	21.90 ± 0.15	0.080	0.00088	0.282 ± 0.026	0.403 ± 0.121	1.0	0.175 ± 0.284
GRB 991208	24.20 ± 0.20	0.040	0.00140	0.048 ± 0.026	0.330 ± 0.099	0.2	4.083 ± 2.994
GRB 991216	25.30 ± 0.20	1.640	0.00860	0.400 ± 0.043	0.288 ± 0.086	2.1	0.898 ± 0.127
GRB 000301C...	28.00 ± 0.30	0.130	0.00629	0.066 ± 0.028	0.156 ± 0.047	0.4	1.054 ± 0.462
GRB 000418	23.80 ± 0.20	0.080	0.00044	0.096 ± 0.027	0.345 ± 0.103	0.5	0.239 ± 0.670

NOTE.—Col. (2): Dereddened host magnitude as referenced in Pian 2002, Djorgovski et al. 2002b, and Sokolov et al. 2001. Col. (3): Estimated extinction in the direction of the GRB host galaxy (Pian 2002). Col. (4): Estimated probability that the assigned host is a chance superposition and not physically related to the GRB (following § 6.1). The half-light radii R_{half} are observed from *HST* imaging (col. [5]) or calculated using the magnitude-radius empirical relationship (col. [6]; see text). For *HST* imaging, uncertainty is taken as the sum of the statistical error and estimated systematic error (0.″025, which is approximately the size of one deconvolved pixel). Otherwise, the uncertainty is taken as 30% of the calculated radius (col. [6]). Col. (7): Estimated host disk scale length. The host-normalized offset $r_0 = R_0/R_{\mathrm{half}}$ given in col. (8) is derived (if possible) from the observed half-light radius or the calculated half-light radius (otherwise). The error on r_0 is σ_r from equation (B4). Note that $r_0 - \sigma_r \leq r \leq r_0 + \sigma_r$ is not necessarily the 68% confidence region of the true offset since the probability distribution is not Gaussian.

[a] Since the GRB position pierces through the Large Magallanic Cloud (Djorgovski et al. 1999), we have added 0.13 mag extinction to the Galactic extinction quoted in Pian 2002. This assumes an average extinction through the LMC of $E(B-V) = 0.05$ (Dutra et al. 2001).

Once the offsets are determined from the final images, we then measure the half-light radii of the host galaxies. For extended hosts, the value of the half-light radius may be obtained directly from aperature curve-of-growth analysis. However, for compact hosts, the instrumental resolution systematically spreads the host flux over a larger area and biases the measurement of the half-light radius to larger values. We attempt to correct for this effect (for all hosts, not just compact hosts) by deconvolving the images with IRAF SCLEAN using an average STIS Clear PSF derived from 10 stars in the final *HST* image of the GRB 990705 field (which were obtained through low Galactic latitude). We then fit curve-of-growth photometry about the host centers and determine the radius at which half the detected light was within such radius. These values, along with associated errors, are presented in Table 3. We tested that the PSFs derived at differing roll angles and epochs had little impact on the determined value of the half-light radius.

5.1. *GRB 970228*

The morphology and offset derivation have been discussed extensively in Bloom et al. (2001), and we briefly summarize the results. In the *HST* STIS image (Fig. 2), the host appears to be essentially a face-on late-type blue dwarf galaxy. At the center is an apparent nucleus manifested as a 6 σ peak north of the transient. There is also an indication of armlike structure extending toward the transient.

This image represents the ideal for astrometric purposes (level 1): both the transient and the host "center" are well localizable in the same high-resolution image. The transient appears outside the half-light radius of the galaxy.

5.2. *GRB 970508*

The host is a compact, elongated and blue galaxy (Bloom et al. 1998a) and is likely undergoing a starburst phase. The optical transient was well detected in the early-time *HST* image (Pian et al. 1998), and the host was well detected (Fig. 2) in the late-time image (Fruchter & Pian 1998). We masked out a $2'' \times 2''$ region around the OT plus host and cross-correlated the two final images using the IRAF CROSSDRIZZLE routine. We used the IRAF SHIFTFIND routine on the correlation image to find the systematic shift between the two epochs. The resulting uncertainty in the shift was quite small, $\sigma = 0.013$, 0.011 pixel in the x and y directions. We also found 37 compact objects common to both images and performed an astrometric mapping in the usual manner. We find $\sigma = 0.344$, 0.354 pixel in the x and y directions. We centered the OT and the host in the normal manner by using the IRAF ELLIPSE task.

The resulting offset is given in Table 2, in which we use the more conservative astrometric mapping uncertainties from using the tie objects, rather than the CROSSDRIZZLE routine. As first noted in Bloom et al. (1998a; Keck imaging) and then in Fruchter & Pian (1998; *HST* imaging), the OT was remarkably close to the apparent center of the host galaxy. The P200→Keck astrometry from Bloom et al. (1998a) produced an rms astrometric uncertainty of 121 mas, compared with an rms uncertainty of 11 mas from *HST*→*HST* astrometry. The largest source of uncertainty from the *HST*→*HST* is the centroid position of the host galaxy.

5.3. *GRB 970828*

The host is identified as the middle galaxy in an apparent three-component system. We discuss the host properties and the astrometry (RADIO→OPT) in more detail in Djorgovski et al. (2001). The total uncertainty in the radio-to-Keck tie is 506 mas (α) and 376 mas (δ).

5.4. *GRB 971214*

By all accounts, the host appears to be a typical L_* galaxy at redshift $z = 3.42$. The Keck→*HST* astrometry is discussed in detail in Odewahn et al. (1998). The offset uncertainty found was $\sigma_r = 70$ mas. The GRB appears located to the east of the host galaxy center but consistent with the east-west extension of the host (see Fig. 2).

5.5. *GRB 980326*

No spectroscopic redshift for this burst was found. However, based on the light curve and the SN hypothesis, the presumed redshift is $z \sim 1$ (see Bloom et al. 1999b). Bloom et al. (1999b) reported that no galaxy was found at the position of the optical transient down to a 3 σ limiting magnitude of $R \approx 27.3$ mag. Given the close spatial connection of other GRBs with galaxies, we posited that a deeper integration would reveal a nearby host. Indeed, Fruchter, Vreeswijk, & Nugent (2001b) recently reported the detection with *HST* STIS imaging of a very faint ($V = 29.25 \pm 0.25$ mag) galaxy within 25 mas of the OT position.

For astrometry we used an *R*-band image from 1998 April 27 when the OT was bright and found the position of the OT on our deep *R*-band image from 1998 December 18. In this deep *R*-band image we found 34 objects in common with the *HST* STIS drizzled image. We confirm the presence of this faint and compact source near the OT position though our astrometry places the OT at a distance of 130 mas ($\sigma_r = 68$ mas).

The galaxy and OT position are shown in Figure 2. The low-level flux to the southeast corner of the image is a rem-

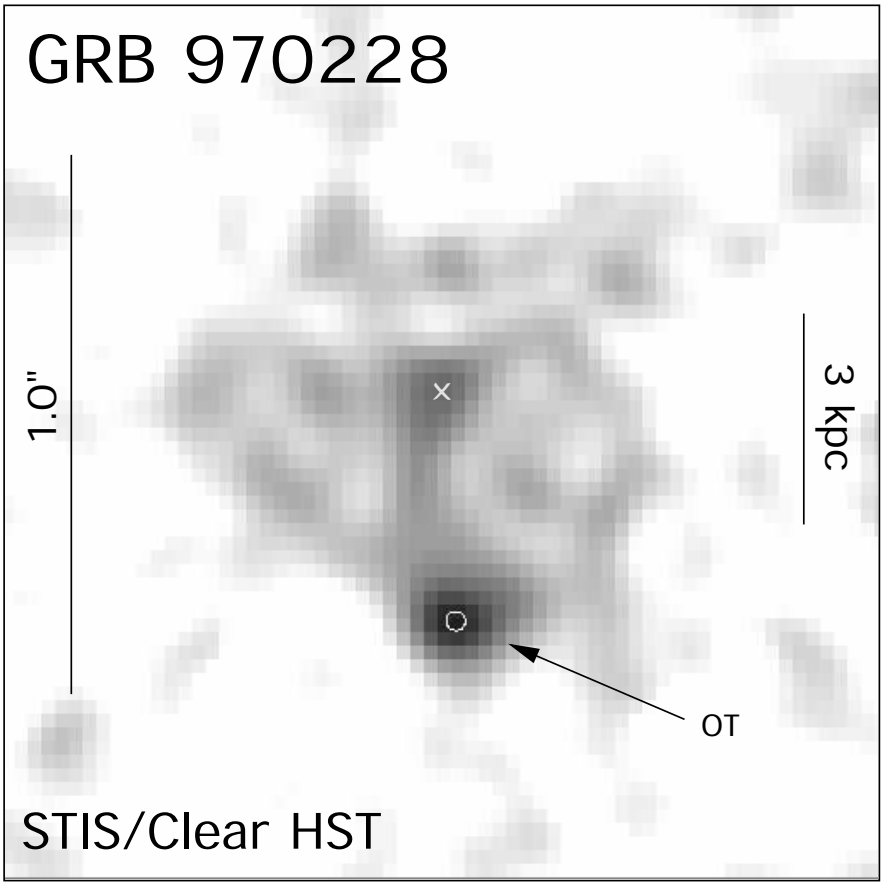

FIG. 2*a*

FIG. 2.—Location of individual GRBs about their host galaxies. The ellipse in each frame represents the 3 σ error contour for the location of the GRB as found in § 5 and in Table 2. The angular scale of each image is different and noted on the left. The scale and stretch were chosen to best show both the detailed morphology of the host galaxy and the spatial relationship of the GRB and the host. The GRB afterglow is still visible in some of the images (GRB 970228 and GRB 991216). In GRB 980425, the location of the associated supernova is noted with an arrow. In all cases in which a redshift is available for the host or GRB afterglow we also provide a physical scale of the region on the right of each image. For all images, north is up and east is to the left.

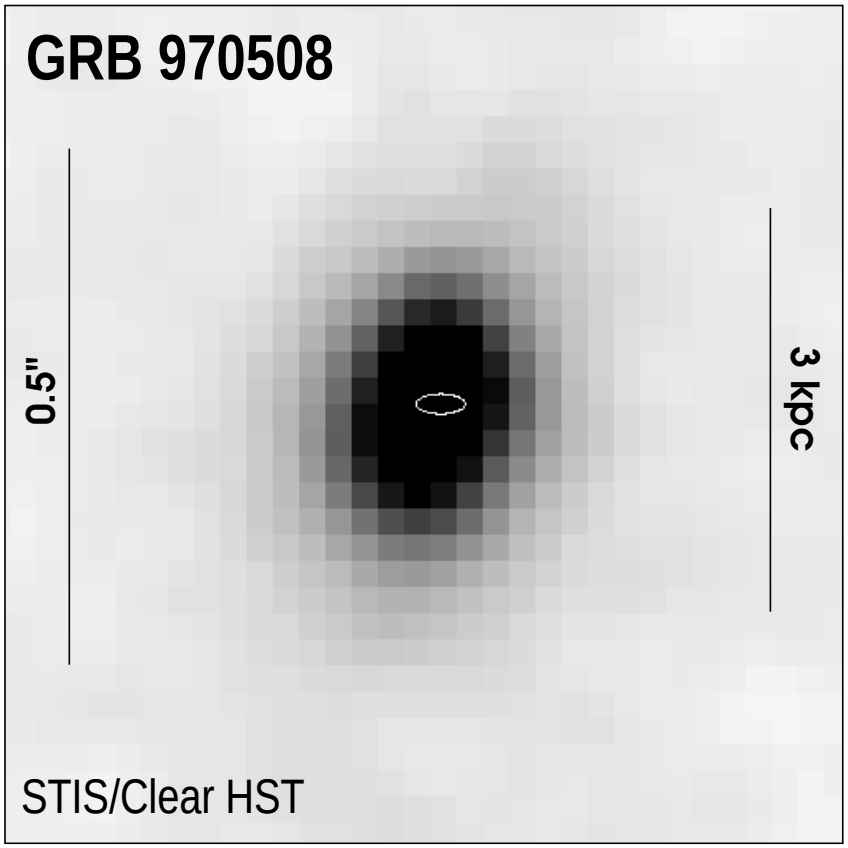
GRB 970508
0.5"
3 kpc
STIS/Clear HST

FIG. 2*b*

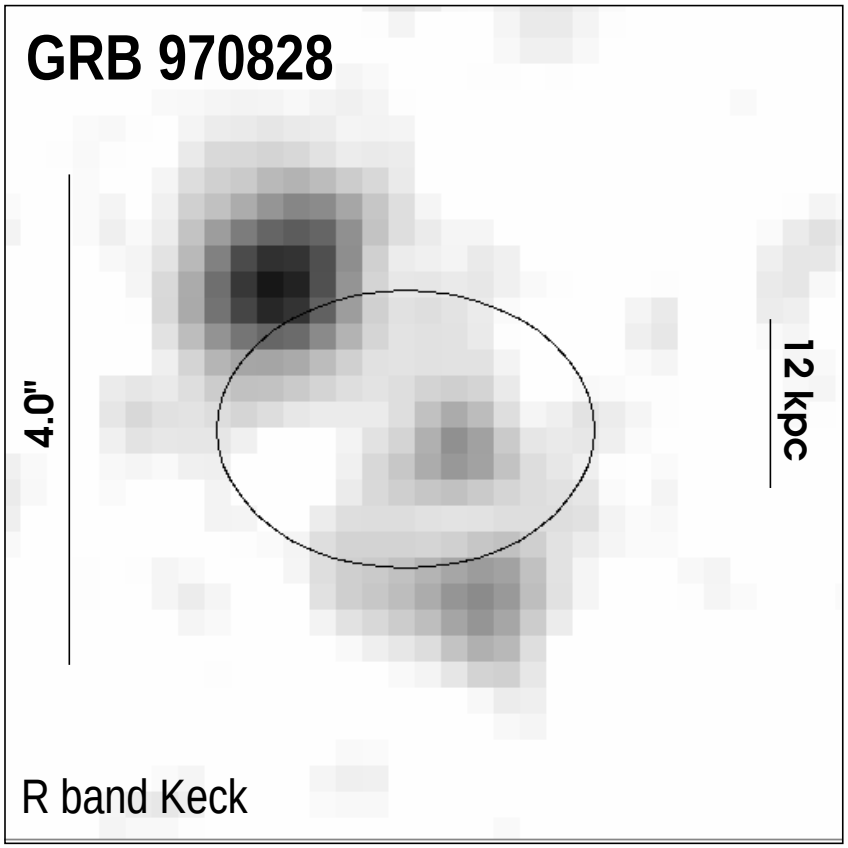
GRB 970828
4.0"
12 kpc
R band Keck

FIG. 2*c*

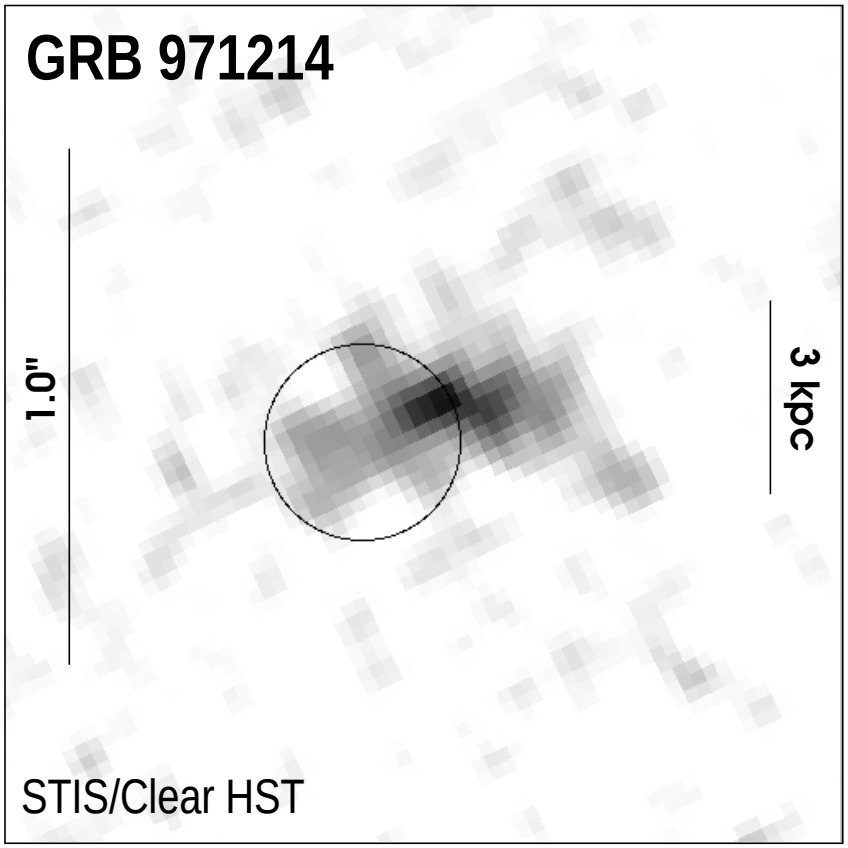
GRB 971214
1.0"
3 kpc
STIS/Clear HST

FIG. 2*d*

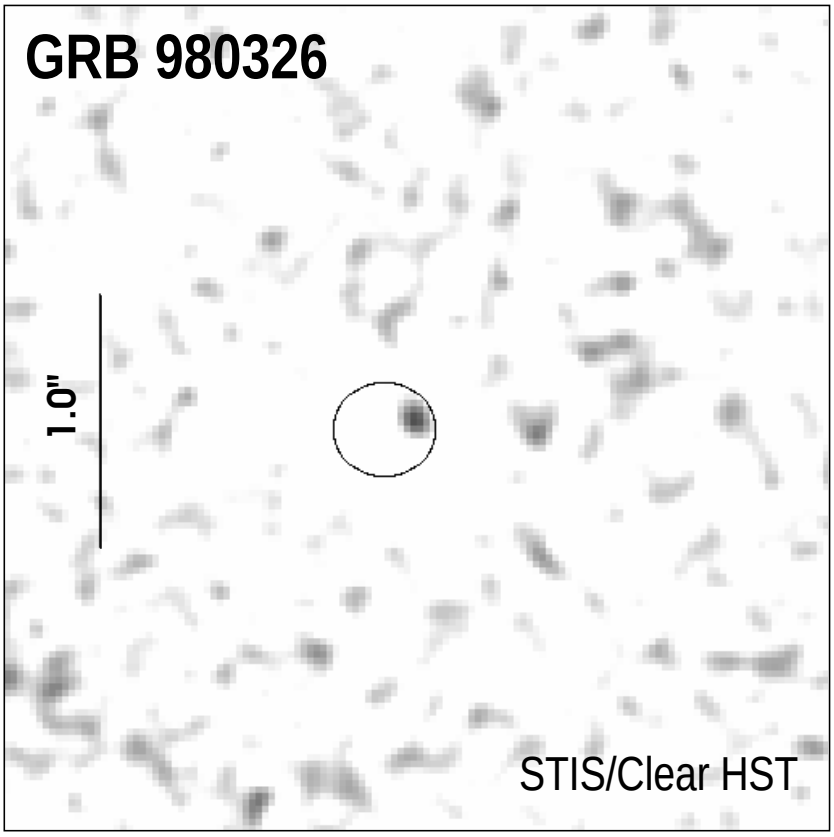
GRB 980326
1.0"
STIS/Clear HST

FIG. 2*e*

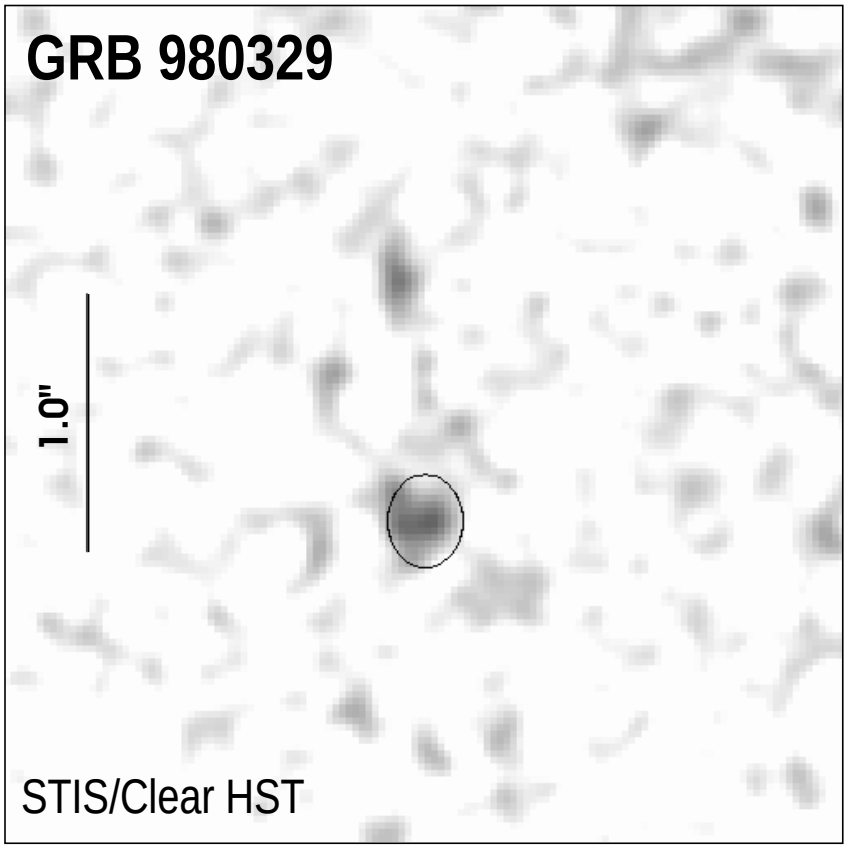
GRB 980329
1.0"
STIS/Clear HST

FIG. 2*f*

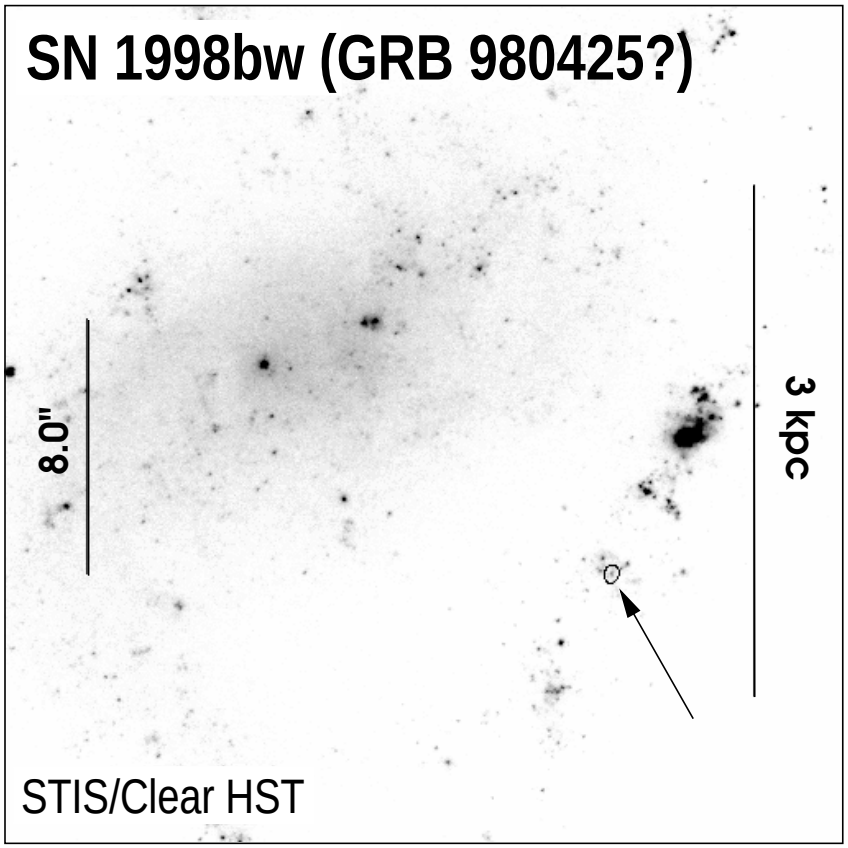
SN 1998bw (GRB 980425?)
8.0"
3 kpc
STIS/Clear HST

FIG. 2*g*

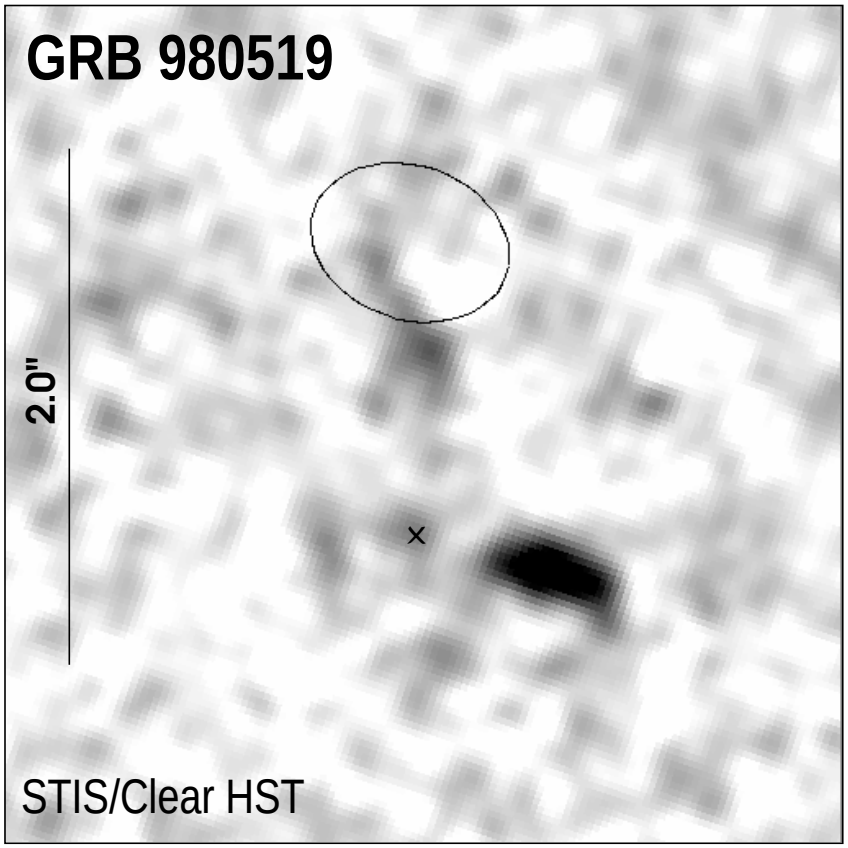
GRB 980519
2.0"
STIS/Clear HST

FIG. 2*h*

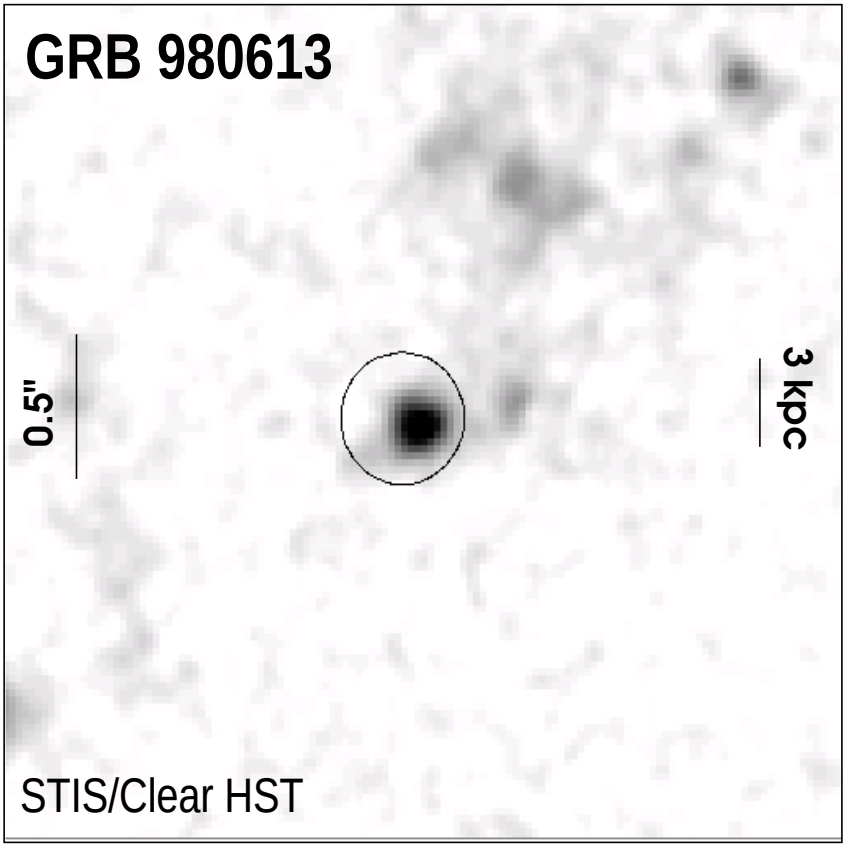
GRB 980613
0.5"
3 kpc
STIS/Clear HST

FIG. 2*i*

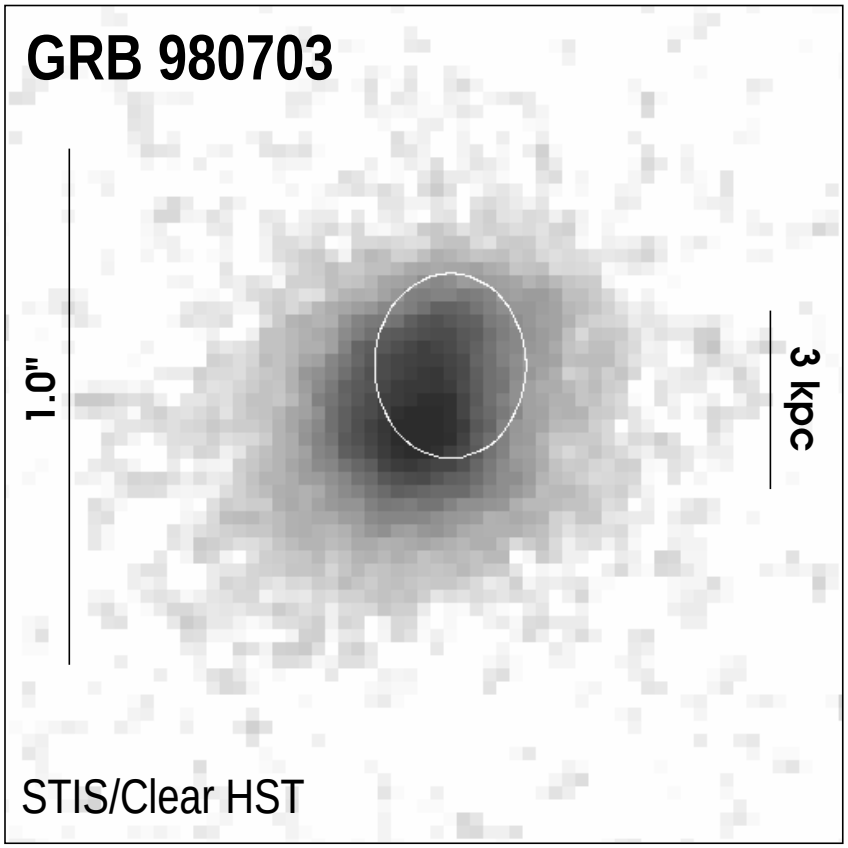
GRB 980703
1.0"
3 kpc
STIS/Clear HST

FIG. 2*j*

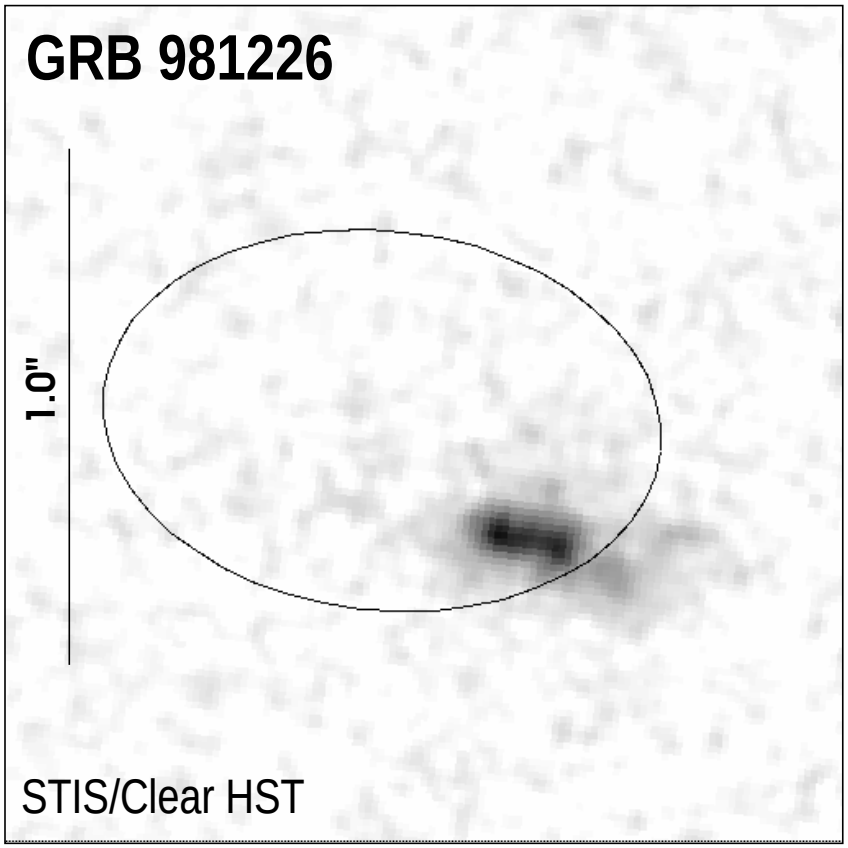
GRB 981226
1.0"
STIS/Clear HST

FIG. 2*k*

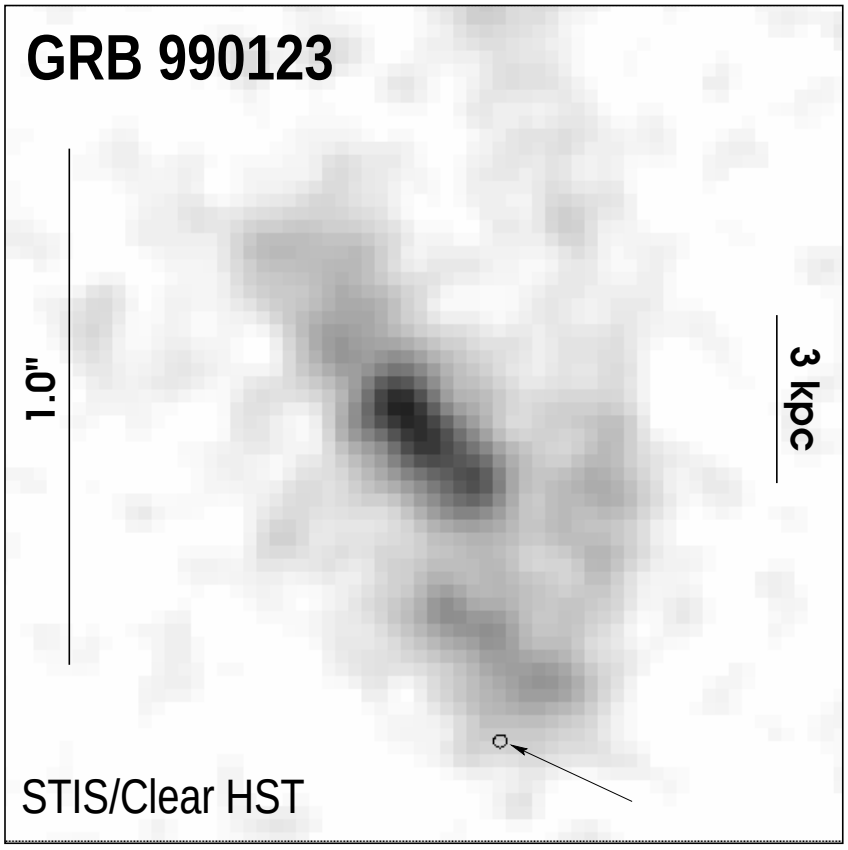
GRB 990123
1.0"
3 kpc
STIS/Clear HST

FIG. 2*l*

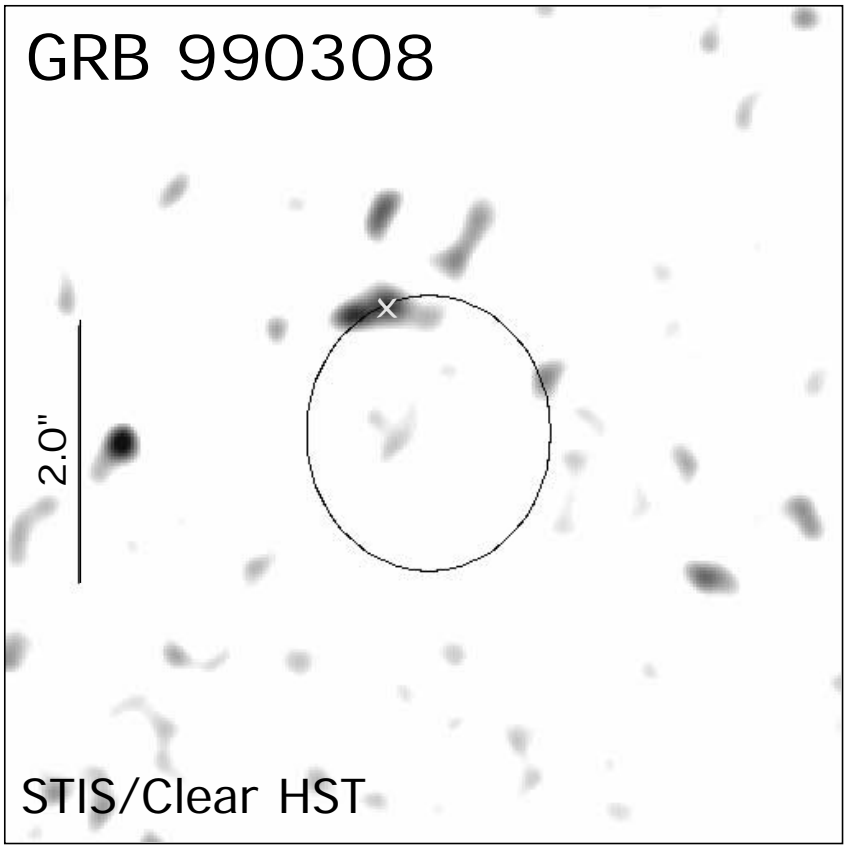
GRB 990308
2.0"
STIS/Clear HST

FIG. 2*m*

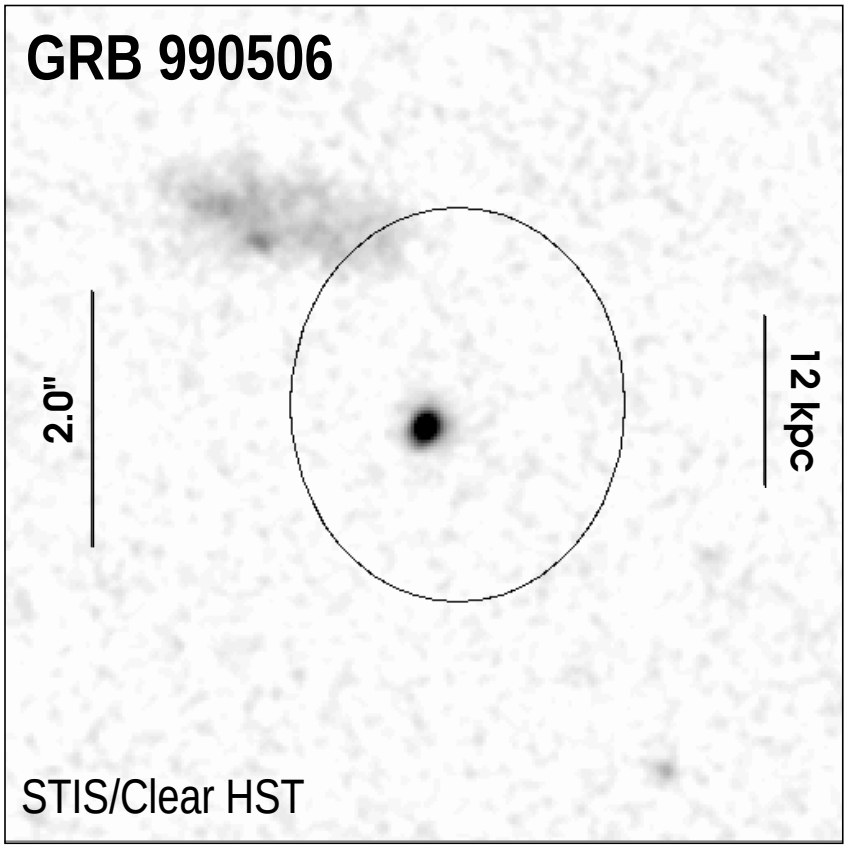
GRB 990506
2.0"
12 kpc
STIS/Clear HST

FIG. 2*n*

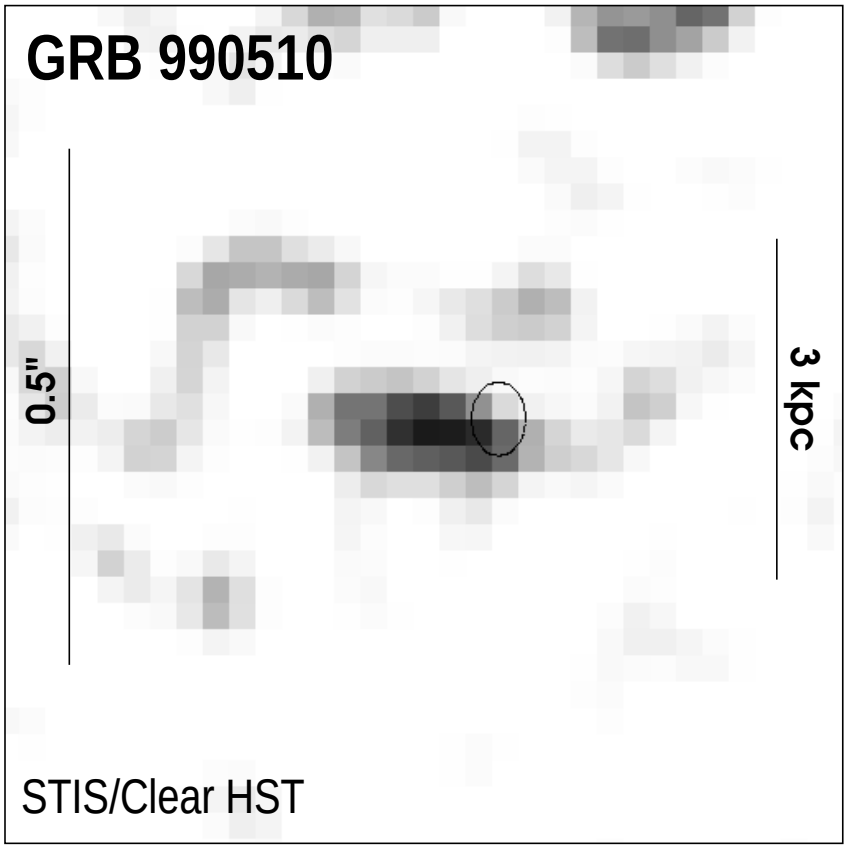
GRB 990510
0.5"
3 kpc
STIS/Clear HST

FIG. 2*o*

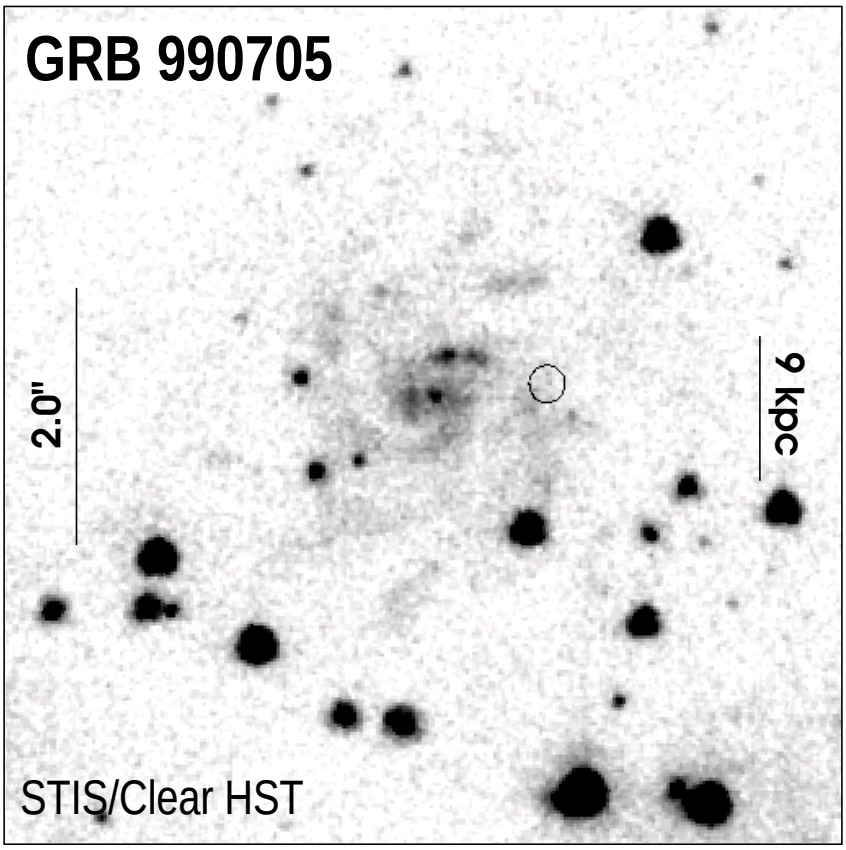
GRB 990705
2.0"
9 kpc
STIS/Clear HST

FIG. 2*p*

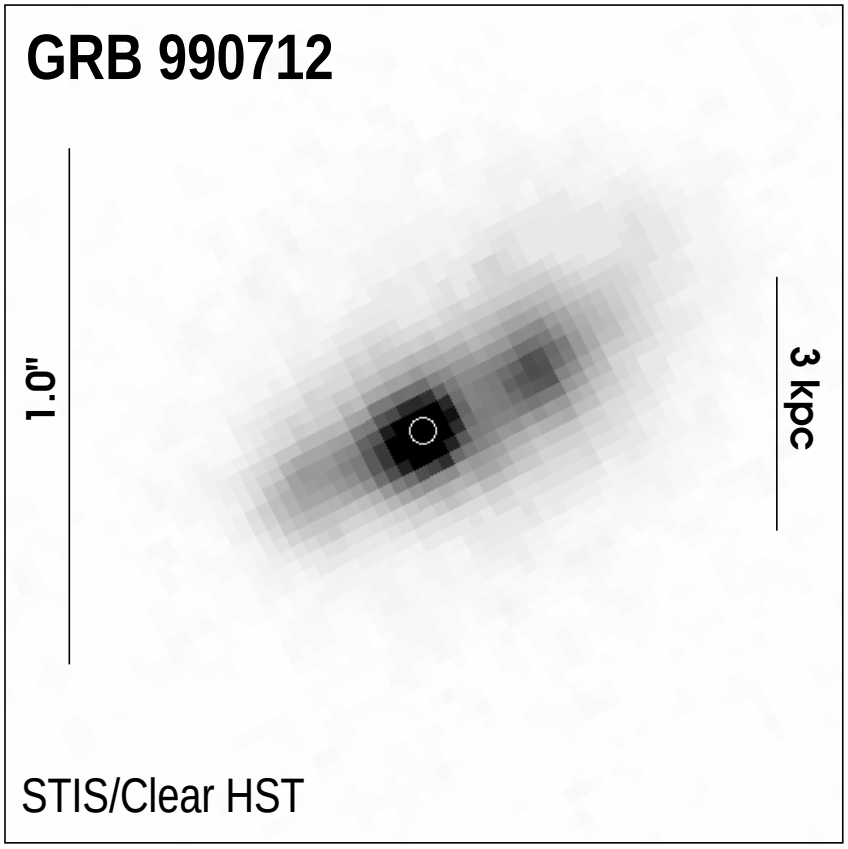
GRB 990712
1.0"
3 kpc
STIS/Clear HST

FIG. 2*q*

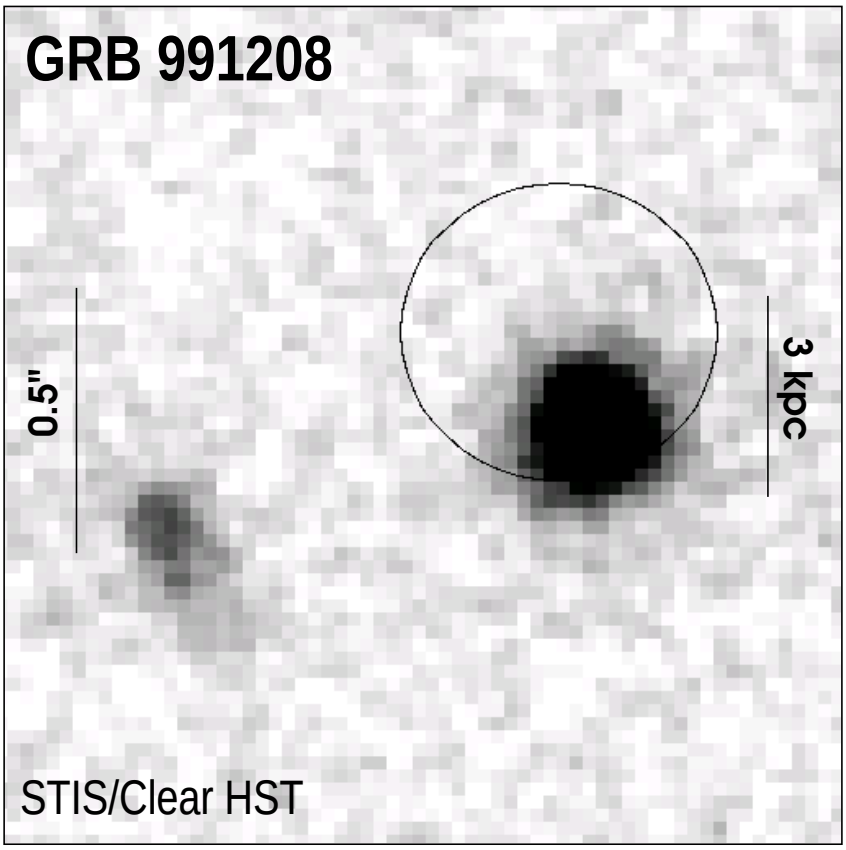
GRB 991208
0.5"
3 kpc
STIS/Clear HST

FIG. 2*r*

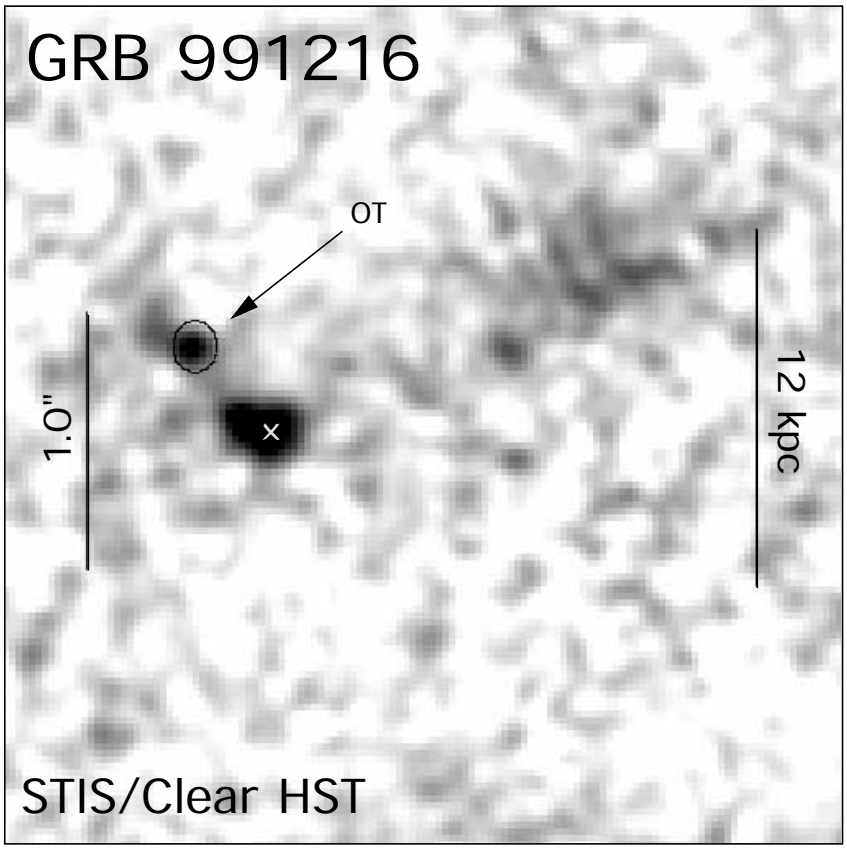
GRB 991216
OT
1.0"
12 kpc
STIS/Clear HST

FIG. 2*s*

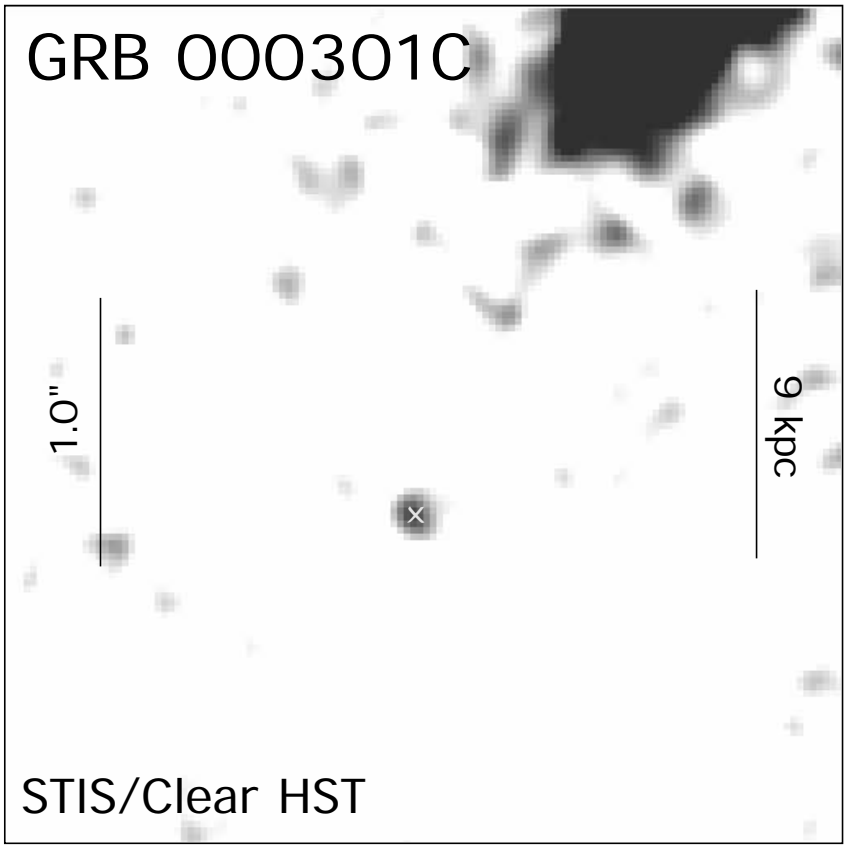
GRB 000301C
1.0"
9 kpc
STIS/Clear HST

FIG. 2*t*

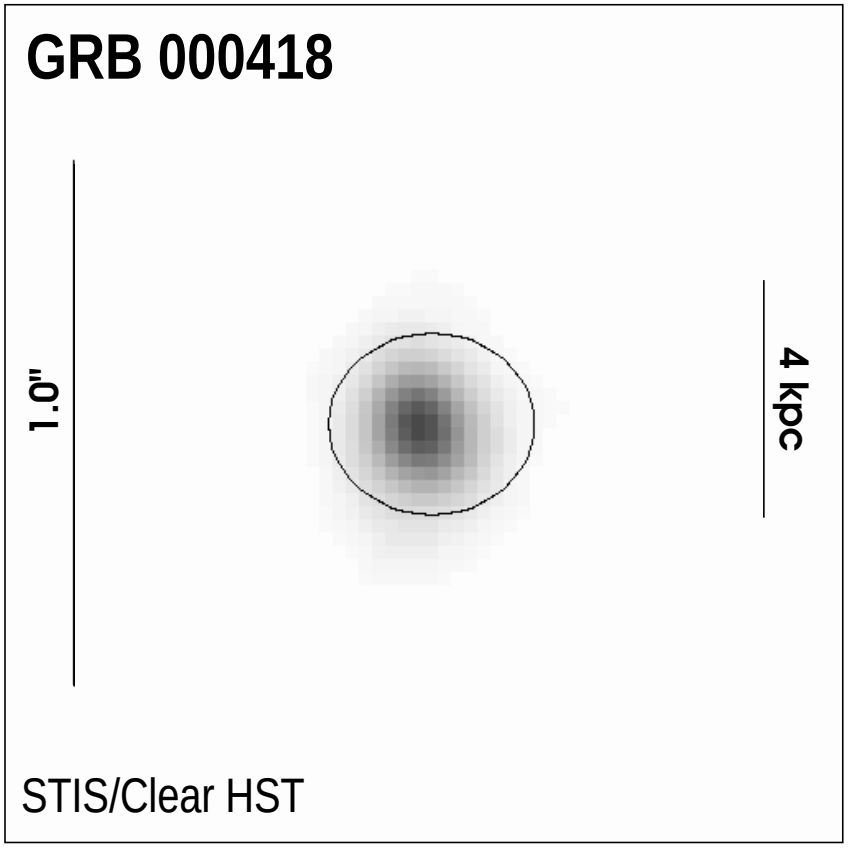
GRB 000418
1.0"
4 kpc
STIS/Clear HST

FIG. 2*u*

nant from a diffraction spike of a nearby bright star. Fruchter et al. (2001b) find that the putative host galaxy is detected at the 4.5 σ level. Adding to the notion that the source is not some chance superposition, we note that the galaxy is the brightest object within 3×3 arcsec^2 of the GRB position. There is also a possible detection of a low surface brightness galaxy $\sim 0\farcs5$ to the east of the galaxy.

5.6. *GRB 980329*

The afterglow of GRB 980329 was first detected at radio wavelengths (Taylor et al. 1998). Our best early-time position was obtained using a Keck *K*-band image of the field observed by J. Larkin and collaborators (Larkin et al. 1998). We recently obtained deep *R* imaging of the field with Keck ESI and detected the host galaxy at $R = 26.53 \pm 0.22$ mag. We found the location of the afterglow relative to the host by using 13 stars in common with the early *K*-band and late *R*-band image.

As shown in Figure 2, the GRB is coincident with a slightly extended faint galaxy. Our determined angular offset (see Table 2) of the GRB from this galaxy is significantly closer to the putative host than the offset determined by Holland (2000b) in late-time *HST* imaging (our astrometric uncertainties are also a factor of ~ 9 smaller). The difference is possibly explained by noting that the Holland (2000d) analysis used the VLA radio position and just three USNO-A2.0 stars to tie the GRB position to the *HST* image.

5.7. *GRB 980425*

The SN 1998bw was well localized at radio wavelengths (Kulkarni et al. 1998b) with an astrometric position relative to the ICRS of 100 mas in each coordinate. Ideally we could calibrate the *HST* STIS image to ICRS to ascertain where the radio source lies. However, without *Hipparcos* Tycho astrometric sources or radio point sources in the STIS field such absolute astrometric positioning is difficult.

Instead, we registered an early ground-based image to the STIS field to determine the differential astrometry of the optical SN with respect to its host. Unfortunately, most early images were relatively shallow exposures to avoid saturation of the bright SN, and so many of the point sources in the STIS field are undetected. The best seeing and deepest exposure from ground-based imaging is from the EMMI ESO 3.5 m New Technology Telescope (NTT) on 1998 May 4.41 (Galama 1999), where the seeing was $0\farcs9$ FWHM. We found six point sources, that were detected in both the STIS CLEAR and the ESO NTT *I*-band image. The use of *I*-band positions for image registration is justified since all six point sources appear red and are therefore unlikely to introduce a systematic error in the relative positioning. Since the number of astrometric tie sources is low, we did not fit for high-order distortions in the ESO image, and instead we fitted for the relative scale in both the *x* and *y* directions, rotation, and shift (five parameters for 12 data points). We compute an rms uncertainty of 40 and 32 mas, respectively, in the *x* and *y* positions of the astrometric tie sources. These transformation uncertainties dominate the error in the positional uncertainty of the SN in the ESO NTT image and so we take the transformation uncertainties as the uncertainty in the true position of the supernova with respect to the STIS host image.

The astrometric mapping places the optical position of SN 1998bw within an apparent star-forming region in the outer spiral arm of the host 2.4 kpc in projection at $z = 0.0088$ to the southwest of the galactic nucleus. Within the uncertainties of the astrometry the SN is positionally coincident with a bright blue knot within this region, probably an H II region. This is consistent with the independent astrometric solutions reported by Fynbo et al. (2000b).

5.8. *GRB 980519*

The GRB afterglow was well detected in our early-time image from the Palomar 200 inch telescope. We found 150 objects common to this image and our intermediate-time Keck image. An astrometric registration between the two epochs was performed using IRAF GEOMAP. Based on this astrometry, Bloom et al. (1998a) reported the OT to be astrometrically consistent with a faint galaxy, the putative host. This is the second-faintest host galaxy (after GRB 990510; see below) observed to date, with $R = 26.1 \pm 0.3$.

We found 25 objects in common with the intermediate-time Keck image and the *HST* STIS image. These tie objects were used to further propagate the OT position onto the *HST* frame. Inspection of our final *HST* image near the optical transient location reveals the presence of low surface brightness emission connecting the two bright elongated structures. Morphologically, the "host" appears to be a pair of tidally interacting galaxies, although this interpretation is subjective. The GRB location is coincident with the dimmer elongated structure to the north. Using the approximate geometric center of the host we estimate the center, albeit somewhat arbitrarily, as the faint knot south of the GRB location and $\sim 0\farcs3$ to the east of the brighter elongated structure. The half-light radius of the system was also measured from this point. From this "center" we find the offset of the GRB given in Table 2.

5.9. *GRB 980613*

The morphology of the system surrounding the GRB is complex and discussed in detail in Djorgovski, Bloom, & Kulkarni (2002a). There we found the OT to be within $\sim 3''$ of five apparent galaxies or galaxy fragments, two of which are very red ($R-K > 5$). In more recent *HST* imaging, the OT appears nearly coincident with a compact high surface brightness feature, which we now identify as the host center. Given the complex morphology, we chose to isolate the feature in the determination of the half-light radius by truncating the curve-of-growth analysis at $0\farcs5$ from the determined center.

5.10. *GRB 980703*

The optical transient was well detected in our early-time image, and, based on the light curve and the late-time image, the light was not contaminated by light from the host galaxy. Berger et al. (2001) recently found that the radio transient was very near the center of the radio emission from the host.

We found 23 objects common to the Keck image and our final reduced *HST* STIS image and computed the geometric transformation. The rms uncertainty of the OT position on the *HST* image was quite small: 49 and 60 mas in the instrumental *x* and *y* coordinates, respectively. We determined the center of the host by using IRAF ELLIPSE and IRAF CENTER, which gave consistent answers to 2 mas in each coordinate.

Recently, Berger et al. (2001) compared the VLBA position of the afterglow with the position of the persistent radio emission from the host. Since both measurements were referenced directly to the ICRS, the offset determined was a factor of $\sim$3 times more accurate than that found by using the optical afterglow; the two offset measurements are consistent within the errors. In the interest of uniformity, we use the optical offset measurement in the following analysis.

5.11. *GRB 981226*

Unfortunately, no optical transient was found for this burst, though a radio transient was identified (Frail et al. 1999). We rely on the transformation between the USNO-A2.0 and the Keck image to place the host galaxy position on the ICRS (see Frail et al. 1999 for further details). We then determine the location of the radio transient in the *HST* frame using 25 compact sources common to both the *HST* and Keck image. In Figure 1 we show as example the tie objects in both the Keck and *HST* image. The tie between the two images is excellent, with an rms uncertainty of 33 and 47 mas, respectively, in the instrumental x and y positions. Clearly, the uncertainty in the radio position on the Keck image dominates the overall location of the GRB on the *HST* image.

The host appears to have a doubly nucleated morphology, perhaps indicative of a merger or interacting system. Holland et al. (2000d) noted, by inspecting both the STIS Longpass and the STIS Clear image, that the northeastern part of the galaxy appeared significantly bluer then the southwestern part. As expected from these colors the center of the host as measured in our late-time R-band Keck lies near ($\sim$50 mas) the centroid of the red (southwestern) portion of the host. We assign the R-band centroid in Keck image as the center of the host.

5.12. *GRB 990123*

This GRB had an extremely bright prompt optical afterglow emission, which was found in archived images from a robotic telescope, the Robotic Optical Transient Search Experiment (Akerlof et al. 1999). We reported on the astrometric comparison of ground-based data with *HST* imaging and found that the bright point source on the southern edge of a complex morphological system was the afterglow (Bloom et al. 1999b). Later *HST* imaging revealed that indeed this source did fade (e.g., Fruchter et al. 1999b) as expected of GRB afterglow.

As seen in Figure 2, the host galaxy is fairly complex, with two bright elongated regions spaced by $\sim$0$''$.5, which run approximately parallel to each other. The appearance of spatially curved emission to the west may be a tidal tail from the merger of two separate systems or a pronounced spiral arm of the brighter elongated region to the north. We choose, again somewhat subjectively, the peak of this brighter region as the center of the system and find the astrometric position of the GRB directly from the first *HST* epoch.

5.13. *GRB 990308*

An optical transient associated with GRB 990308 was found by Schaefer et al. (1999). Though the transient was detected at only one epoch (3.3 hr after the GRB; Schaefer et al. 1999) it was observed in three bandpasses, twice in R band. Later time Keck imaging revealed no obvious source at the location of the transient to $R = 25.7$, suggesting that the source had faded by at least $\sim$7.5 mag in R band.

A deep *HST* exposure of the field was obtained by Holland (2000a), who reported that the Schaefer et al. position derived from the USNO-A2.0 was consistent with two faint galaxies.

We found the offset by two means. First, we found an absolute astrometric solution using 12 USNO-A2.0 stars in common with the later time Keck image. The *HST* STIS and the Keck R-band image were then registered using 27 objects in common. Second, we found a differential position by using early ground-based images kindly provided by B. Schaefer to tie the optical afterglow position directly to the Keck (then to the *HST*) image. Both methods give consistent results though the differential method is, as expected, more accurate.

Our astrometry places the OT position further east from the two faint galaxies than the position derived by Holland (2000a). At a distance of 0$''$.73 to the north of our OT position there appears to be a low surface brightness galaxy near the detection limit of the STIS image (see Fig. 2), similar to the host of GRB 980519 (there is also, possibly, a very faint source 0$''$.23 southwest of the OT position, but the reality of its detection is questionable). Because of the faintness and morphological nature of the source, a detection confidence limit is difficult to quantify, but we are reasonably convinced that the source is real. At $V \sim 27$ mag, the nondetection of this galaxy in previous imaging is consistent with the current STIS detection. Since the angular extent of the galaxy spans $\sim$25 drizzled STIS pixels ($\sim$0$''$.63), more high-resolution *HST* imaging is not particularly useful for confirming the detection of the galaxy. Instead, deeper ground-based imaging with a large aperture telescope would be more useful.

5.14. *GRB 990506*

The Keck astrometric comparison with the radio position was given in Taylor et al. (2000), with a statistical error of 250 mas. We transferred this astrometric tie to the *HST* STIS image using eight compact sources common to both the Keck and *HST* images of the field near GRB 990506. The resulting uncertainty is negligible compared with the uncertainties in the radio position on the Keck image. As first reported in Taylor et al. (2000), the GRB location appears consistent with a faint compact galaxy. Hjorth (2000) later reported that the galaxy appears compact even in the STIS imaging.

5.15. *GRB 990510*

This GRB is well known for having exhibited the first clear evidence of a jet manifested as an achromatic break in the light curve (e.g., Harrison et al. 1999; Stanek et al. 1999). We discovered the host galaxy in late-time *HST* STIS imaging[7] (Bloom 2000) with $V = 28.5 \pm 0.5$. Registration of the early epoch when the OT was bright reveals the OT occurred 64 ± 9 mas west and 15 ± 12 mas north of the center of the host galaxy. This amounts to a significant displacement of 66 ± 9 mas or 600 pc at a distance of $z = 1.62$ (Galama et al. 1999). The galaxy is extended with a position

[7] See http://gcn.gsfc.nasa.gov/gcn/.

angle P.A. = 80°.5 ± 1°.5 (east of north) and an ellipticity of about ~0.5.

In retrospect, the host does appear to be marginally detected in the 1999 July imaging, as well as the later 2000 April image, although at the time no galaxy was believed to have been detected (Fruchter et al. 1999a).

5.16. *GRB 990705*

Masetti et al. (2000) discovered the infrared afterglow of GRB 990705 projected on the outskirts of the Large Magellanic Cloud. At the position of the afterglow, Masetti et al. (2000) noted an extended galaxy seen in ground-based *V*-band imaging; they identified this galaxy as the host. Holland et al. (2000a) reported on *HST* imaging of the field and noted, thanks to the large size (~2″) of the galaxy and resolution afforded by *HST*, an apparent face-on spiral at the location of the transient. We retrieved the public *HST* data and compared the early images provided by N. Masetti with our final reduced *HST* image. Consistent with the position derived by Holland et al. (2000a), we find that the transient was situated on the outskirts of a spiral arm to the west of the galaxy nucleus and just north of an apparent star-forming region.

5.17. *GRB 990712*

This GRB has the lowest measured redshift of a "cosmological" GRB with $z = 0.4337$ (Hjorth et al. 2000). Unfortunately, the astrometric location of the GRB appears to be controversial, though there is no question that the GRB occurred within the bright galaxy pictured in Figure 2. Hjorth et al. 2000 found that the only source consistent with a point source in the earlier *HST* image was the faint region to the northwest side of the galaxy and concluded that the source was the optical transient. However, Fruchter et al. (2000d) found that this source did not fade significantly. Instead the Fruchter et al. analysis showed, by subtraction of two *HST* epochs, that a source did fade near the bright region to the southeast. While the fading could be due to AGN activity instead of the presence of a GRB afterglow, we adopt the conclusion of Fruchter et al. for astrometry and place conservative uncertainties on the location relative to the center as 75 mas (3 pixels) in both right ascension and declination for 1 σ errors. We did not conduct an independent analysis to determine this GRB offset.

5.18. *GRB 991208*

In our early *K*-band image of the field, we detect the afterglow, as well as seven suitable tie stars to our late ESI image. The host galaxy is visible in the ESI image, and the subsequent offset was reported by us (Diercks et al. 2000). An *HST* image was later obtained and reported by Fruchter et al. (2000e), confirming the presence of the host galaxy.

We reduced the public *HST* STIS data on this burst and found the offset in the usual manner by tying the OT position from Keck to the *HST* frame. The GRB afterglow position falls near a small compact galaxy. A fainter galaxy, to the southeast, may also be related to the GRB-host galaxy system (see Fig. 2).

5.19. *GRB 991216*

We used nine compact objects in common with our early Keck image (seeing FWHM = 0″.66) and the late-time *HST* STIS imaging to locate the transient. As noted first by Vreeswijk et al. (2000), the OT is spatially coincident with a faint apparent point source in the *HST* STIS image. Our astrometric accuracy of $\sigma_r = 32$ mas of the OT position is about 4 times better than that of Vreeswijk et al. (2000). Thanks to this we can confidently state that the OT coincides with a point source on the *HST* STIS image. We believe this point source, as first suggested by Vreeswijk et al., is the OT itself.

The "location" of the host galaxy is difficult to determine. The OT does appear to reside to the southwest of faint extended emission (object N from Vreeswijk et al. 2000), but it is also located to the northeast of a brighter extended component (object S from Vreeswijk et al. 2000). There appears to be a faint bridge of emission connecting the two regions, as well as the much larger region to the west of the OT (see Fig. 2). In fact these three regions may together compose a large low surface brightness system. Again, somewhat arbitrarily, we take the center of the "host" to be the peak of object S.

5.20. *GRB 000301C*

Fruchter, Metzger, & Petro (2000a), in intermediate-time (2000 April) imaging of the field of GRB 000301C, detected a faint unresolved source coincident with the location of the GRB afterglow; the authors reckoned the source to be the faded afterglow itself. In the most recent imaging on 2001 February the same group detected a somewhat fainter, compact object very near the position of the transient. Given the time (~1 yr) since the GRB the authors suggested that the afterglow should have faded below the detection level and that therefore this object is the host of GRB 000301C (Fruchter & Vreeswijk 2001a)

We confirm the detection of this source and measure the offset by using earlier time imaging from *HST*. Though no emission-line redshift of this source has been obtained, given its proximity to the GRB it likely resides at $z = 2.03$, inferred from absorption spectroscopy (Smette et al. 2001; Castro et al. 2000) of the OT.

In Figure 2 we present the late-time image from *HST* STIS. A galaxy 2″.13 from the transient to the northwest is detected at $R = 24.25 \pm 0.08$ mag and may be involved in possible microlensing of the GRB afterglow (e.g., Garnavich, Loeb, & Stanek 2000)

5.21. *GRB 000418*

We reported the detection of an optically bright component and an infrared bright component at the location of GRB 000418 (Bloom et al. 2000a). Metzger et al. (2000) later reported that *HST* STIS imaging of the field revealed that the OT location was 0″.08 ± 0″.15 east of the center of the optically bright component, a compact galaxy.

For our astrometry we used an early Keck *R*-band image and the late *HST* STIS image. The astrometric uncertainty is improved over the Metzger et al. (2000) analysis by a factor of 2.4. Within errors, the OT is consistent with the center of the compact host.

6. OBSERVED OFFSET DISTRIBUTION

6.1. *Angular Offset*

As seen in Table 2 and § 5, there are 20 GRBs for which we have a reliable offset measurement from self-*HST*, *HST*→*HST*, *HST*→GB, GB→GB, or RADIO→OPT

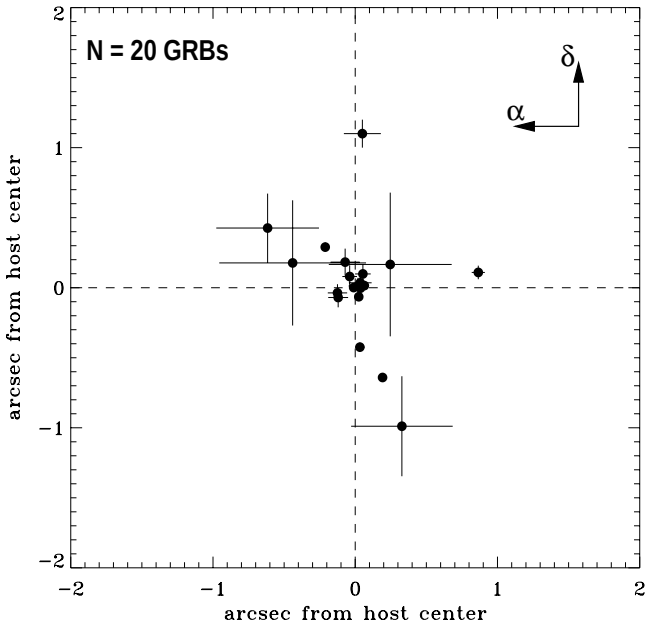

FIG. 3*a*

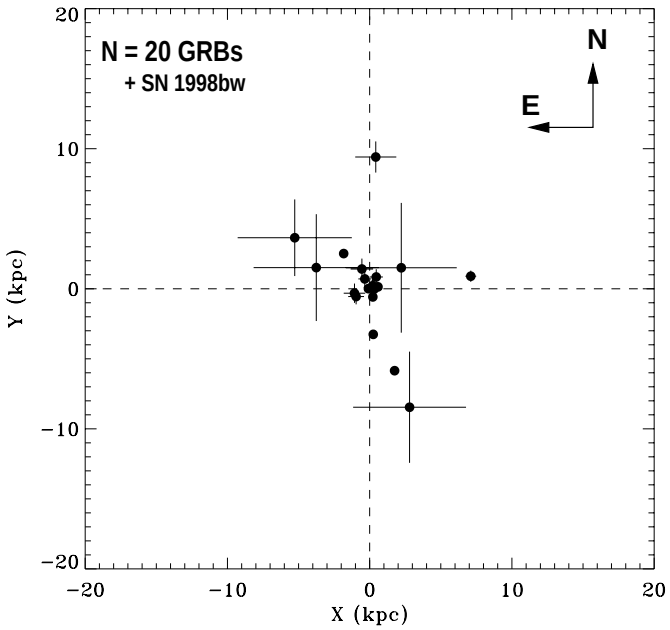

FIG. 3*b*

FIG. 3.—*Left*: Angular distribution of 20 gamma-ray bursts about their presumed host galaxy. The error bars are 1 σ and reflect the total uncertainty in the relative location of the GRB and the apparent host center. The offset of GRB 980425 from its host is suppressed for clarity since, relative to all the others, the redshift GRB was so small. *Right*: Projected physical offset distribution of 20 gamma-ray bursts (now including SN1998bw/GRB 980425) about their presumed host galaxies. The physical offset is assigned assuming $H_0 = 65$ km s^{-1} Mpc^{-1}, $\Lambda = 0.7$, and $\Omega_m = 0.3$ and assuming the GRB and the presumed host are at the same redshift. When no redshift has been directly measured a redshift is assigned equal to the median redshift ($z = 0.966$) of all GRBs with measured redshifts (see text).

astrometric ties. There are several representations of this data worth exploring. In Figure 3 we plot the angular distribution of GRBs about their presumed host galaxy. In this figure and in the subsequent analysis we exclude GRB 980425 because the association of this GRB with SN 1998bw is still controversial. More importantly (for the purposes of this paper) the relation of GRB 980425 to the classical "cosmological" GRBs is unclear (Schmidt 1999) given that, if the association proved true, the burst would have been underluminous by a factor of $\sim 10^5$ (Galama et al. 1998; Bloom et al. 1998a).

As can be seen from Table 2 and Figure 3, well-localized GRBs appear on the sky close to galaxies. The median projected offset of the 20 GRBs from their putative host galaxies is $0''.17$—sufficiently small that almost all the identified galaxies must be genuine hosts (see below). In detail, three of the bursts show no measurable offset from the centroid of their compact hosts (GRB 970508, 980703, and 000418), whereas five bursts appear well displaced ($\gtrsim 0''.3$) from the center of their host at a high level of significance. Three additional bursts detected via radio afterglows (GRB 970828, 981226, and 990506) and GRB 990308 (poor astrometry of the discovery image due to large pixels and shallow depth) suffer from larger uncertainties (rms $\approx 0''.3$) but have plausible host galaxies.

As discussed in Appendix A, GB→GB or GB→*HST* astrometry could systematically suffer from the effects of differential chromatic refraction, albeit on the 5–10 mas level. The *HST*→*HST* measured offsets of GRB 970228, 970508, 990123, 990510, 990712, and 000301C are immune from DCR effects. Since optical transients in general appear red and their hosts blue, DCR will systematically appear to pull OTs away from their hosts in the parallactic direction toward the horizon. Comparing the observed offset directions parallactic at the time of each OT observation in Table 2, we find no systematic correlation, thus confirming that DCR does not appear to play a dominant role in determining the differential offsets of OTs from their hosts.

On what basis can we be confident that the host assignment is correct for a particular GRB? Stated more clearly in the negative is the question, "What is the probability of finding an unrelated galaxy (or galaxies) within the localization error circle of the afterglow (3 σ) or, in the case in which the localization error circle is very small, whether a galaxy found close to a GRB localization is an unrelated galaxy seen in projection?" This probability, assuming that the surface distribution of galaxies is uniform and thus follows a Poisson distribution (i.e., we ignore clustering of galaxies), is

$$P_{i,\mathrm{ch}} = 1 - \exp(-\eta_i) \, , \tag{1}$$

where the subscript "ch" indicates "chance." Here

$$\eta_i = \pi r_i^2 \sigma(\leq m_i) \tag{2}$$

is the expected number of galaxies in a circle with effective radius r_i and

$$\sigma(\leq m_i) = \frac{1}{3600^2 \times 0.334 \log_e 10} \times 10^{0.334(m_i - 22.963) + 4.320} \text{ galaxy arcsec}^{-2} \tag{3}$$

is the mean surface density of galaxies brighter than R-band magnitude of m_i, found using the results from Hogg et al. (1997). Since GRBs are observed through some Galactic extinction, the surface density of galaxies at a given limiting flux is reduced; therefore, we use the reddened host galaxy magnitude for m_i (col. [2] minus col. [3] of Table 3).

There are few possible scenarios for determining r_i at a given magnitude limit. If the GRB is very well localized inside the detectable light of a galaxy then $r_i \approx 2R_{\rm half}$ is a reasonable estimate for the effective radius. If the localization is poor and there is a galaxy inside the uncertainty position, then $r_i \approx 3\ \sigma_{R_0}$. If the localization is good, but the position is outside the light of the nearest galaxy, then $r_i \approx (R_0^2 + 4R_{\rm half}^2)^{1/2}$. Therefore, we take $r_i = \max\left[2R_{\rm half}, 3\ \sigma_{R_0}, (R_0^2 + 4R_{\rm half}^2)^{1/2}\right]$ as a conservative estimate of the effective radius. Here the quantity R_0 is the radial separation between the GRB and the presumed host galaxy, $R_{\rm half}$ is the half-light radius, and σ_{R_0} is the associated rms error (see Table 2).

If no "obvious" host is found (i.e., $P_{\rm ch} \gtrsim 0.1$) then we often seek deeper imaging observations, which will in general decrease the estimated r_i as more and more galaxies are detected. However, the estimate for η_i should remain reasonable since the surface density of background galaxies continues to grow larger with increasing depth. This is to say that there is little penalty to pay in statistically relating sky positions to galaxies by observing to fainter depths.

The values for $P_{i,{\rm ch}}$ are computed and presented in Table 3. As expected, GRBs that fall very close to a galaxy (e.g., GRB 970508, 980703, or 990712) are likely to be related to that galaxy. Similarly, GRB localizations with poor astrometric accuracy (e.g., GRB 990308 or GRB 970828) yield larger probabilities that the assigned galaxy is unrelated.

In the past, most authors (including ourselves) did not endeavor to produce a probability of chance association, instead opting to assume that these assigned galaxies are indeed the hosts. Nevertheless, we believe these estimates are conservative; for instance, van Paradijs et al. (1997) estimated that $P_{\rm ch}(970228) = 0.0016$, which is 5.8 times smaller than our estimate. Again, we emphasize that the estimated probabilities are constructed a posteriori so there is no exact formula to determine the true $P_{\rm ch}$.

The probability that *all* supposed host galaxies in our sample are random background galaxies is

$$P(n_{\rm ch} = m = {\rm all}) = \prod_{k=1}^{m} P_k\ ,$$

with $m = 20$ and P_k found from equation (1) for each GRB k. Not surprisingly, this number is extremely small, $P({\rm all}) = 2 \times 10^{-60}$, ensuring that at least some host assignments must be correct.

The probability that *all* galaxies are physically associated (i.e., that none are chance superpositions of a random field galaxy) is

$$P(n_{\rm ch} = 0) = \prod_{k=1}^{m}(1 - P_k) = 0.483\ .$$

In general, the chance that n assignments will be spurious out of a sample of $m \geq n$ assignments is

$$P(n_{\rm ch}) = \frac{1}{n_{\rm ch}!}\overbrace{\sum_{i}^{m}\sum_{j\neq i}^{m}\cdots}^{n_{\rm ch}}\left[\overbrace{P_i \times P_j \times \cdots}^{n_{\rm ch}}\prod_{k\neq i\neq j\neq\cdots}^{m}(1 - P_k)\right]\ . \tag{4}$$

$P(n_{\rm ch})$ reflects the probability that we have generated a number $n_{\rm ch}$ of spurious host galaxy identifications. For our sample, we find that $P(1) = 0.395$, $P(2) = 0.106$, and $P(3) = 0.015$ and so the number of spurious identifications is likely to be small, $\sim$1–2. Indeed, if the two GRBs with the largest $P_{\rm ch}$ are excluded (GRB 970828 and GRB 990308) then $P(n_{\rm ch} = 0)$ jumps to 0.76. Thus we are confident that almost all our identifications are quite secure.

The certainty of our host assignments of the nearest galaxy to a GRB finds added strength by using redshift information. In *all* cases in which an absorption redshift is found in a GRB afterglow (GRB 970508, 980613, 990123, 980703, 990712, and 991216) the highest redshift absorption system is observed to be at nearly the same emission redshift as the nearest galaxy. Therefore, with these bursts clearly the nearest galaxy cannot reside at a higher redshift than the GRB. The galaxy may simply be a foreground object, that gives rise both to nebular line emission and the absorption of the afterglow originating from a higher redshift. However, using the observed number density evolution of absorbing systems, Bloom et al. (1997) calculated that statistically in $\gtrsim$80% of such absorption cases, the GRB could reside no further than 1.25 times the absorption redshift. For example, if an emission-absorption system is found at $z = 1.0$ then there is only a $\lesssim$20% chance that the GRB could have occurred beyond redshift $z = 1.25$ without another absorption system intervening. Though this argument cannot prove that a given GRB progenitor originated from the assigned host, the effect of absorption or emission redshifts is to confine the possible GRB redshifts to a shell in redshift space, reducing the number of galaxies that could possibly host the GRB and increasing the chance that the host assignment is correct. Therefore, given this argument and the statistical formulation above, we proceed with the hypothesis that, as a group, GRBs are indeed physically associated with galaxies assigned as hosts.

6.2. *Physical Projection*

Of the 20 GRBs with angular offsets five have no confirmed redshift and the angular offset is thus without a physical scale. These bursts have hosts fainter than $R \approx 25$ mag and, given the distribution of other GRB redshifts with these host magnitudes, it is reasonable to suppose that the five bursts originated somewhere in the redshift range $z = 0.5$–5. It is interesting to note (with our assumed cosmology) that despite a luminosity distance ratio of 37 between these two redshifts, the angular scales are about the same: $D_\theta(z = 0.5)/D_\theta(z = 5) \approx 1$. In fact over this entire redshift range, 6.6 kpc arcsec^{-1} $< D_\theta(z) <$ 9.1 kpc arcsec^{-1}, which renders the conversion of angular displacement to physical projection relatively insensitive to redshift. For these five bursts, then, we assign the median D_θ of the other bursts with known redshifts so that $D_\theta = 8.552$ kpc arcsec^{-1} (corresponding to a redshift of $z = 0.966$) and scale the observed offset uncertainty by an additional 30%. Here, we

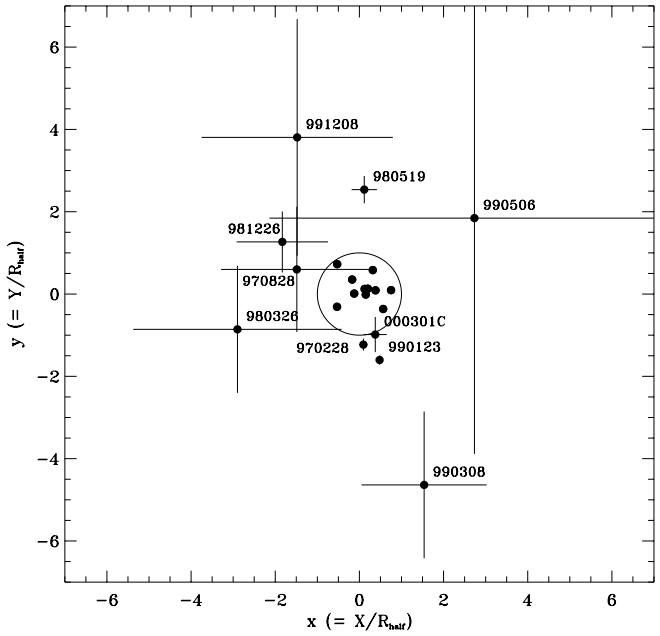

FIG. 4*a*

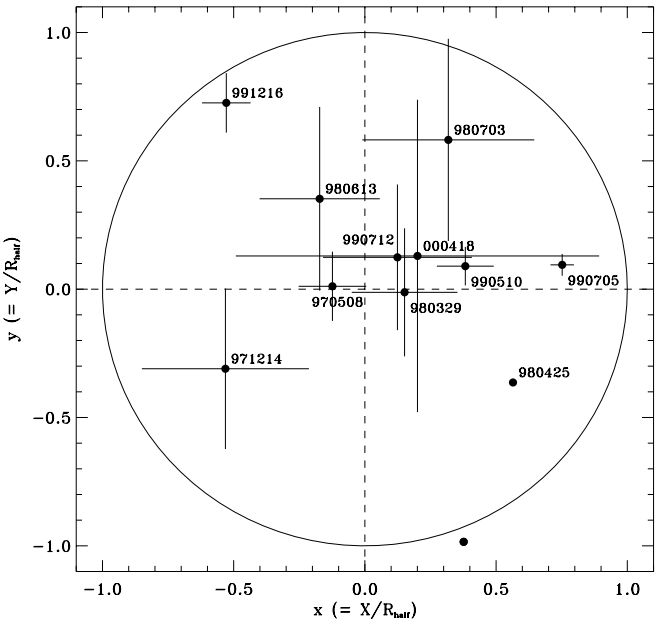

FIG. 4*b*

FIG. 4.—Host-normalized offset distribution. The dimensionless offsets are the observed offsets (X_0, Y_0) normalized by the host half-light radius ($R_{\rm half}$) of the presumed host galaxy. See text for an explanation of how the half-light radius is found. The 1 σ error bars reflect the uncertainties in the offset measurement and in the half-light radius. As expected if GRBs occur where stars are formed, there are 10 GRBs (plus 1998bw/GRB 980425) inside and 10 GRBs outside the half-light radius of their host. All GRBs outside one half-light radius (*circle; left*) are labeled. All GRBs observed to be internal to one half-light radius are labeled (*right*).

use the GRB redshifts (and, below, host magnitudes) compiled in the review by Kulkarni et al. (2000). The resulting physical projected distribution is depicted in Figure 3 and given in Table 2. The median projected physical offset of the 20 GRBs in the sample is 1.31 kpc or 1.10 kpc including only those 15 GRBs for which a redshift was measured. The minimum offset found is just 91 $\pm$ 90 pc from the host center (GRB 970508).

6.3. *Host-normalized Projected Offset*

If GRBs were to arise from massive stars we would then expect that the distribution of GRB offsets would follow the distribution of the light of their hosts. As can be seen in Figure 2, qualitatively this appears to be the case since almost all localizations fall on or near the detectable light of a galaxy.

The next step in the analysis is to study the offsets, but normalized by the half-light radius of the host. This step then allows us to consider all the offsets in a uniform manner. The half-light radius, $R_{\rm half}$, is estimated directly from STIS images with sufficiently high signal-to-noise ratio, and in the remaining cases we use the empirical half-light radius–magnitude relation of Odewahn et al. (1996); we use the dereddened R-band magnitudes found in the GRB host summaries from Djorgovski et al. (2002b) and Sokolov et al. (2001). Table 3 shows the angular offsets and the effective radius used for scaling. Where the empirical half-light radius–magnitude relation is used, we assign an uncertainty of 30% to $R_{\rm half}$.

The median of the distribution of normalized offsets is 0.976 (Table 3). That this number is close to unity suggests a strong correlation of GRB locations with the light of the host galaxies. The same strong correlation can be graphically seen in Figure 4, where we find that half the galaxies lie inside the half-light radius, and the remaining lie outside the half-light radius. We remark that the effective wavelength of the STIS bandpass and the ground-based R band corresponds to that of the rest-frame UV, and thus GRBs appear to be traced quite faithfully by the UV light, which mainly arises from the youngest and thus massive stars. We will examine the distribution in the context of massive-star progenitors more closely in § 7.2.

6.4. *Accounting for the Uncertainties in the Offset Measurements*

A simple way to compare the normalized offsets with the expectations of various progenitor models (see § 7) is through the histogram of the offsets. However, because of the small number of offsets, the usual binned histogram is not very informative. In addition, the binned histogram implicitly assumes that the observables can be represented by δ-functions, and this is not appropriate for our case, in which several offsets are comparable to the measurement uncertainty.

To this end we have developed a method to construct a probability histogram (PH) that takes into account the errors on the measurements. Simply put, we treat each measurement as a probability distribution of offset (rather than a δ-function) and create a smooth histogram by summing over all GRB probability distributions. Specifically, for each offset i we create an individual PH distribution function, $p_i(r)dr$, representing the probability of observing a host-normalized offset r for that burst. The integral of $p_i(r)dr$ is normalized to unity. The total PH is then constructed as $p(r)dr = \sum_i p_i(r)dr$ and plotted as a shaded region curve in Figure 5; see Appendix B for further details.

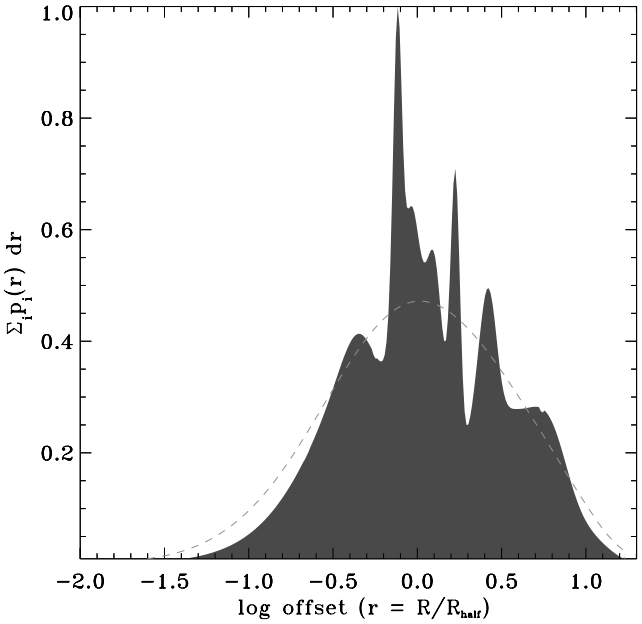

FIG. 5.—GRB offset distribution as a function of normalized galactocentric radius. The normalized offset is $r = R/R_{\rm half}$, where R is the projected galactocentric offset of the GRB from the host and $R_{\rm half}$ is the half-light radius of the host. This distribution is essentially a smooth histogram of the data, but one that takes into account the uncertainties in the measurements: the sharper peaks are due to individual offsets for which the significance (r_0/σ_{r_0}) of the offset is high. That is, if a GRB offset is well determined its contribution to the distribution will appear as a δ-function centered at $r = r_0$. The dashed curve is the distribution under the curve (*dark*) but smoothed with a Gaussian of FWHM = 0.7 dex in r. Strikingly, the peak of the probability is near one half-light radius, a qualitative argument for the association of GRBs with massive-star formation. We compare in detail this distribution with predicted progenitor distributions in § 7.

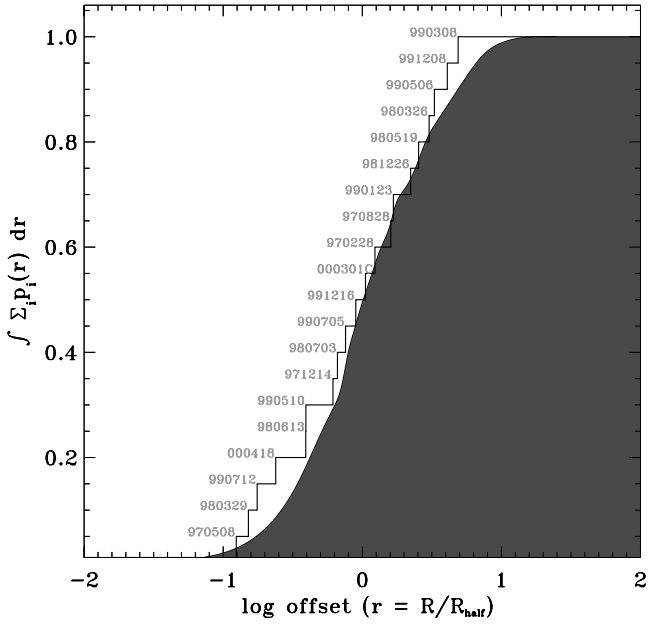

FIG. 6.—Cumulative GRB offset distribution as a function of host half-light radius. The solid jagged line is the data in histogram form. The smooth curve is the probability histogram (PH) constructed with the formalism of Appendix B and is the integral of the curve depicted in Fig. 5. The GRB identifications are noted alongside the solid histogram. In this figure and in Fig. 5, SN 1998bw/GRB 980425 has not been included.

The total cumulative probability histogram $\int_0^r p(r)dr$ is depicted as the solid smooth curve in Figure 6. There is, as expected, a qualitative similarity between the cumulative total PH distribution and the usual cumulative histogram distribution.

7. TESTING PROGENITOR MODEL PREDICTIONS

Given the observed offset distribution, we are now in the position to pose the question: Which progenitor models are favored by the data? Clearly, GRBs as a class do not appear to reside at the centers of galaxies and so we can essentially rule out the possibility that *all* GRBs localized to date arise from nuclear activity.

7.1. *Delayed Merging Remnant Binaries* (*BH-NS and NS-NS*)

In general, the expected distributions of merging remnant binaries are found by using population synthesis models for high-mass binary evolution to generate synthetic remnant binaries. The production rate of such binaries from other channels (such as three-body encounters in dense stellar clusters) are assumed to be small relative to isolated binary evolution. Because of gravitational energy loss, the binary members eventually coalesce but may travel far from their birth site before doing so. The locations of coalescence are determined by integrating the synthetic binary orbits in galactic potential models.

Bloom et al. (1999d), Fryer et al. (1999), and Bulik, Belczyński, & Zbijewski (1999) have simulated the expected radial distribution of GRBs in this manner. All three studies essentially agree on the NS-NS differential offset distributions as a function of host galaxy mass. (Note that the displayed distance axis, when compared with the differential distribution, is erroneously too large by a factor of 10 in the *cumulative* offset prediction plot in Figure 22 of Fryer et al. 1999.) Fryer et al. (1999) suggest that the Bloom et al. (1999d) synthesis may have incorrectly predicted an overabundance of compact binaries with small merger ages, because the population synthesis did not include a nonzero helium star radius; this is not the case although an arithmetic error in our code may account for the discrepancy (S. Sigurdsson 2001, private communication).

The formation scenarios of BH-NS binaries are less certain than that of NS-NS binaries. Both Fryer et al. (1999) and Belczyński, Bulik, & Zbijewski (2000) suggest that so-called "hypercritical accretion" (Bethe & Brown 1998) dominates the birthrate of BH-NS binaries. Briefly, hypercritical accretion occurs when the primary star evolves off the main sequence and explodes as a supernova, leaving behind a neutron star. Mass is rapidly accreted from the secondary star (in red giant phase) during common envelope evolution, causing the primary neutron star to collapse to a black hole. The secondary then undergoes a supernova explosion, leaving behind an NS. As in NS-NS binary formation, only some BH-NS systems will remain bound after having received systemic velocity kicks from two supernovae explosions.

One important difference is that BH-NS binaries are in general more massive (total system mass $M_{\rm tot} \approx 5\ M_\odot$) than NS-NS binaries ($M_{\rm tot} \approx 3\ M_\odot$). Furthermore, the coalescence timescale after the second supernova is shorter that in NS-NS binaries because of the BH mass. Therefore, despite

similar evolutionary tracks BH-NS binaries could be retained more tightly to host galaxies than NS-NS binaries (Bloom et al. 1999d; Belczyński et al. 2000). Belczyński et al. (2000) quantified this expected trend, showing that on average, BH-NS binaries merge about a few times closer to galaxies than NS-NS binaries. Surprisingly, Fryer et al. (1999) found that BH-NS binaries merged *farther* from galaxies than NS-NS binaries, but this result was not explained by Fryer et al. (1999). Nevertheless, just as with NS-NS binaries, a substantial fraction of BH-NS binaries will escape the potential well of the host galaxy and merge far outside the host. For example, even in massive galaxies such as the Milky Way, these studies show that roughly 25% of mergers occur more than 100 kpc from the center of a host galaxy.

Before comparing in detail the predicted and observed distributions, it is illustrative to note that the observed distribution appears qualitatively inconsistent with the delayed merging remnant binaries. All the population synthesis studies mentioned thus far find that approximately 50% of merging remnants will occur outside $\approx$10 kpc when the mass of the host is less than or comparable to the mass of the Milky Way. Comparing this expectation with Figure 3, where no bursts lie beyond 10 kpc from their host, the simplistic Poisson probability that the observed distribution is the same as the predicted distribution is no larger than 2×10^{-3}.

To provide a more quantitative comparison of the observed distribution with the merging remnant expectation, we require a model of the location probability of GRB mergers about their hosts. These models, which should in principle vary from host to host, have a complex dependence on the population synthesis inputs, the location of star formation within the galaxies, and the dark matter halo mass.

No dynamical or photometric mass of a GRB host has been reported to date. However, since GRB hosts are blue starbursts (e.g., Djorgovski et al. 2002b) it is not unreasonable to suspect that their masses will lie in the range 0.001 to $0.1 \times 10^{11}\ M_\odot$ (e.g., Östlin et al. 2001). The most obvious exceptions to this are the hosts of GRB 971214 and GRB 990705, which are likely to be near L_*. The observed median effective disk scale length of GRB hosts is $r_e = 1.1$ kpc though GRB hosts clearly show a diversity of sizes (Table 3, col. [5]). This value of r_e is also close to the median effective scale radii found in the Östlin et al. (2001) study of nearby compact blue galaxies.

To compare the observed and predicted distributions we use galactic models a–e from Bloom et al. (1999d), corresponding to hosts with mass in the range $(0.009–0.62) \times 10^{11}\ M_\odot$ and disk scale radii (r_e) of 1 and 3 kpc. Following the discussion above, we also construct a new model (a^*), which we consider the most representative of GRB hosts galaxies, with $v_{\rm circ} = 100$ km s^{-1}, $r_{\rm break} = 1$ kpc, and $r_e = 1.5$ kpc ($M_{\rm gal} = 9.2 \times 10^9\ M_\odot$).

We project these predicted *radial* distribution models by dividing each offset by a factor of 1.15 since the projection of a merger site onto the plane of the sky results in a smaller observed distance to the host center than the radial distance. We determined the projection factor of 1.15 by a Monte Carlo simulation projecting a three-dimensional distribution of offsets onto the sky. The median projected offset is thus 87% of the three-dimensional radial offset.

The observed distribution is compared with the predicted distributions and shown in Figure 7 (later, in Fig. 8, we compare the observed distribution with the massive-star prediction). We summarize the results in Table 4. Only model *d* ($M = 6.3 \times 10^{10}\ M_\odot$, $r_e = 3$ kpc) could be consistent with the data ($P_{\rm KS} = 0.063$), but this galactic model has a larger disk and is probably more massive than most GRB hosts. Instead, for the "best bet" model, a^*, the one-sided Kolmogorov-Smirnov probability that the observed sample derives from the same predicted distribution is $P_{\rm KS} = 2.2 \times 10^{-3}$, in agreement with our simplistic calculation above; that is, the location of GRBs appears to be inconsistent with the NS-NS and NS-BH hypothesis.

If GRBs do arise from systems that travel far from their birth site, then there is a subtle bias in determining the offset to the host. If the progenitors are ejected from the host by more than half the distance between the host and the nearest

TABLE 4

Comparison of Observed Offset Distributions with Various Progenitor Model Predictions

	Comparison Model				$P_{\rm KS}$			
Progenitor (1)	Name (2)	r_e (kpc) (3)	$v_{\rm circ}$ (km s^{-1}) (4)	Mass ($M_\odot$) (5)	Observed (6)	Synth (7)	Synth (replaced) (8)	Fraction of $P_{\rm KS} \geq 0.05$ (9)
Collapsar–promptly bursting binary.....	Expon. disk	$R_{\rm half}/1.67$	...	...	0.454	0.409	0.401	0.996
NS-NS, BH-NS.....	a*	1.5	100	9.2×10^9	9.5×10^{-4}	2.2×10^{-3}	2.2×10^{-3}	0.003
	a	1.0	100	9.2×10^9	6.9×10^{-3}	1.7×10^{-2}	1.8×10^{-2}	0.139
	b	1.0	100	2.8×10^{10}	4.9×10^{-3}	2.0×10^{-2}	2.0×10^{-2}	0.243
	c	3.0	100	2.8×10^{10}	3.5×10^{-5}	4.7×10^{-5}	4.7×10^{-5}	0.001
	d	1.0	150	6.3×10^{10}	2.5×10^{-2}	6.0×10^{-2}	6.3×10^{-2}	0.553
	e	3.0	150	6.3×10^{10}	5.7×10^{-5}	1.3×10^{-4}	1.3×10^{-4}	0.001

Note.—Col. (2): Names correspond to the model distribution compared against the data, with the letters corresponding to population synthesis models from Bloom et al. 1999d. For the NS-NS and BH-NS comparisons, we believe that a* best represents the observed host galaxy properties (see text). Col. (6)–(8): KS probability that the data are drawn from the model. Col. (6): Direct comparison of the models to the data without accounting for the uncertainties and measurements in the data. Col. (7): Median KS probability derived from our Monte Carlo modeling (Appendix C). Col. (8): Median KS probability derived from our Monte Carlo modeling but in which offsets thrown out due to high $P_{\rm ch}$ are replaced by synthetic offsets drawn from the model distribution. In general this pushes $P_{\rm KS}$ to larger values, but the resulting median of the distribution is strongly affected (since $P_{\rm ch}$ is near zero for most offsets). Col. (9): Fraction of synthetic data sets with $P_{\rm KS} \geq 0.05$.

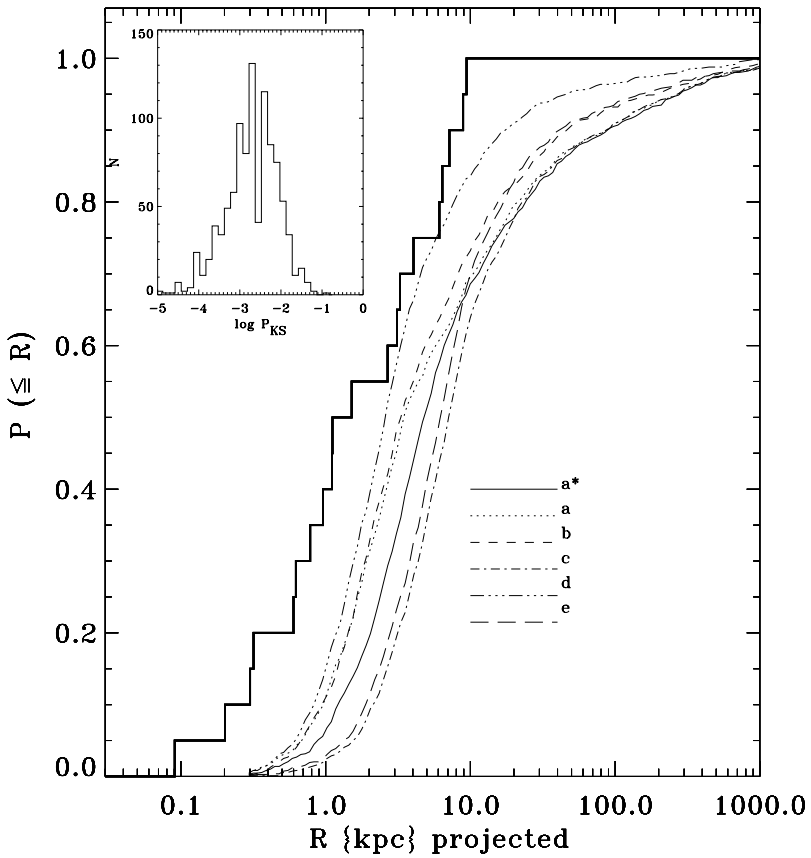

FIG. 7.—Offset distribution of GRBs compared with delayed merging remnant binaries (NS-NS and BH-NS) prediction. The models, depicted as smooth curves, are the radial distributions in various galactic systems that have been projected by a factor of 1.15 (see text). The letters denote the model distributions from Table 2 of Bloom et al. (1999d); a^* is the galactic model that we consider the most representative of GRB hosts galaxies ($v_{\rm circ} = 100$ km s^{-1}, $r_{\rm break} = 1$ kpc, $r_e = 1.5$ kpc, $M_{\rm gal} = 9.2 \times 10^9 M_\odot$). The cumulative histogram is the observed data set. The inset shows the distribution of KS statistics (based on the maximum deviation from the predicted and observed distribution) of 1000 synthetic data sets compared with model a^*. Even with conservative assumptions (see text) the observed GRB distribution is inconsistent with the prediction: in only 0.3% of synthetic data sets is $P_{\rm KS} \geq 0.05$. Instead, the collapsar–promptly bursting remnant progenitor model appears to be a better representation of the data (see Fig. 8).

(projected) galaxy, then the transient position will appear unrelated to any galaxies (the wrong host will be assigned, of course) but $P_{\rm ch}$ will always appear high no matter how deep the host search is. We try to account for this effect in our modeling (Appendix C) by synthetically replacing observed (small) offsets that are associated with a high value of $P_{\rm ch}$ with new generally larger offsets drawing from the expected distribution of offsets for a particular galactic model. This then biases the distribution of $P_{\rm KS}$ statistics toward *higher* values (by definition) but the median values of $P_{\rm KS}$ are largely unaffected (see Table 4).

7.2. *Massive Stars* (*Collapsars*) *and Promptly Bursting Binaries* (*BH-He*)

As discussed, collapsars produce GRBs in star-forming regions, as will BH-He binaries. The localization of GRB 990705 near a spiral arm is, of course, tantalizing smaller scale evidence of the GRB–star formation connection. Ideally, the burst sites of individual GRBs could be studied in detail with imaging and spectroscopy and should, if the collapsar–promptly bursting binary origin is correct, reveal that the burst sites are H II regions. Unfortunately, the distances to GRBs preclude a detailed examination of the specific burst sites on a resolution scale of tens of parsecs (the typical size for a star-forming region) with current instrumentation. Adaptive optics laser–guide star imaging may prove quite useful in this regard, as will IR imaging with the *Next Generation Space Telescope*.

Weaker evidence for a star formation connection exists in that no GRB to date has been observed to be associated with an early-type galaxy (morphologically or spectroscopically), though in practice it is often difficult to discern galaxy type with the data at hand. Indeed most well-resolved hosts appear to be compact star-forming blue galaxies, spirals, or morphological irregulars.

Above we have demonstrated that GRBs follow the UV (rest frame) light of their host galaxies. However, the comparison has been primarily mediated by a single parameter, the half-light radius and the median normalized offset. We now take this comparison one step further. For the GRB hosts with high signal-to-noise ratio *HST* detections (e.g., GRB 970508, 971214, and 980703) our analysis shows that the surface brightness is well approximated by an exponential disk. We use this finding as the point of departure for a simplifying assumption about all GRB hosts: we assume an exponential disk profile such that the surface brightness of the host galaxy scales linearly with the galactocentric radius in the disk. We further assume that the star formation rate of massive stars scales with the observed optical light of the host; this is not an unreasonable assumption given that *HST* STIS imaging probes rest-frame UV light, an excellent tracer of massive stars, at GRB redshifts.

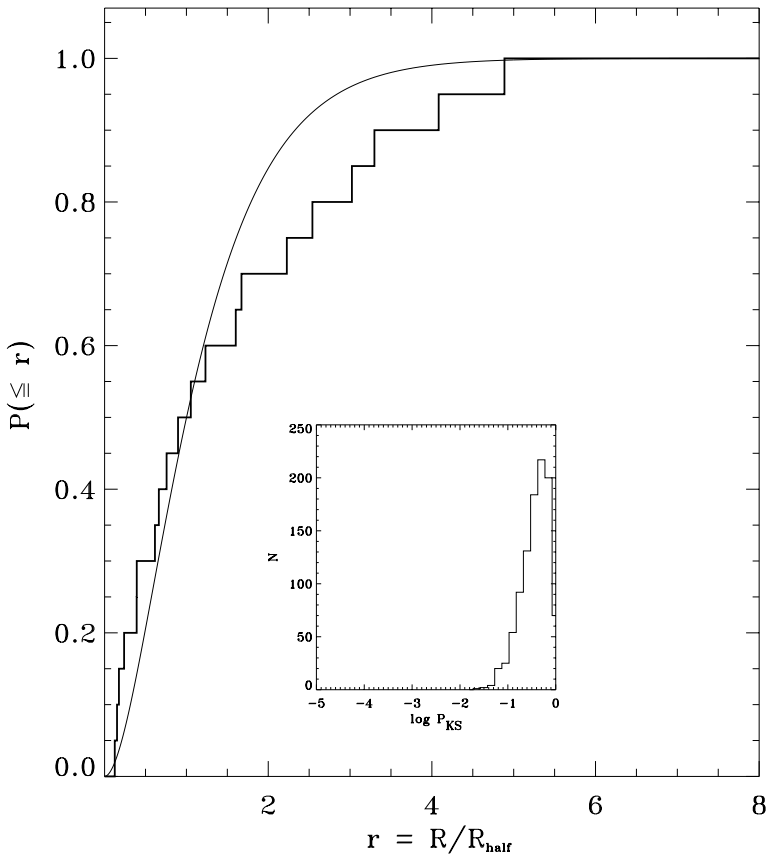

FIG. 8.—Offset distribution of GRBs compared with the host galaxy star formation model. The model, an exponential disk, is shown as the smooth curve and was chosen as an approximation to the distribution of the location of collapsars and promptly bursting remnant binaries (BH-He). The cumulative histogram is the observed data set. The inset shows the distribution of KS statistics (based on the maximum deviation from the predicted and observed distribution) of 1000 synthetic data sets. Since the observed KS statistic is near the median in both cases, we are assured that errors on the measurements do not bias the results of the KS test, and therefore the KS test is robust. The observed GRB distribution provides a good fit to the model, considering we make few assumptions to perform the comparison. In reality the location of star formation in GRB hosts will be more complex than in a simple exponential disk model.

Again, clearly not all host galaxies are disklike (Fig. 2) so this assumption is not strictly valid in all cases. If r_e is the disk scale length, the half-light radius of a disk galaxy is $R_{\rm half} = 1.67 \times r_e$, so that the simplistic model of the number density of massive-star formation regions in a galaxy is

$$N(r)dr \propto r \exp(-1.67r)dr\ , \qquad (5)$$

where $r = R/R_{\rm half}$. In reality, the distribution of massive-star formation in even normal spiral galaxies is more complex, with a strong peak of star formation in the nuclear region and troughs between spiral arms (e.g., Rana & Wilkinson 1986; Buat, Deharveng, & Donas 1989). We make an important assumption when comparing the observed distribution with the star formation disk model: that each GRB occurs in the disk of its host (see discussion below). Dividing the observed offset by the apparent half-light radius host essentially performs a crude deprojection.

We find the probability that the observed distribution could be derived from the simplistic distribution of massive-star regions (eq. [5]) is $P_{\rm KS} = 0.454$ (i.e., the two distributions are consistent). In Appendix C we show that these results are robust even given the measurement uncertainties. This broad agreement between GRB positions and the UV light of their hosts is remarkable in the sense that the model for massive-star locations is surely too simplistic; even in classic spiral galaxies (which most GRB hosts are not) star formation is a complex function of galactocentric radius, with peaks in galactic centers and spiral arms. Furthermore, surface brightness dimming with redshift causes galaxies to appear more centrally peaked, resulting in a systematic underestimate of $R_{\rm half}$.

8. DISCUSSION AND SUMMARY

We have determined the observed offset distribution of GRBs by astrometrically comparing localizations of GRB afterglows with optical images of the field surrounding each GRB. In all cases, the GRB location appears "obviously" associated with a galaxy—either because the position is superposed atop a galaxy or very near ($\lesssim 1\farcs2$) a galaxy in an otherwise sparse field. In fact, irrespective of the validity of individual assignments of hosts, the offset distribution may be considered a distribution of GRB positions from the nearest respective galaxy at least as bright as $R \approx 28$ (note that in most cases the host galaxies are much brighter, typically $R = 24$–26 mag). We find that at most a few of the 20 GRBs could be unrelated physically to their assigned host and that there is about a 50% chance that all GRBs are correctly assigned to their hosts (see § 6.1).

We then compare the distribution of GRB locations about their respective hosts with the *predicted* radial offset distribution of merging binary remnants. This comparison

is complicated by an unknown projection factor for each burst: if a GRB occurs near an edge-on disk galaxy there exists no model-independent manner to determine the true three-dimensional radial offset of the GRB from the center of the host. Indeed, in a few cases (e.g., GRB 980519 and GRB 991216) even the "center" of the host is not well defined and we must estimate a center visually. In all other cases, we find the centers by using a luminosity-weighted centroid surrounding the central peak of the putative host.

To compare the GRB offsets with those predicted by the NS-NS and NS-BH binary models, we make a general assumption about the projection factor and, to facilitate a comparison in physical units (that is, offsets in kiloparsecs rather than arcseconds), we assign an angular diameter distance to the five hosts without a confirmed distance (§ 6.2). We have shown that the conversion of an angular offset to physical projection is relatively insensitive to the actual redshift of the host. We estimate that the probability that the observed GRB offset distribution is the same as the predicted distribution of NS-NS and BH-NS binaries is $P \lesssim 2 \times 10^{-3}$. Insofar as the observed distribution is representative (see below) and the predicted distribution is accurate, our analysis renders BH-NS and NS-NS progenitor scenarios unlikely for long-duration GRBs.

Having cast doubt on the merging remnant hypothesis, we test whether the offset distribution is consistent with the collapsar (or BH-He) class. Since massive stars (and promptly merging binaries) explode where they are born, we have compared the observed GRB offset distribution with a very simplistic model of massive-star formation in late-type galaxies: an exponential disk. After normalizing each GRB offset by its host half-light radius we compare the distribution with a KS test and find good agreement: $P_{\rm KS} = 0.454$. We have shown that these KS results, based on the assumption of δ-function offsets, are robust even after including the uncertainties in the offset measurements.

Thus far we have neglected discussion of the observational biases that have gone into the localizations of these 20 GRBs. The usual problems plaguing supernova detection, such as the brightness of the central region of the host and dust obscuration, are not at issue for detection of the *prompt* high-energy emission (i.e., X-rays and gamma-rays) of GRBs since the high-energy photons penetrate dust. If the intrinsic luminosity of GRBs is only a function of the inner workings of the central engine (that is, GRBs arise from internal shocks and not external shocks), then the luminosity of a GRB is independent of ambient number density. Therefore, prompt X-ray localizations from *BeppoSAX* and gamma-ray locations from the IPN should not be a function of the global properties of GRB environment; only intrinsic GRB properties such as duration and hardness will affect the prompt detection probability of GRBs.

The luminosity of the afterglows is, however, surmised to be a function of the ambient number density. Specifically, the afterglow luminosity will scale as $\sqrt{n}$, where n is the number density of hydrogen atoms in the 1–10 pc region surrounding the GRB explosion site (see Mészáros, Rees, & Wijers 1998). While $n \approx 0.1$–10 cm^{-3} in the interstellar medium, the ambient number density is probably $n \approx 10^{-4}$–10^{-6} in the intergalactic medium. Thus GRB afterglows in the intergalactic medium (IGM) may appear $\sim 10^{-3}$ times fainter than GRB afterglows in the interstellar medium (ISM; and even more faint compared with GRBs that occur in star-forming regions where the number densities are higher than in the ISM). If only a small fraction of GRBs localized promptly in X-rays and studied well at optical and radio wavelengths were found as afterglow, the ambient density bias may be cause for concern. However, this is not the case. As of 2001 June, 29 of 34 bursts localized by prompt emission were later found as X-ray, optical, and/or radio afterglow (see Frail et al. 2000); that is, almost all GRBs have detectable X-ray afterglow. Therefore, *no more than about 10% of GRBs localized by BeppoSAX could have occurred in significantly lower density environments* such as the IGM; thus, we do not believe that our claim against the delayed merging binaries is affected by this bias.

What about the nondetection of GRB afterglow at optical–radio wavelengths? Roughly half of GRBs promptly localized in the gamma-ray or X-ray bands are not detected as optical or radio afterglow (Frail et al. 2000; Lazzati, Covino, & Ghisellini 2002). While many of these "dark" GRBs must be due to observing conditions (lunar phase, weather, time since burst, etc.), at least some fraction may be due to intrinsic extinction local to the GRB. If so, then these GRBs are likely to be centrally biased since the optical column densities are strongest in star-forming regions and giant molecular clouds. Therefore, *any optically obscured GRBs that do not make it into our observed offset sample will be preferentially located in the disk*. We do not therefore believe the ambient density bias plays any significant role in causing GRBs to be localized preferentially closer to galaxies; in fact, the opposite may be true.

The good agreement between our simplistic model for the location of massive stars and the observed distribution is one of the strongest arguments yet for a collapsar (or promptly bursting binaries) origin of long-duration GRBs. However, the concordance of the predicted and observed distributions is necessary to prove the connection, although not sufficient.

We may now begin to relate the offsets to the individual host and GRB properties. For instance, for the GRBs that lie in close proximity to their host centers (GRB 970508, 980703, and 000418), there is a striking similarity between their hosts—all appear compact and blue with high central surface brightness, suggesting that these hosts are nuclear starburst galaxies (none show spectroscopic evidence for the presence of an AGN).

In fact, the closeness of some GRBs to their host centers signifies that our simplistic model for star formation may require modification. This is not unexpected since in the Galaxy star formation as a function of Galactocentric radius does not follow a pure exponential disk but is vigorous near the center and is strongly peaked around $R \sim 5$ kpc (see Kennicutt 1989). As more accurate offsets are amassed, these subtle distinctions in the GRBs offset distribution may be addressed.

The authors thank the staff of the W. M. Keck Foundation and the staff at the Palomar Observatories for assistance. We thank the anonymous referee for very insightful comments; in particular, the referee pointed out (and suggested the fix for) the bias in offset assignment if GRBs are ejected far from their host galaxies. The referee also pointed out that we did not establish that GRBs are preferentially aligned with the major axes of their hosts (as we had claimed in an earlier version of the paper). We applaud E. Berger and D. Reichart for close reads of various drafts of the

paper. We also thank M. Davies for encouraging us to compare several NS-NS models with the data rather than just one. We acknowledge the members of the Caltech-NRAO-CARA GRB collaboration and P. van Dokkum, K. Adelberger, and R. Simcoe for helpful discussions. We thank N. Masetti for allowing us access to early ground-based data on GRB 990705 and B. Schaefer for kindly providing *QUEST* images of the afterglow associated with GRB 990308. This work was greatly enhanced by the use of data taken as part of A Public Survey of the Host Galaxies of Gamma-Ray Bursts with *HST* (No. 8640; principal investigator, S. Holland). J. S. B. gratefully acknowledges the fellowship and financial support from the Fannie and John Hertz Foundation. S. G. D. acknowledges partial support from the Bressler Foundation. S. R. K. acknowledges support from NASA and the NSF. The authors wish to extend special thanks to those of Hawaiian ancestry on whose sacred mountain we are privileged to be guests. Without their generous hospitality, many of the observations presented herein would not have been possible.

APPENDIX A

POTENTIAL SOURCES OF ASTROMETRIC ERROR

A1. DIFFERENTIAL CHROMATIC REFRACTION

Ground-based imaging always suffers from differential chromatic refraction (DCR) introduced by the atmosphere. The magnitude of this refraction depends strongly ($\propto 1/\lambda_{\rm eff}^2$) on the effective wavelength ($\lambda_{\rm eff}$) of each object, the air mass of the observation, and the air temperature and pressure. With increasing air mass, images are dispersed by the atmosphere and systematically stretched in the parallactic direction in the sense that bluer objects shift toward the zenith and redder objects shift toward the horizon. Other sources of refraction, such as turbulent refraction (e.g., Lindegren 1980), are statistical in nature and serve only to increase the uncertainty in our astrometric solution.

Here we show that DCR, in theory, will not dominate our offset determinations. Since all our early ground-based imaging was conducted with air mass ($\sec z$) $\lesssim 1.6$ we take as an extreme example an image with air mass $\sec z = 2$, where z is the observed zenith angle. It is instructive to determine the scale of systematic offset shifts introduced when compared with either late-time ground-based or *HST* imaging where refractive distortions are negligible. Following Gubler & Tytler (1998), the differential angular distortion between two point sources at an apparent angular separation along the zenith, Δz, may be broken into a color and a zenith distance term. Assuming nominal values for the altitude of the Keck Telescopes on Mauna Kea, atmospheric temperature, humidity and pressure, at an effective wavelength of the R-band filter, $\lambda_{\rm eff}(R) = 6588$ Å (Fukugita et al. 1996), the zenith distance term is 16 mas for an angular separation of $30''$ at an air mass of $\sec z = 2$. The zenith term is approximately linear in angular distance, and so, in practice, even this small effect will be accounted for as a first-order perturbation to the overall rotation, translation, and scale mapping between a Keck and *HST* image. In other words, we can safely neglect the zenith term contribution to the DCR.

We now determine the color term contribution. Optical transients of GRBs are in general redder in appearance (apparent $V-R \approx 0.5$ mag) than their host galaxies (apparent $V-R \sim 0.2$ mag). We assume the average astrometric tie object has $V-R = 0.4$ mag. If the OT is observed through an air mass of $\sec z = 2$ and then the galaxy is observed at a later time through an air mass of, for example, $\sec z = 1.2$, then DCR will induce a $\sim$30 mas centroid shift between the OT and the host galaxy if the two epochs are observed in B band (see Fig. 2 of Alcock et al. 1999). In R band, the filter used in almost all our ground-based imaging for the present work, the DCR strength is about 20% smaller than in B band because of the strong dependence of refraction on wavelength. Therefore we can reasonably assume that DCR should *systematically* affect only our astrometric precision at the 5–10 mas level. Such an effect could, in principle, be detected as a systematic offset in the direction of the parallactic angles of the first epochs of GRB afterglow observations. In § 6.1 we claim that no such systematic effect is present in our data. DCR could of course induce a larger *statistical* scatter in the uncertainty of an astrometric transformation between epochs since individual tie objects are not, in general, the same color and each will thus experience its own DCR centroid shift.

Bearing in mind that DCR is probably negligible we can minimize the effects of DCR by choosing small fields and similar spectral responses of the offset data sets. The *HST* fields are naturally small, and there are enough tie stars when compared with deep ground-based imaging. However, since the spectral response of the *HST* STIS CCD is so broad, extended objects with color gradients will have different apparent relative locations when compared with our deep ground-based R-band images. As such, in choosing astrometric tie objects, we pay particular attention to choosing objects that appear compact (half-light radii $\lesssim 0\farcs3$) on the STIS image.

A2. FIELD DISTORTION

Optical field distortion is another source of potential error in astrometric calibration. Without correcting for distortion in STIS, the maximum distortion displacement (on the field edges) is $\sim$35 mas (Malumuth & Bowers 1997). This distortion is corrected to a precision at the sub-milliarcsecond level on individual STIS exposures with IRAF DITHER (Malumuth & Bowers 1997). Malumuth & Bowers (1997) also found that the overall plate scale appears to be quite stable, with rms changes at the 0.1% level. We confirmed this result by comparing two epochs of imaging on GRB 990510 and GRB 970508 that span about 1 year. The relative plate scale of the geometric mapping between final reductions was unity to within 0.03%.

We do not correct for optical field distortion before mapping ground-based images to *HST*. While there may be considerable distortion (about a few times 100 mas) across whole ground-based CCD images, these distortions are correlated on small

scales. Therefore, when mapping a 50×50 arcsec^2 portion of a Keck image with an *HST* image, the intrinsic differential distortions in the Keck image tend to be small ($\lesssim$30–50 mas). Much of the distortion is accounted for in the mapping by the higher order terms of the fit, and any residual differential distortions simply add scatter to the mapping uncertainties.

APPENDIX B

DERIVATION OF THE PROBABILITY HISTOGRAM (PH)

Histogram binning is most informative when there are many more data points than bins and the bin sizes are much larger than the errors on the individual measurements. Unfortunately, the set of GRB offsets is contrary to both these requirements. We require a method to display the data as in the traditional histogram, but in which the errors on the measurements are accounted for. Instead of representing each measurement as a δ-function, we will represent each measurement as a probability distribution as a function of offset.

What distribution function is suitable for offsets? When the offset is much larger than the error, then the probability that the burst occurred at the measured displacement should approach a δ-function. When the offset is much larger than zero, then the probability distribution should appear essentially Gaussian (assuming the error on the measurement is Gaussian). However, when the observed offset is small and the error on the measurement nonnegligible with respect to the observed offset, the probability distribution is decidedly non-Gaussian since the offset is a positive quantity. The distribution we seek is similar to the well-known Rice distribution (see Rice 1954), only more general.

We derive the probability histogram (PH) as follows. For each GRB offset, i, we construct an individual probability distribution function, $p_i(r)dr$, of the host-normalized offset (r_i) of the GRB given the observed values for $X_{0,i}$, $Y_{0,i}$, the host half-light radius, $R_{i,\mathrm{half}}$, and the associated uncertainties. To simplify the notation in what follows, we drop the index, i, and let all lower case parameters represent dimensionless numbers; for example, the value $x_0 = \mathrm{X}_0/R_{\mathrm{half}}$, where R_{half} is the host half-light radius. Without loss of generality, we can subsume (by quadrature summation) the uncertainties in the host center, the astrometric transformation, and the GRB center into the error contribution in each coordinate. We assume that these statistical coordinate errors are Gaussian distributed with σ_x and σ_y with, for example,

$$\sigma_x = \frac{X_0}{R_{\mathrm{half}}}\sqrt{\frac{\sigma_{X_0}^2}{X_0^2} + \frac{\sigma_{R_{\mathrm{half}}}^2}{R_{\mathrm{half}}^2}}\,.$$

Therefore, we can construct the probability $p(x, y)dxdy$ of the true offset at some distance x and y from the measured offset location (x_0, y_0):

$$p(x,y)dx\,dy = \frac{1}{2\pi\sigma_x\sigma_y}\exp\left[-\frac{1}{2}\left(\frac{x^2}{\sigma_x^2} + \frac{y^2}{\sigma_y^2}\right)\right]dx\,dy\,, \tag{B1}$$

assuming the errors in the x and y are uncorrelated. This is a good approximation since, while the astrometric mappings generally include cross terms in X and Y, these terms are usually small. If $\sigma_x = \sigma_y$, then equation (B1) reduces to the Rayleigh distribution in distance from the observed offset, rather than the host center.

The probability distribution about the host center is found with an appropriate substitution for x and y in equation (B1). In Figure 9 we illustrate the geometry of the problem. The gray-scale distribution shows $p(x, y)dxdy$ about the offset point x_0 and y_0. Let $\phi = \arctan(y_0/x_0)$ and transform the coordinates in equation (B1) by using $\psi = \phi + \theta$, $x = r\cos\psi - x_0$ and $y = r\sin\psi - y_0$. The distribution we seek, the probability that the true offset lies a distance r from the host center, requires a marginalization of $\int_\psi p_i(r, \psi)drd\psi$ over ψ,

$$\begin{aligned} p_i(r)dr &= \int_\psi p_i(r,\psi)dr\,d\psi \\ &= \frac{Jdr}{2\pi\sigma_x\sigma_y}\int_0^{2\pi}\exp\left[-\frac{1}{2}\left(\frac{x(r,\psi)^2}{\sigma_x^2} + \frac{y(r,\psi)^2}{\sigma_y^2}\right)\right]d\psi\,, \end{aligned} \tag{B2}$$

finding $J = r$ as the Jacobian of the coordinate transformation. In general, equation (B2) must be integrated numerically using the observed values x_0, y_0, σ_x, and σ_y. The solution is analytic, however, if we assume that $\sigma_x \rightarrow \sigma_r$ and $\sigma_y \rightarrow \sigma_r$, so that

$$\begin{aligned} p_i(r)dr &\approx \frac{r}{\pi\sigma_r^2}\exp\left(-\frac{r^2 + r_0^2}{2\sigma_r^2}\right)\int_{\theta=0}^{\pi}\exp\left(\frac{rr_0\cos\theta}{\sigma_r}\right)d\theta\,dr \\ &\approx \frac{r}{\sigma_r^2}\exp\left(-\frac{r^2 + r_0^2}{2\sigma_r^2}\right)I_0\left(\frac{rr_0}{\sigma_r^2}\right)dr\,, \end{aligned} \tag{B3}$$

where $I_0(x)$ is the modified Bessel function of zeroth order and $r_0 = (x_0^2 + y_0^2)^{1/2}$.

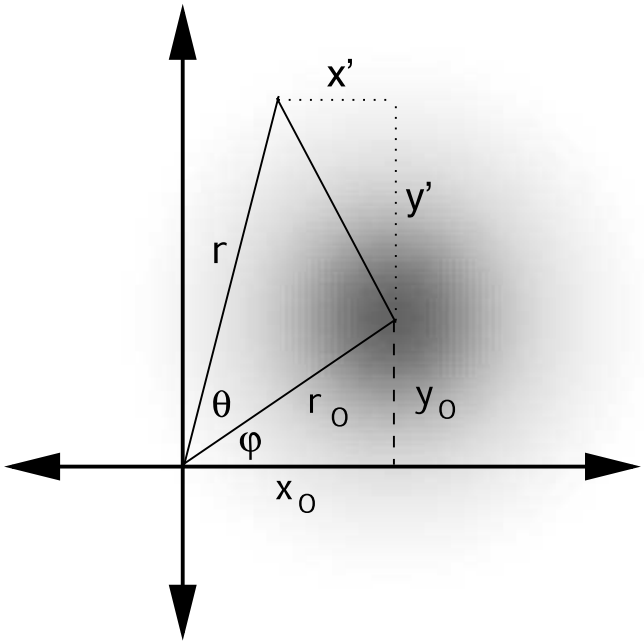

FIG. 9.—Geometry for the offset distribution probability calculation in Appendix B

Equation (B3) is readily recognized as the Rice distribution and is often used to model the noise characteristics of visibility amplitudes in interferometry; visibility amplitudes, like offsets, are positive-definite quantities. Only when $\sigma_x = \sigma_y = \sigma_r$ is the probability distribution exactly a Rice distribution, which is usually the case for interferometric measurements since the real and imaginary components of the fringe phasor have the same rms.

Equation (B2) is a generalized form of the Rice distribution but can be approximated as a Rice distribution by finding a suitable value for σ_r. We find that by letting

$$\sigma_r = \frac{1}{r_0}\sqrt{(x_0\sigma_x)^2 + (y_0\sigma_y)^2} \tag{B4}$$

equation (B3) approximates (to better than 30%) the exact form of the probability distribution in equation (B2) as long as $\sigma_x \lesssim 2\sigma_y$ (or vise versa). In Figure 10 we show two example offset probability distributions in exact and approximate form. Note that $r_0 - \sigma_r \leq r \leq r_0 + \sigma_r$ is not necessarily the 68% percent confidence region of the true offset since the probability distribution is not Gaussian. The exact form is used to construct the data representations in Figures 5–8.

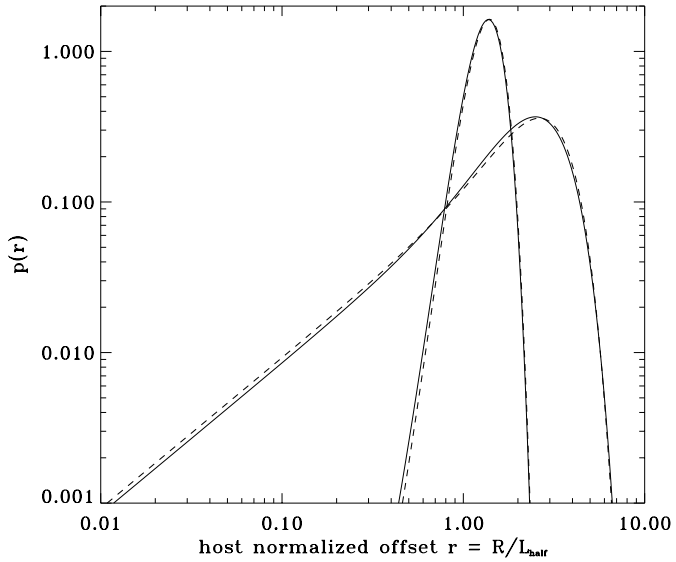

FIG. 10.—Example offset distribution functions $p(r)$. Depicted are two probability distribution curves for $(X_0, Y_0, \sigma_{X_0}, \sigma_{Y_0}, R_{\rm half}, \sigma_{R_{\rm half}})$ = (0.″033, 0.″424, 0.″034, 0.″034, 0.″31, 0.″05) for GRB 970228 and (0.″616, 0.″426, 0.″361, 0.″246, 0.″314, 0.″094) for GRB 981226 for the lower and upper peaked distributions, respectively. The solid line is the exact solution (eq. [B2]), and the dashed line is the approximate solution (eq. [B3]). Here as in the text the host-normalized offset $r = R/R_{\rm half}$, where R is the galactocentric offset of the GRB from the host and $R_{\rm half}$ is the half-light radius of the host.

APPENDIX C

TESTING THE ROBUSTNESS OF THE KS TEST

How robust are the estimates of probabilities found by comparing the observed distribution and the predicted progenitor offset distributions? Since there are different uncertainties on each offset measurement, the KS test is not strictly the appropriate statistic to determine the likelihood that the observed distribution could be drawn from the same underlying (predicted) distribution. One possibility is to construct synthetic sets of observed data from the model by using the observed uncertainties. However, a small uncertainty (say 0.″2 in radius observed to be paired with an equally small offset) that is randomly assigned to a large offset from a Monte Carlo distribution has a different probability distribution than if assigned to a small offset (since the distribution in r is physical only for positive r). Instead, we approach the problem from the other direction by using the data themselves to assess the range in KS statistics given our data. We construct $k = 1000$ synthetic cumulative physical offset distributions using the smoothed probability offset distributions $p_i(r)dr$ for each GRB. As before r is the offset in units of host half-light radius. For each simulated offset distribution k we find a set $\{r_i\}_k$ such that

$$P[0, 1] = \frac{\int_0^{r_i} p_i(l)dl}{\int_0^{\infty} p_i(l)dl} ,$$

where $P[0, 1]$ is a uniform random deviate over the closed interval [0, 1]. In addition, since some of the host assignments may be spurious chance superpositions, we use the estimate of $P_{\rm ch}$ (§ 6.1; Table 3) to selectively remove individual offsets from a given Monte Carlo realization of the offset data set. GRBs with relatively secure host assignments remain in more realizations than those without. So, for instance, the offset of GRB 980703 ($P_{\rm ch} = 0.00045$) is used in all realizations, but the offset of GRB 970828 ($P_{\rm ch} = 0.07037$) is retained in only 93% of the synthetic data sets.

We evaluate the KS statistic as above for each synthetic set and record the result. Figure 8 depicts the cumulative probability distribution compared with the simple exponential disk model. The inset of the figure shows the distribution of KS statistics for the set of synthetic cumulative distributions constructed as prescribed above. In both cases, as expected, the *observed* KS probability falls near the median of the synthetic distribution. The distribution of KS statistics is not significantly affected by retaining all GRB offsets equally (that is, assuming $P_{\rm ch} = 0.0$ for every GRB offset). In Table 4 we present the result of the Monte Carlo modeling. Using this distribution of KS statistics we can now assess the robustness of our comparison result: given the data and their uncertainties, the probability that the observed GRB offset distribution is the same as the model distribution of star formation (exponential disk) is $P_{\rm KS} \geq 0.05$ in 99.6% of our synthetic data sets.

REFERENCES

Akerlof, C., et al. 1999, Nature, 398, 400
Alcock, C., et al. 1999, ApJ, 521, 602
Anderson, J., & King, I. R. 1999, PASP, 111, 1095
Bartunov, O. S., Tsvetkov, D. Y., & Filimonova, I. V. 1994, PASP, 106, 1276
Belczyński, K., Bulik, T., & Zbijewski, W. 2000, A&A, 355, 479
Berger, E., Kulkarni, S. R., & Frail, D. A. 2001, ApJ, 560, 652
Bethe, H. A., & Brown, G. E. 1998, ApJ, 506, 780
Bloom, J. S. 2000, GRB Circ. Network 756
Bloom, J. S., Diercks, A., Galama, T. J., Mahabal, A., Kulkarni, S. R., Harrison, F. A., Mao, P., & Helfand, D. 2000a, GRB Circ. Network 689
Bloom, J. S., Diercks, A., Kulkarni, S. R., Djorgovski, S. G., & Frayer, D. T. & Scoville, N. Z. 1999a, GRB Circ. Network 480
Bloom, J. S., Djorgovski, S. G., Gal, R. R., Kulkarni, S. R., & Kelly, A. 1998a, GRB Circ. Network 87
Bloom, J. S., Djorgovski, S. G., & Kulkarni, S. R. 2001, ApJ, 554, 678
Bloom, J. S., Djorgovski, S. G., Kulkarni, S. R., & Frail, D. A. 1998b, ApJ, 507, L25
Bloom, J. S., et al. 1998c, ApJ, 508, L21
Bloom, J. S., & Kulkarni, S. R. 2000b, GRB Circ. Network 702
Bloom, J. S., et al. 1999b, Nature, 401, 453
Bloom, J. S., Kulkarni, S. R., Djorgovski, S. G., Gal, R. R., Eichelberger, A., & Frail, D. A. 1998d, GRB Circ. Network 149
Bloom, J. S., Kulkarni, S. R., Harrison, F., Prince, T., Phinney, E. S., & Frail, D. A. 1998e, ApJ, 506, L105
Bloom, J. S., et al. 1999c, ApJ, 518, L1
Bloom, J. S., Sigurdsson, S., & Pols, O. R. 1999d, MNRAS, 305, 763
Bloom, J. S., Sigurdsson, S., Wijers, R. A. M. J., Almaini, O., Tanvir, N. R., & Johnson, R. A. 1997, MNRAS, 292, L55
Boella, G., Butler, R. C., Perola, G. C., Piro, L., Scarsi, L., & Bleeker, J. A. M. 1997, A&AS, 122, 299
Brandt, N., & Podsiadlowski, P. 1995, MNRAS, 274, 461
Briggs, M. S., Pendleton, G. N., Kippen, R. M., Brainerd, J. J., Hurley, K., Connaughton, V., & Meegan, C. A. 1999, ApJS, 122, 503
Buat, V., Deharveng, J. M., & Donas, J. 1989, A&A, 223, 42
Bulik, T., Belczyński, K., & Zbijewski, W. 1999, MNRAS, 309, 629
Carter, B. 1992, ApJ, 391, L67
Castro, S. M., Diercks, A., Djorgovski, S. G., Kulkarni, S. R., Galama, T. J., Bloom, J. S., Harrison, F. A., & Frail, D. A. 2000, GRB Circ. Network 605
Cheng, K. S., & Wang, J. 1999, ApJ, 521, 502
Chevalier, R. A., & Li, Z. 2000, ApJ, 536, 195
Cline, T. L., et al. 1999, A&AS, 138, 557
Costa, E., et al. 1997, Nature, 387, 783
de Bernardis, P., et al. 2000, Nature, 404, 955
Deutsch, E. W. 1999, AJ, 118, 1882
Diercks, A., Bloom, J. S., Galama, T. J., & Kulkarni, S. R. 2000, GRB Circ. Network 764
Djorgovski, S. G., Bloom, J. S., & Kulkarni, S. R. 2002a, ApJL, in press
Djorgovski, S. G., Frail, D. A., Kulkarni, S. R., Bloom, J. S., Odewahn, S. C., & Diercks, A. 2001, ApJ, 562, 654
Djorgovski, S. G., et al. 2002b, in Proc. IX Marcel Grossmann Meeting, ed. V. Gurzadyan, R. Jantzen, & R. Ruffini (Singapore: World Scientific), in press
———. 1999, GRB Circ. Network 368
Dutra, C. M., Bica, E., Clariá, J. J., Piatti, A. E., & Ahumada, A. V. 2001, A&A, 371, 895
Eichler, D., Livio, M., Piran, T., & Schramm, D. N. 1989, Nature, 340, 126
Epps, H. W., & Miller, J. S. 1998, Proc. SPIE, 3355, 48
Esin, A. A., & Blandford, R. 2000, ApJ, 534, L151
Fenimore, E. E., Epstein, R. I., & Ho, C. 1993, A&AS, 97, 59
Fenimore, E. E., Ramirez-Ruiz, E., & Wu, B. 1999, ApJ, 518, L73
Filippenko, A. V. 1997, ARA&A, 35, 309
Finger, G., Biereichel, P., Mehrgan, H., Meyer, M., Moorwood, A. F., Nicolini, G., & Stegmeier, J. 1998, Proc. SPIE, 3354, 87
Fishman, G. J., & Meegan, C. A. 1995, ARA&A, 33, 415
Frail, D. A. 1999, GRB Circ. Network 451
Frail, D. A., et al. 1999, ApJ, 525, L81
Frail, D. A., Kulkarni, S. R., Nicastro, S. R., Feroci, M., & Taylor, G. B. 1997, Nature, 389, 261
Frail, D. A., et al. 2001, ApJ, 562, L55
———. 2000, in AIP Conf, Proc. 526, Gamma-Ray Bursts, ed. R. M. Kippen, R. S. Mallozzi, & G. J. Fishman (Fifth Huntsville Symp.) (New York: AIP), 298
Frontera, F., Costa, E., dal Fiume, D., Feroci, M., Nicastro, L., Orlandini, M., Palazzi, E., & Zavattini, G. 1997, A&AS, 122, 357
Fruchter, A., Ferguson, H., Popper, J., Gibbons, R., Sahu, K., & Pian, E. 1999a, GRB Circ. Network 386
Fruchter, A., Metzger, M., & Petro, L. 2000a, GRB Circ. Network 701
Fruchter, A., & Pian, E. 1998, GRB Circ. Network 151
Fruchter, A., Sahu, K., Gibbons, R., Petro, L., & Ferguson, H. 2000b, GRB Circ. Network 565
Fruchter, A., Smette, A., Gull, T., Ferguson, H., Petro, L., Rhoads, J., & Sahu, K. 2000c, GRB Circ. Network 627

Fruchter, A., Thorsett, S., & Pian, E. 1999b, GRB Circ. Network 354
Fruchter, A., & Vreeswijk, P. 2001a, GRB Circ. Network 1063
Fruchter, A., Vreeswijk, P., Hook, R., & Pian, E. 2000d, GRB Circ. Network 752
Fruchter, A., Vreeswijk, P., & Nugent, P. 2001b, GRB Circ. Network 1029
Fruchter, A., Vreeswijk, P., Sokolov, V., & Castro-Tirado, A. 2000e, GRB Circ. Network 872
Fruchter, A. S., & Hook, R. N. 1997, Proc. SPIE, 3164, 120
Fruchter, A. S., et al. 1999c, ApJ, 516, 683
Fryer, C. L., & Woosley, S. E. 1998, ApJ, 502, L9
Fryer, C. L., Woosley, S. E., & Hartmann, D. H. 1999, ApJ, 526, 152
Fukugita, M., Ichikawa, T., Gunn, J. E., Doi, M., Shimasaku, K., & Schneider, D. P. 1996, AJ, 111, 1748
Fynbo, J. P. U., Jensen, B. L., Hjorth, J., Pedersen, H., & Gorosabel, J. 2000a, GRB Circ. Network 570
Fynbo, J. U., et al. 2000b, ApJ, 542, L89
Galama, T. 1999, Ph.D. thesis, Univ. Amsterdam
Galama, T. J., et al. 2000, ApJ, 536, 185
———. 1999, GCN 313
———. 1998, Nature, 395, 670
Garnavich, P. M., Loeb, A., & Stanek, K. Z. 2000, ApJ, 544, L11
Goodman, J. 1986, ApJ, 308, L47
Groot, P. J., et al. 1998a, ApJ, 493, L27
———. 1998b, ApJ, 502, L123
Gubler, J., & Tytler, D. 1998, PASP, 110, 738
Hakkila, J., Meegan, C. A., Pendleton, G. N., Briggs, M. S., Horack, J. M., Hartmann, D. H., & Connaughton, V. 1998, in AIP Conf. Ser. 428, Gamma-Ray Bursts, ed. C. A. Meegan, R. Preece, & T. Koshut (Fourth Huntsville Symp.) (Woodbury, New York: AIP), 236
Hansen, B. M. S., & Phinney, E. S. 1997, MNRAS, 291, 569
Harrison, F. A., et al. 1999, ApJ, 523, L121
Hjorth, J. 2000, GRB Circ. Network 731
Hjorth, J., Andersen, M. I., Pedersen, H., Jaunsen, A. O., Costa, E., & Palazzi, E. 1998, GRB Circ. Network 109
Hjorth, J., Holland, S., Courbin, F., Dar, A., Olsen, L. F., & Scodeggio, M. 2000, ApJ, 534, L147
Hogg, D. W., Pahre, M. A., McCarthy, J. K., Cohen, J. G., Blandford, R., Smail, I., & Soifer, B. T. 1997, MNRAS, 288, 404
Holland, S. 2000a, GRB Circ. Network 726
———. 2000b, GRB Circ. Network 778
Holland, S., et al. 2000a, GRB Circ. Network 753
———. 2000b, GRB Circ. Network 698
———. 2000c, GRB Circ. Network 704
———. 2000d, GRB Circ. Network 749
———. 2000e, GRB Circ. Network 778
Hurley, K. 2000, GRB Circ. Network 736
Hurley, K., Cline, T., Mazets, E., & Golenetskii, S. 2000a, GRB Circ. Network 791
Hurley, K., Mazets, E., Golenetskii, S., & Cline, T. 2000b, GRB Circ. Network 801
Jager, R., et al. 1997, A&AS, 125, 557
Jaunsen, A. O., et al. 1998, GRB Circ. Network 78
Johnson, H. M., & MacLeod, J. M. 1963, PASP, 75, 123
Kells, W., Dressler, A., Sivaramakrishnan, A., Carr, D., Koch, E., Epps, H., Hilyard, D., & Pardeilhan, G. 1998, PASP, 110, 1487
Kennicutt, R. C. 1989, ApJ, 344, 685
Kimble, R. A., et al. 1998, ApJ, 492, L83
Klebesadel, R. W., Strong, I. B., & Olson, R. A. 1973, ApJ, 182, L85
Kobayashi, S., & Sari, R. 2001, ApJ, 551, 934
Kulkarni, S. R., et al. 1998a, Nature, 393, 35
———. 1998b, Nature, 395, 663
———. 2000, Proc. SPIE, 4005, 9
Kumar, P. 1999, ApJ, 523, L113
Lamb, D. Q. 1995, PASP, 107, 1152
Larkin, J., Ghez, A., Kulkarni, S., Djorgovski, S., Frail, D., & Taylor, G. 1998, GRB Circ. Network 51
Lazzati, D., Compana, S., & Ghisellini, G. 1999, MNRAS, 304, L31
Lazzati, D., Covino, S., & Ghisellini, G. 2002, MNRAS, in press
Lazzati, D., et al. 2001, A&A, 378, 996
Lindegren, L. 1980, A&A, 89, 41
MacFadyen, A. I., & Woosley, S. E. 1999, ApJ, 524, 262
Malumuth, E. M., & Bowers, C. W. 1997, in The 1997 *HST* Calibration Workshop with a New Generation of Instruments, ed. S. Casertano, R. Jedrzejewski, C. D. Keyes, & M. Stevens (Baltimore: STScI), 144
Masetti, N., et al. 2000, A&A, 354, 473
McLean, I. S., et al. 1998, Proc. SPIE, 3354, 566
Mészáros, P., Rees, M. J., & Wijers, R. A. M. J. 1998, ApJ, 499, 301
Metzger, M., Fruchter, A., Masetti, N., Palazzi, E., Pian, E., Klose, S., & Stecklum, B. 2000, GRB Circ. Network 733
Metzger, M. R., Djorgovski, S. G., Kulkarni, S. R., Steidel, C. C., Adelberger, K. L., Frail, D. A., Costa, E., & Fronterra, F. 1997a, Nature, 387, 879
Metzger, M. R., Kulkarni, S. R., Djorgovski, S. G., Gal, R., Steidel, C. C., & Frail, D. A. 1997b, IAU Circ. 6588
Mirabal, N., Halpern, J. P., & Wagner, R. M. 2000, GRB Circ. Network 650
Monet, D. G. 1998, BAAS, 193(12003)
Narayan, R., Paczyński, B., & Piran, T. 1992, ApJ, 395, L83
Nicklas, H., Seifert, W., Boehnhardt, H., Kiesewetter-Koebinger, S., & Rupprecht, G. 1997, Proc. SPIE, 2871, 1222
Odewahn, S. C., et al. 1998, ApJ, 509, L5
Odewahn, S. C., Windhorst, R. A., Driver, S. P., & Keel, W. C. 1996, ApJ, 472, L13
Oke, J. B., et al. 1995, PASP, 107, 375
Östlin, G., Amram, P., Bergvall, N., Masegosa, J., Boulesteix, J., & Márquez, I. 2001, A&A, 374, 800
Paczyński, B. 1986, ApJ, 308, L43
———. 1995, PASP, 107, 1167
———. 1998, ApJ, 494, L45
Panaitescu, A., & Kumar, P. 2000, ApJ, 543, 66
Phinney, E. S. 1991, ApJ, 380, L17
Pian, E. 2002, in Supernovae and Gamma-Ray Bursters, ed. K. W. Weiler (Berlin: Springer), in press
Pian, E., et al. 1998, ApJ, 492, L103
Piran, T. 1999, Phys. Rep., 314, 575
Piro, L. 2001, GRB Circ. Network 959
Piro, L., et al. 1999, ApJ, 514, L73
———. 2000, Science, 290, 955
Portegies Zwart, S. F., & Spreeuw, H. N. 1996, A&A, 312, 670
Rana, N. C., & Wilkinson, D. A. 1986, MNRAS, 218, 497
Reaves, G. 1953, PASP, 65, 242
Rees, M. J. 1999, A&AS, 138, 491
Reichart, D. E. 1999, ApJ, 521, L111
———. 2001, ApJ, 554, 643
Rice, S. O. 1954, Selected Papers on Noise and Stochastic Processes, ed. N. Wax (New York: Dover), 238
Sahu, K. C., et al. 1997, Nature, 387, 476
———. 2000, ApJ, 540, 74
Schaefer, B. E., et al. 1999, ApJ, 524, L103
Schmidt, M. 1999, ApJ, 523, L117
Smette, A., et al. 2001, ApJ, 556, 70
Sokolov, V. V., et al. 2001, A&A, 372, 438
Stanek, K. Z., Garnavich, P. M., Kaluzny, J., Pych, W., & Thompson, I. 1999, ApJ, 522, L39
Stone, R. C. 1989, AJ, 97, 1227
Stornelli, M., Celidonio, G., Muller, J. M., in't Zand, J. I., Amati, L., Feroci, M., & Gandolfi, G. 2000, GRB Circ. Network 540
Taylor, G. B., Beasley, A. J., Frail, D. A., Kulkarni, S. R., & Reynolds, J. E. 1999, A&AS, 138, 445
Taylor, G. B., Bloom, J. S., Frail, D. A., Kulkarni, S. R., Djorgovski, S. G., & Jacoby, B. A. 2000, ApJ, 537, L17
Taylor, G. B., Frail, D. A., Kulkarni, S., Shepherd, D. S., Feroci, M., & Frontera, F. 1998, ApJ, 502, L115
Taylor, J. H. 1994, Rev. Mod. Phys., 66, 711
Uglesich, R., Mirabal, N., Halpern, J., Kassin, S., & Novati, S. 1999, GRB Circ. Network 472
van Dyk, S. D. 1992, AJ, 103, 1788
van Paradijs, J., et al. 1997, Nature, 386, 686
van Paradijs, J., Kouveliotou, C., & Wijers, R. A. M. J. 2000, ARA&A, 38, 379
Vietri, M., Perola, C., Piro, L., & Stella, L. 1999, MNRAS, 308, L29
Vreeswijk, P. M., Fruchter, A., Ferguson, H., & Kouveliotou, C. 2000, GRB Circ. Network 751
Vreeswijk, P. M., et al. 1999, GRB Circ. Network 310
Waxman, E., & Draine, B. T. 2000, ApJ, 537, 796
Weth, C., Mészáros, P., Kallman, T., & Rees, M. J. 2000, ApJ, 534, 581
Wijers, R. A. M. J., Bloom, J. S., Bagla, J., & Natarajan, P. 1998, MNRAS, 294, L13
Woosley, S. E. 1993, ApJ, 405, 273
Yoshida, A., Namiki, M., Otani, C., Kawai, N., Murakami, T., Ueda, Y., Shibata, R., & Uno, S. 1999, A&AS, 138, 433